SCUOLA DI DOTTORATO
UNIVERSITÀ DEGLI STUDI DI MILANO-BICOCCA

Department of

Materials Science

PhD program in Materials Science and Nanotechnology Cycle XXXIV

Curriculum in Materials Science

# Anion Conducting Polymers for Fuel Cells and Electrolyzers

Surname: Bonizzoni Name: Simone

Registration number: 846171

Tutor: Prof. Piercarlo Mustarelli

Co-tutor: Prof. Riccardo Ruffo

Coordinator: Prof. Marco Bernasconi

**ACADEMIC YEAR 2021/2022**

**Look, if you had**
**One shot or one opportunity**
**To seize everything you ever wanted**
**In one moment**
**Would you capture it**
**Or just let it slip?**

**Lose yourself - Eminem**

# Abstract:

Green hydrogen, as energy vector, is expected to replace fossil hydrocarbon fuels. In a circular hydrogen-based economy, electrolyzer and fuel cell technologies play a crucial role in vector generation and conversion, respectively. In particular, Anion Exchange Membrane Fuel Cells (AEMFCs) and ELectrolyzers (AEMELs) are expected to represent a breakthrough with respect to the state of the art, allowing the use of low-cost catalysts, in principle avoiding Platinum Group Metals (PGM) and other Critical Raw Materials.

My PhD work was focused on the development of anionic conducting polymers to be applied in membranes for AEMFCs and AEMELs. I investigated the chemical modification of different classes of polymers, including perfluorinated systems (Aquivion®), aliphatic polyketones, and polystyrene. The employed methodologies were organic chemistry procedures e.g. Paal-Knorr reaction, Baeyer-Villiger oxidation, methylation processes. The polymers and the related membranes were characterized with a wide ensemble of techniques, including elemental and thermal analysis, FTIR and solid-state NMR spectroscopies, scanning electron microscopy. The functional properties of the membranes were investigated by electrochemical impedance spectroscopy and polarization curves.

The most interesting results were obtained from Aquivion® modification. The membranes obtained following this route show interesting and promising properties for fuel cell and electrolyzer applications. In particular, modified Aquivion® membranes show excellent stability in alkaline environment. The results of Aquivion® modification have been published on two international journals, and the polyketones functionalization work is undergoing publication.

**TABLE OF CONTENTS**

# Chapter 1: Introduction

In recent decades, energy production in a sustainable way, with low environmental impact and with a reduced and controlled production of greenhouse gases, has pushed energy research towards the use of new alternative and renewable energy sources[1,2]. At present, most energy production is based on the utilization of fossil fuels such as petroleum products and natural gas as the primary source, producing the main atmosphere pollution such as $CO_2$, $SO_x$, $NO_x$.[3]

A possible alternative solution to the fossil fuels application is a circular economy based on hydrogen as energy vector in which electrolyzer and fuel cell technologies play a crucial role in vector generation and conversion, respectively[4]. From the electrochemical oxidation of hydrogen, water, electricity and heat are obtained, consequently, the application of hydrogen vector is considered green, eco-sustainable and renewable. In order to realize this system, the fuel cell and water electrolyzer technologies must be improved.

## Fuel cell

Fuel Cells are electrochemical devices that can convert the chemical energy of a fuel and an oxidizing reagent into electricity thanks to electrochemical processes. These devices are composed by two electrodes (in green), which are separated by an electrolyte, and two gas diffusers, which allow the supply of the reagents.

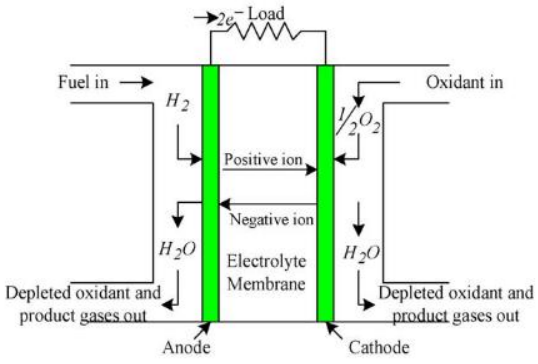


**Fig. 1.** Fuel cell operation diagram.

*Figure 1-1 General scheme of fuel cell of PEMFC and AEMFC*[5]

The electrode where the Oxidation Reaction (OR) takes place is called anode compartment, while the other one, where the Redaction Reaction (RR) takes place, is called cathode compartment. Considering the couple hydrogen-oxygen, when the fuel cell is working, the hydrogen is oxidized at the anode, while the oxygen is reduced at the cathode.

According to the figure 1, if the fuel cell works with a proton exchange membrane, the electrons generated in the process will be balanced by the migration of protons from the anode to the cathode through the proton membrane and the half-reactions are:

Anode:

$$H_2 \rightarrow 2\ H^+ + 2\ e^-$$

Cathode:

$$½\ O_2 + 2\ e^- + 2\ H^+ \rightarrow H_2O$$

Global reaction:

$$H_2 + ½\ O_2 \rightarrow H_2O$$

if the fuel cell works with an anionic exchange membrane, the electrons generated in the process will be balanced by the migration of $OH^-$ from the cathode to the anode through the alkaline membrane and the half-reactions are:

Anode:

$$H_2 + 2\ OH^- \rightarrow 2\ H_2O + 2\ e^-$$

Cathode:

$$½\ O_2 + H_2O + 2\ e^- \rightarrow 2\ OH^-$$

Global reaction:

$$H_2 + ½\ O_2 \rightarrow H_2O$$

The Proton Exchange Membrane Fuel Cells (PEMFC) are getting increasing interest for their intrinsic properties such as the deliverability power (up to 100 KW[4]) and the short wait time before providing energy (few seconds), which allow this technology to have a wide range of applicability, from mobile

devices to automotive industry[6]. The commercial PEMFCs are composed of a Proton Exchange Membrane, such as Nafion® (Dupont) or Aquivion® (Solvay), graphite or nickel electrodes, and platinum and platinum alloys as electrocatalysts (EC) for anode and cathode, respectively. This type of FC works with an extreme low pH value and it implies a restricted choice of electrocatalysts (ECs) to those of the Platinum Metal Group (PMG). This represents the main disadvantage to PEMFC scalability, because the use of platinum or its alloys increases the final cost of the devices. Moreover, these kinds of ECs are very sensitive to environmental pollution, thus reducing the life time of the device[7]. To solve some of these drawbacks, Anion Exchange Membranes (AEM) are investigated as possible replacement of PEMFCs. The main advantage of working with higher pH values is the possibility to extend the ECs choice to low-cost and more abundant metals, such as iron, nickel[8]. Consequently, it is possible to reduce the final cost of the FC and to make the device more robust against environmental pollution. In addition, the Oxygen Reduction Reaction (ORR) is facilitate. The drawbacks of the higher pH values are correlated to the low chemical stability of AEM in alkaline environment and the less conductivity of hydroxide ions with respect to protons (1-2 orders of magnitude)[9]

## Aquivion perfluorinated polymer

Polyfluorinated polymers are largely used as proton exchange membranes thanks to their very high conductivity, chemical and electrochemical stability. Despite their elevated cost, these polymers find application in commercial low temperature fuel cell and water Electrolyzer[4,10]. The main polyfluorinated PEM commercially available are Nafion® (Dupont), 3M ionomer (3M), Aquivion® (Solvay), which differ by the length of the protogenic side chain. Below, the main characteristics and differences between Nafion® and Aquivion® are reported.

### Nafion®

The first significant step in membrane research and development occurred in 1966 with Dupont's production of Nafion®. This perfluorinated polymer exhibited significantly improved properties including doubling the specific conductivity and a four-fold increase in the lifetime[11]. These properties allowed Nafion® to quickly replace other membranes and made it the industry standard[4].

Its structure consists of a polytetrafluoroethylene (PTFE) backbone with fluorodiether side chains ending with sulfonic acid [11].

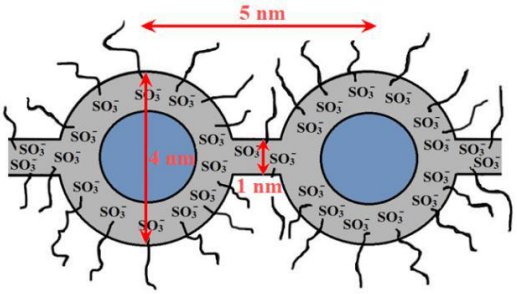


*Figure 1-2 – Sketch of Nafion® cluster structure*[12]

The transport of ions in this material is described with the network-cluster model by Gierke et al.[13], according to which the membrane is a mixture of two phases with hydrophobic and hydrophilic domains. The hydrophobic domains are made by PTFE portion, while the hydrophilic domains are clusters established within the hydrated membrane containing the sulfonic acid groups, water, and protons as showed in figure 2. These clusters are connected by channels to assure the proton conductivity. The charge transport in the membrane can be described as a combination of Grotthuss mechanism and the vehicle mechanism as showed in figure 3[14].

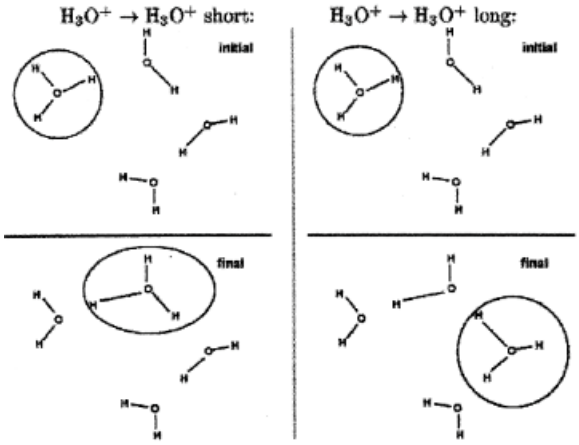


*Figure 1-3 – Sketch of short- and long-range mechanism*[15]

The first one describes the charge transport with low-water contents through $H_3O^+$ ions, while the vehicle mechanism describes the transport of the hydronium ions through diffusion caused by electroosmotic drag with the formation of Zundel ($H_5O_2^+$) and Eigen ($H_9O_4^+$) ions[4,15].

Despite of the good performance under conventional operating conditions (60–80 ◦C, low temperature FC), usually it is not suitable for high temperature PEM fuel cells applications[16]. It is well documented in literature that in this temperature range the proton conductivity of pristine PFSA ionomers is insufficient owing to a breakdown of the proton transport mechanism triggered by: the dehydration of the materials and the collapse of the elastic modulus of the membranes[17]. The first drawback causes a decrease of proton conductivity according to the "vehicle" mechanism for proton conduction whereas the latter problem leads quickly the backbone structure to collapse[16,17]. Another important failure mode is chemical degradation, defined as ionomer damage and loss in membrane functionality and integrity, i.e. the breakage of perfluorocarbon backbone and side chain groups of polymer membrane. Radical attack is the major cause of chemical degradation. Two possible mechanisms for radical generation have been proposed: hydrogen peroxide decomposition due to the incomplete reduction at the cathode side (ORR) or the reaction of hydrogen and oxygen on platinum catalyst. For the former case, many studies have verified that the presence of $H_2O_2$ in drain water, in exhaust gas and in the membrane[11].

**Aquivion®**

Aquivion® (Solvay, Specialty Polymers SpA) is a PerFluoroSulfonic Acid (PFSA) ionomer constituted by a hydrophobic polytetrafluoroethylene (PTFE)-like backbone and hydrophilic side chains ending with sulfonic acid that provides protons; this property is mandatory for fuel cell operation[18].

Since the chemical structure is like the one observed in Nafion®, this polymer presents many characteristics seen before, such as ion transport modes and chemical degradation and radical attack, however, it differs from the mechanic point of view. In spite of the similarity in chemical structure with other ionomers currently available on the market such as Nafion® (DuPont de Nemours) and 3M ionomer (3M company), Aquivion® has a shorter side chain length (figure 4)[19].

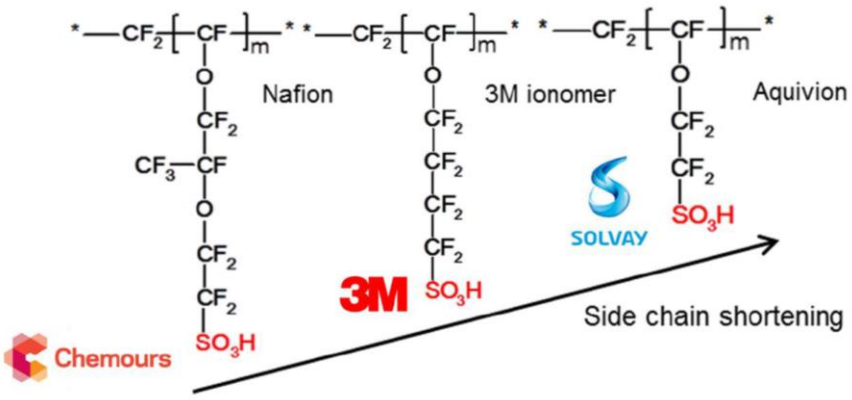


*Figure 1-4 - Comparison of the structures of Nafion®, 3M Ionomer®, Aquivion*[18]

The shorter side chain in Aquivion® allows higher glass transition temperature (e.g. higher softening temperature, figure 5), higher capability to retain and absorb cathode produced water (e.g. self-humidification ability) and high conductivity and water mobility especially in low humidity conditions[20,21].

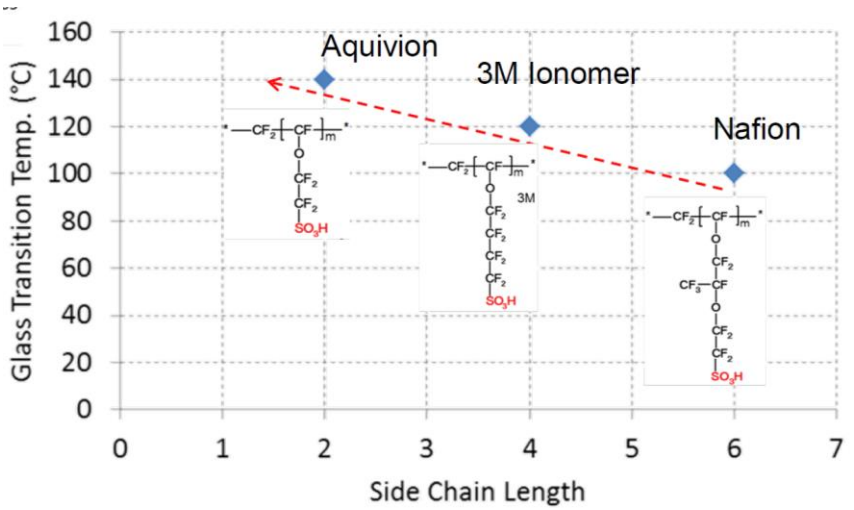


*Figure 1-5 - Glass transitions temperature of Nafion®, 3M Ionomer®, Aquivion® in function of side chain length*[18]

The capability of surviving and having better performances at higher working temperature (≈130°C, target temperature for automotive application)[16] without major issues, is, again, explained by the larger crystallinity (i.e. mechanical toughness, inversely proportional to -$SO_3H$ loading), higher glass transition temperature and lower equivalent weight of Aquivion®, ensuring better mechanical properties and producing higher conductivity and an increase of catalyst utilization[16].

## Aliphatic polyketones

The aliphatic polyketones are most produced by polymerizing carbon monoxide with one or more α-olefins e.g. ethylene, propylene, styrene, vinyl chloride, acrylonitrile [22,23]. According to the nature of these olefins, a very wide type of polymers such us poly(ethyl-ketone), poly(propyl-ketone), poly(styrene-ketone), poly(vinylpiridine-ketone) could be obtained [22–24].

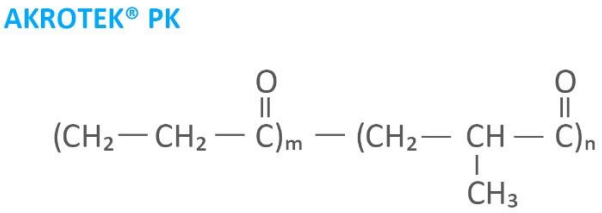


*Figure 1-6 Structure of AKROTEK_PK*[25]

The first commercial aliphatic polyketones is poly(ethyl-ketone)[26]. In 1982 J. Dent (Shell) employed a new $Pd^{2+}$-based catalyst system that allows to produce linear, perfectly alternating carbon monoxide - ethylene copolymer with high molecular weight [27]. In 1996 Shell commercialized its carbon monoxide – ethylene – propylene terpolymer as "*Carilon*". In 2000, Shell announced that *Carilon* was withdrawing from their marketplace [27]. Therefore, the copolymer poly(ethyl-ketone) and the terpolymer poly(ethyl-propyl-ketone) still remain very attractive raw materials due to the low cost and high availability of their monomers and also for the wide versatility of ketone groups inside the backbone[23,28]. For these reasons, we have investigated these materials as possible polymer matrix for fuel cell and electrolyzer applications.

**Synthesis of poly(ethyl-ketone):**

The aliphatic polyketones are produced by co-polymerization between carbon monoxide and olefin such as ethylene or propylene[23]. In general, the main working conditions for these process are a pressure about 50 - 60 bar and a temperature about 90 - 100 °C, in presence of $Pd^{2+}$- based catalyst[29,30]. For these working conditions, autoclave is necessary. In particular, in order to have a homogeneous poly(ethyl-ketone), the carbon monoxide and ethylene must be mixed before entering in the autoclave, consequently, a premixing zone is required (See A1). This implant allows

the synthesis of all polyketones using gaseous or liquid olefins. During my PhD period, I designed the structure part of the implant for the synthesis poly(ethyl-ketone) (See A1) but, unfortunately, due to technical and security problems, which do not depend on me, the implant has not yet been tested. For this reason, I decided to use the commercial aliphatic polyketones AKROTECH_PK (figure 6).

**Chemical modification:**

The poly(ethyl-ketone) can be easily functionalized thanks to the wide reactivity of ketone group. Observing the polymer structure, three different modification sites can be identified.

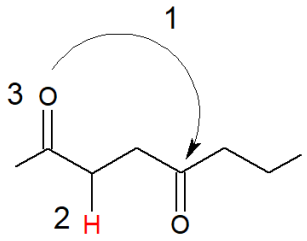


*Figure 1-7 - Scheme of PK with the possible modification pathway*

According to the figure 7 , the first is the Pall-Knorr reaction, the second pathway involves the alpha-hydrogen then the third employs oxidation/reduction of the oxygen of carboxyl group. Below, the main properties of these synthesis route are reported

**First method - Pall-Knorr reactions**

Pall-Knorr reactions are very attractive from the point of view mechanical and thermal properties because they allow to introduce a heteroatomic ring inside the backbone of poly(ethyl-ketone). Generally, an 1,4-diketones unit forms a 5-member ring including a heteroatom like nitrogen, oxygen, sulfur creating a pyrrole, furan and thiophene derivates (figure 8)[31].

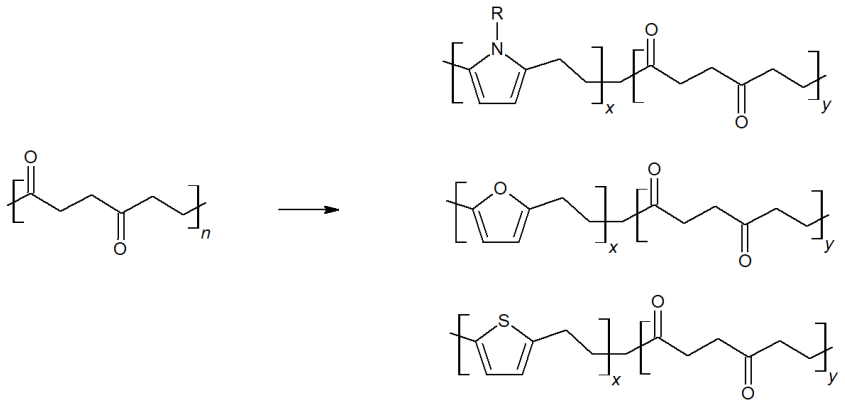

*Figure 1-8 - Scheme of possible Pall-Knorr products*

The pyrrole-based derivates are produced by reaction of the 1,4-diketones units with ammonia of primary amines[32,33]. The Furan rings are introduced in the polymer by using strong dehydrating agent e.g. anhydride phosphoric[23,31] . The thiophene-based derivates are produced by using the Lawson's reagent[23,34].

**Second method - Alpha hydrogen**

The alpha-hydrogen of ketone groups shows a weak acid behavior due to the keto-enol tautomerism equilibrium[35,36]. If the polymer is treated with a basic chemical, I can remove this proton away, generating a strong carbon-based nucleophilic group which can be used for nucleophilic substitution or addition. For this method, the grafting of polyketones with allyl group is reported [37] .

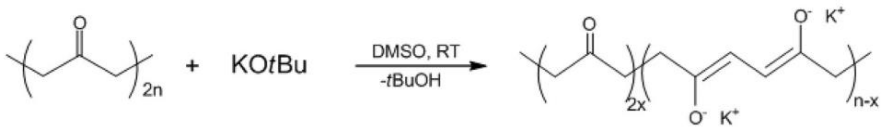


*Figure 1-9 - Scheme of the enol formation[37]*

**Third method – Reduction of carboxyl oxygen**

In this group are included the reactions which involve the C=O double bond for examples ketone reduction or methylenation reaction. The reduction of ketone introduces the hydroxyl group in the structure and generate a new chirogenic center. The introduction of the hydroxyl groups opens to new synthesis ways based on oxygen nucleophilic substitution typical of alcohol compound,

however it affects the mechanical properties giving a softer polymer matrix due to the decreasing of carboxyl group contents[23]. The synthesis of polyol polymer using $Bu_4NBH_4$ [31] and the synthesis polyamine and polythiol with Cu-based catalyst [23] are reported.

**Other reaction**

In literature, is also reported the well-known Baeyer-Villiger oxidation that allows the conversion of ketone into ester group[31].

## Polystyrene:

The polystyrene and its copolymer are thermoplastic materials with good mechanical and thermal properties, high chemical resistance [38]. Those polymers are used for wide applications such as packaging or as structure materials[39,40] Usually these polymers are produced by polymerization processes[38].

For the application as anion exchange membranes, polystyrene materials are produced from specific monomers thanks to polymerization and copolymerization procedures[41] or they could be obtained by direct modification of the their backbone[42]. For the direct modification the main procedures applied are the chloromethylation[43–45], radical grafting[43].

## Bibliography


1. Züttel A, Remhof A, Borgschulte A, Friedrichs O. Hydrogen: The future energy carrier. *Philos Trans R Soc A Math Phys Eng Sci*. 2010;368(1923):3329-3342. doi:10.1098/rsta.2010.0113

2. Mandal TK, Gregory DH. Hydrogen: A future energy vector for sustainable development. *Proc Inst Mech Eng Part C J Mech Eng Sci*. 2010;224(3):539-558. doi:10.1243/09544062JMES1774

3. Nicoletti G, Arcuri N, Nicoletti G, Bruno R. A technical and environmental comparison between hydrogen and some fossil fuels. *Energy Convers Manag*. 2015;89:205-213. doi:10.1016/j.enconman.2014.09.057

4. Di Noto V, Zawodzinski TA, Herring AM, Giffin GA, Negro E, Lavina S. Polymer electrolytes for a hydrogen economy. *Int J Hydrogen Energy*. 2012;37(7):6120-6131. doi:10.1016/j.ijhydene.2012.01.080

5. Kirubakaran A, Jain S, Nema RK. A review on fuel cell technologies and power electronic interface. *Renew Sustain Energy Rev*. 2009;13(9):2430-2440. doi:10.1016/j.rser.2009.04.004

6. Satyapal S, Cell F, Office T. Hydrogen and Fuel Cells Perspective and Opportunities American Nuclear Society Meeting – Nuclear Hybrid Systems Panel. 2017.

7. Merle G, Wessling M, Nijmeijer K. Anion exchange membranes for alkaline fuel cells: A review. *J Memb Sci*. 2011;377(1-2):1-35. doi:10.1016/j.memsci.2011.04.043

8. Pan ZF, An L, Zhao TS, Tang ZK. Advances and challenges in alkaline anion exchange membrane fuel cells. *Prog Energy Combust Sci*. 2018;66:141-175. doi:10.1016/j.pecs.2018.01.001

9. Cheng J, He G, Zhang F. A mini-review on anion exchange membranes for fuel cell applications: Stability issue and addressing strategies. *Int J Hydrogen Energy*. 2015;40(23):7348-7360. doi:10.1016/j.ijhydene.2015.04.040

10. Weber AZ, Mench MM, Meyers JP, Ross PN, Gostick JT, Liu Q. Redox flow batteries: A review. *J Appl Electrochem*. 2011;41(10):1137-1164. doi:10.1007/s10800-011-0348-2

11. Smitha B, Sridhar S, Khan AA. Solid polymer electrolyte membranes for fuel cell applications

- A review. *J Memb Sci*. 2005;259(1-2):10-26. doi:10.1016/j.memsci.2005.01.035

12. Lebedeva M V., Ragutkin A V., Antropov AP, Yashtulov NA. The features of bimetallic Pt-Ru nanoparticles formation on the Nafion membrane for electrodes of chemical power sources. *IOP Conf Ser Mater Sci Eng*. 2020;744(1). doi:10.1088/1757-899X/744/1/012007

13. Wu B, Zhao M, Shi W, et al. The degradation study of Nafion/PTFE composite membrane in PEM fuel cell under accelerated stress tests. *Int J Hydrogen Energy*. 2014;39(26):14381-14390. doi:10.1016/j.ijhydene.2014.02.142

14. Kornyshev AA, Kuznetsov AM, Spohr E, Ulstrup J. Kinetics of Proton Transport in Water. 2003:3351-3366. doi:10.1021/jp020857d

15. Kuwertz R, Kirstein C, Turek T, Kunz U. Influence of acid pretreatment on ionic conductivity of Nafion® membranes. *J Memb Sci*. 2016;500:225-235. doi:10.1016/j.memsci.2015.11.022

16. Stassi A, Gatto I, Passalacqua E, et al. Performance comparison of long and short-side chain perfluorosulfonic membranes for high temperature polymer electrolyte membrane fuel cell operation. *J Power Sources*. 2011;196(21):8925-8930. doi:10.1016/j.jpowsour.2010.12.084

17. Negro E, Vittadello M, Vezzù K, Paddison SJ, Di Noto V. The influence of the cationic form and degree of hydration on the structure of Nafion™. *Solid State Ionics*. 2013;252:84-92. doi:10.1016/j.ssi.2013.09.017

18. Polymers SS. Aquivion ® PFSA Functional Polymers Dev't Group Solvay Specialty Polymers. 2019.

19. Le Bideau J, Viau L, Vioux A. Ionogels, ionic liquid based hybrid materials. *Chem Soc Rev*. 2011;40(2):907-925. doi:10.1039/c0cs00059k

20. Radice S, Oldani C, Merlo L, Rocchia M. Aquivion® PerfluoroSulfonic Acid ionomer membranes: A micro-Raman spectroscopic study of ageing. *Polym Degrad Stab*. 2013;98(6):1138-1143. doi:10.1016/j.polymdegradstab.2013.03.015

21. Alberti G, Di Vona ML, Narducci R. New results on the visco-elastic behaviour of ionomer membranes and relations between T-RH plots and proton conductivity decay of Nafion ® 117 in the range 50-140 °c. *Int J Hydrogen Energy*. 2012;37(7):6302-6307. doi:10.1016/j.ijhydene.2011.07.134

22. Data RUSA. United States Patent (19). 1996;(19).

23. Sommazzi A, Garbassi F. Olefin-carbon monoxide copolymers. *Prog Polym Sci*. 1997;22(8):1547-1605. doi:10.1016/S0079-6700(97)00009-9

24. Rogoff KS. Chapter 1: Introduction and Overview. *Curse Cash*. 2017:1-12. doi:10.1515/9781400883219-002

25. AKRO-PLASTIC. *AKROTEK® PK-HM Natural (7536)*.; 2022.

26. Shkrabo DM, Zhizhin GN, Kuzik LA, Garbuzova IA. Ethylene - carbon monoxide copolymer ('Carilon') vibrational spectra and study of nanometer films on gold covered substrate. *Vib Spectrosc*. 1998;17(2):155-162. doi:10.1016/S0924-2031(98)00023-X

27. Melton GH, Peters EN, Arisman RK. *Engineering Thermoplastics*. Elsevier; 2011. doi:10.1016/B978-1-4377-3514-7.10002-9

28. Zehetmaier PC, Vagin SI, Rieger B. Functionalization of aliphatic polyketones. *MRS Bull*. 2013;38(3):239-244. doi:10.1557/mrs.2013.49

29. Sang S, Zhang J, Wu Q, Liao Y. Influences of Bentonite on conductivity of composite solid alkaline polymer electrolyte PVA-Bentonite-KOH-H2O. *Electrochim Acta*. 2007;52(25):7315-7321. doi:10.1016/j.electacta.2007.06.004

30. Benetollo F, Bertani R, Bombieri G, Toniolo L. Synthesis, characterization and X-ray structure of [Pd(dppp)(H2O)(TsO)][TsO] (dppp = 1,3-bis(diphenylphosphino)propane; TsO = p-CH3C6H4SO3), a catalytic species in COC2H4 copolymerization. *Inorganica Chim Acta*. 1995;233(1-2):5-9. doi:10.1016/0020-1693(95)04505-4

31. Nozaki K, Ito S. *Alkene/CO Copolymerization*. Vol 3. Elsevier B.V.; 2012. doi:10.1016/B978-0-444-53349-4.00086-8

32. Nawn G, Vezzù K, Cavinato G, et al. Opening Doors to Future Electrochemical Energy Devices: The Anion-Conducting Polyketone Polyelectrolytes. *Adv Funct Mater*. 2018;28(29):1-10. doi:10.1002/adfm.201706522

33. Ataollahi N, Vezzù K, Nawn G, et al. A Polyketone-based Anion Exchange Membrane for Electrochemical Applications: Synthesis and Characterization. *Electrochim Acta*. 2017;226:148-157. doi:10.1016/j.electacta.2016.12.150

34. Jiang Z, Sanganeria S, Sen A. Polymers incorporating backbone thiophene, furan, and alcohol functionalities formed through chemical modifications of alternating olefin–carbon monoxide copolymers. *J Polym Sci Part A Polym Chem*. 1994;32(5):841-847. doi:10.1002/pola.1994.080320505

35. Loudon M. *Chimica Organica*.; 2010.

36. Clayden J, Greeves N, Warren S. *Organic Chemistry*. Second edi. (Press O university, ed.).

37. Jung YS, Canlier A, Hwang TS. An efficient and facile method of grafting Allyl groups to chemically resistant polyketone membranes. *Polymer (Guildf)*. 2018;141:102-108. doi:10.1016/j.polymer.2018.03.007

38. Ma H, Huang J. Tactic polystyrene and styrene copolymers. *Stereoselective Polym with Single-Site Catal*. 2007:363-398. doi:10.1002/14356007.a21

39. Puype F, Samsonek J, Knoop J, Egelkraut-Holtus M, Ortlieb M. Evidence of waste electrical and electronic equipment (WEEE) relevant substances in polymeric food-contact articles sold on the European market. *Food Addit Contam - Part A Chem Anal Control Expo Risk Assess*. 2015;32(3):410-426. doi:10.1080/19440049.2015.1009499

40. Martins JN, Klohn TG, Bianchi O, Fiorio R, Freire E. Dynamic mechanical, thermal, and morphological study of ABS/textile fiber composites. *Polym Bull*. 2010;64(5):497-510. doi:10.1007/s00289-009-0200-6

41. Tsai TH, Maes AM, Vandiver MA, et al. Synthesis and structure-conductivity relationship of polystyrene-block- poly(vinyl benzyl trimethylammonium) for alkaline anion exchange membrane fuel cells. *J Polym Sci Part B Polym Phys*. 2013;51(24):1751-1760. doi:10.1002/polb.23170

42. Khomein P, Ketelaars W, Lap T, Liu G. Sulfonated aromatic polymer as a future proton exchange membrane: A review of sulfonation and crosslinking methods. *Renew Sustain Energy Rev*. 2021;137(September 2019):110471. doi:10.1016/j.rser.2020.110471

43. Golubenko D V., Van der Bruggen B, Yaroslavtsev AB. Novel anion exchange membrane with low ionic resistance based on chloromethylated/quaternized-grafted polystyrene for energy efficient electromembrane processes. *J Appl Polym Sci*. 2020;137(19):1-10. doi:10.1002/app.48656

44. Vinodh R, Ilakkiya A, Elamathi S, Sangeetha D. A novel anion exchange membrane from polystyrene (ethylene butylene) polystyrene: Synthesis and characterization. *Mater Sci Eng B Solid-State Mater Adv Technol*. 2010;167(1):43-50. doi:10.1016/j.mseb.2010.01.025

45. Zeng QH, Liu QL, Broadwell I, Zhu AM, Xiong Y, Tu XP. Anion exchange membranes based on quaternized polystyrene-block-poly(ethylene-ran-butylene)-block-polystyrene for direct methanol alkaline fuel cells. *J Memb Sci*. 2010;349(1-2):237-243. doi:10.1016/j.memsci.2009.11.051

# Chapter 2: Aquivion®-based anion exchange polymer

Polyfluorinated polymers are largely used as proton exchange membrane thanks to their very high conductivity, chemical and electrochemical stability. Despite their elevated cost, these polymers find application in commercial low temperature fuel cell and water Electrolyzer[1–3]. The main polyfluorinated PEM commercially available are Nafion® (Dupont), 3M ionomer (3M), Aquivion® (Solvay), which differ by the length of the protogenic side chain.

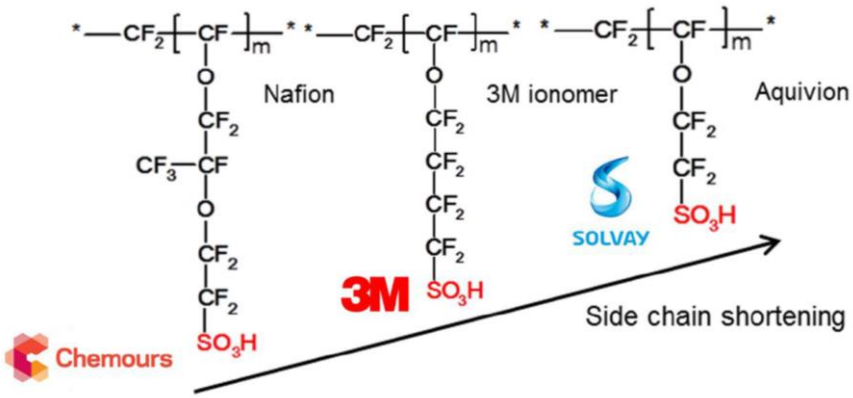


*Figure 2-1 - Comparison of the structures of Nafion®, 3M Ionomer®, Aquivion®* [4]

The side chain shortening affects the mechanical properties of the material as reducing the chain length, increases the glass transition temperature of the polymers as shown in figure 2. This implies that Aquivion® membranes show better mechanical properties, e.g. lower gas permeability, than the other at the same working conditions.

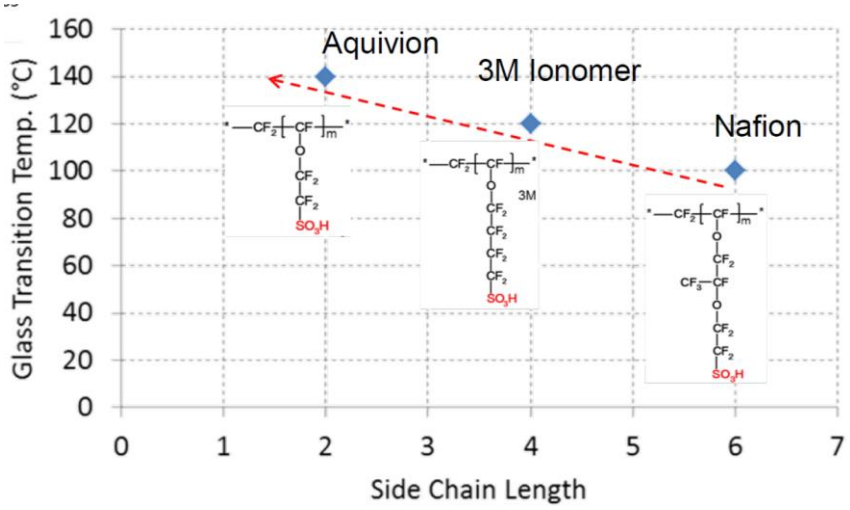


*Figure 2-2 - Glass transitions temperature of Nafion®, 3M Ionomer®, Aquivion® in function of side chain length* [4]

In this chapter, I report the conversion of commercial proton exchange Aquivion® membranes into N-(quaternary ammonium)alkylsulfonamide anion exchange membrane.

## 2.1 – Synthesis of sulfonamide anion exchange membranes

### 2.1.1 – Activation

Before the modification, the protonic membranes must be regenerated in order to active all the available sites[5,6]. The membranes were soaked sequentially in distilled water at 80°C for 1 h, 3% $H_2O_2$ at 80°C 1 h, distilled water at 80°C for 1 h, 1 M $H_2SO_4$ at 80°C for 1 h. After that, the membranes were washed in distilled water at 80°C at least three times until the pH value of washing solution become neutral. This fact is import to guarantee that diamine reacts only with active sites.

### 2.1.2 - Synthesis overview

This process is based on the conversion of side-chain sulfonic acid group into N-(quaternary ammonium)alkylsulfonamide. The anion Aquivion® membranes were prepared by reaction with primary-ternary diamine and the modification was carried out with the following steps: sulfonamide bond formation (step_1a and 1b), methylation (step_2) and ionic exchange (step_3).

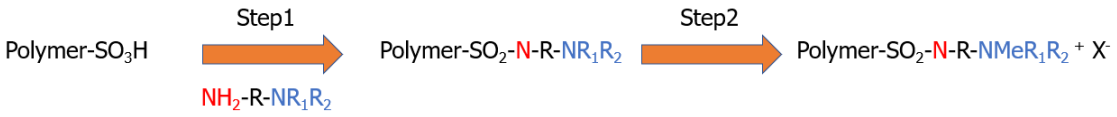


*Figure 2-3- General scheme of Aquivion® modification*

## Step_1a

The step_1a is the acid-basic reaction between the sulfonic acid group of polyfluorinated polymer and the diamines forming their salt. For this specific work, E98S12 and E98S05 Aquivion® membranes and the N,N,2,2-tetramethyl-1,3-propandiamine are used. In this particular diamine, the primary ammine is more by three order of magnitude basic than the ternary due to 6-member ring configuration [7]. Consequently, the nitrogen of primary amine is used for the sulfonamide bond formation while the ternary amine can be used for quaternary ammonium group conversion[8].

The pristine membranes were immersed in distilled water for 1 hour at room temperature, then 500% excess of N,N,2,2-tetramethyl-1,3-propandiamine is added and let to react for 1 day under stirring. After that, the membranes were washed three times with ethanol and then dried in vacuum at 50°C for 1 hour.

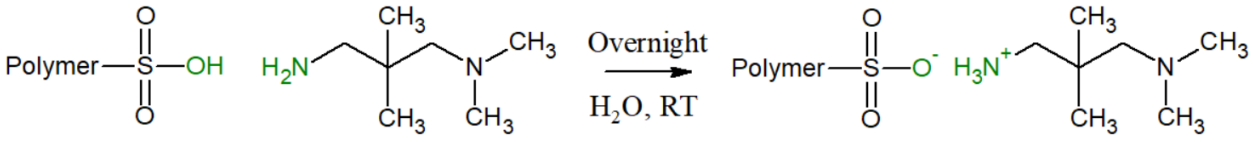


*Figure 2-4 -Scheme of step_1a*

## Step_1b

The step_1b is the dehydration of the new salt in favor to the sulfonamide covalent bond generation. It consists in a heat process up to 250°C for 1 hour according the TGA and DSC results (see fig. 9-10). For this process a slowly increase of the temperature is necessary to prevent bubbles or bends in the membranes.

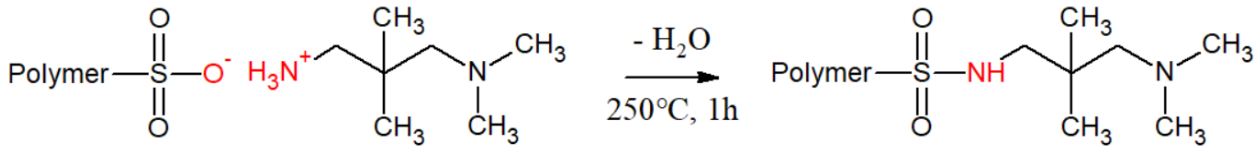


*Figure 2-5 - Scheme of step_1b*

## Step_2

In step_2, the ternary nitrogen of N-alkilsulfonamide was methylated giving the quaternary ammonium group and a charged polymer. The membranes were soaked in acetonitrile for 1 hour and then ten-times excess of iodomethane is added and let react for 14 hours at 40°C in reflux condition. After that, membranes were washed with acetonitrile and water, dried in vacuum at 80°C for 1 hour. The samples were obtained in I-form and then were brought in homemade wet-box with controlled nitrogen atmosphere (see appendix A2).

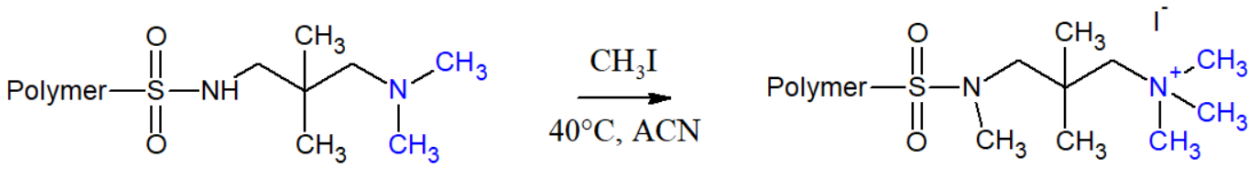


*Figure 2-6 -Scheme of step_2*

## Step_3

The step_3 is the ionic exchange to obtain the membranes with the preferred anion according to the application for example $Cl^-$ or $OH^-$. The membranes were immersed in 1 M KOH solution for 1 day and washed with distilled water until the pH value became neutral. This step was carried out in wet-box.

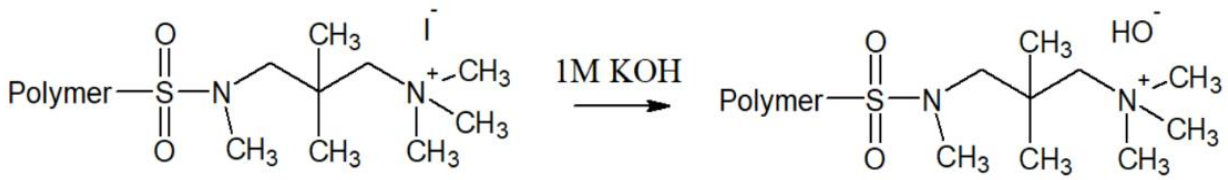


*Figure 2-7 - Scheme of step_3*

## 2.2 – Physico-chemical characterization

During the synthesis processes, the samples were characterized in order to monitor and control the modification progress and also to better understand their physico-chemical properties. The polymer structure was investigated with FTIR and solid-state NMR, the thermal properties was studied with TGA and DSC. On the functionalized membranes SEM images and contact angle measurements were performed.

### 2.2.1 – Pristine Aquivion® membrane

#### Structure investigation

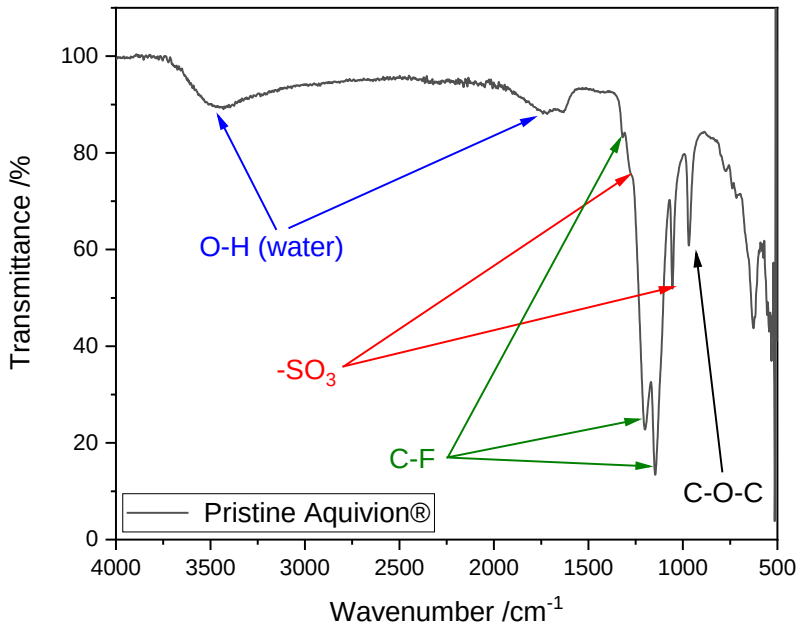


*Figure 2-8 - FTIR spectrum of pristine Aquivion®*

In Aquivion® spectrum (figure 8) the main signals are the O-H stretching, asymmetric and symmetric bending of water at 3500, 1720, 1630 $cm^{-1}$, the stretching of $CF_2$ group at 1320, 1200, 1146 $cm^{-1}$ [9,10]. It's possible to observe at 966 $cm^{-1}$ the stretching of C-O-C linking of side chain and the asymmetric and symmetric stretching of $SO_3$ group at 1278 and 1056 $cm^{-1}$ [9,10]. In particular, the last signal may shift depending on the counterion[11].

The $^{13}C$ MAS NMR spectrum allows to investigate the polymer structure and its change. In particular, the High-Power Decoupling (HPDEC) experiment allows to see the main signal of Aquivion® material at 110 ppm that is correlated to $CF_2$ portion. This signal could be used as internal standard for the next NMR spectra. The two small peaks at 210 and 10 ppm are attributed as spinning side band of $CF_2$ signal (marked with * in fig. 9).

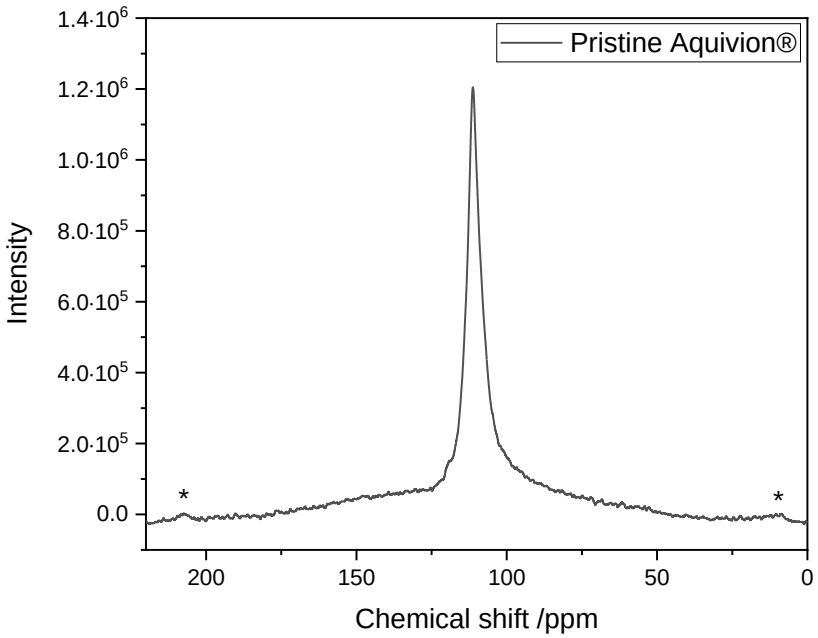


*Figure 2-9 – $^{13}C$-HPDEC NMR spectrum of Pristine Aquivion®: the spinning side band are marked with **

## Thermal properties

The TGA curve of pristine material shows a 5 % mass loss below 170°C, correlated to moisture released, and the beginning of the multi-step thermal degradation at 300°C as showed in figure 10.

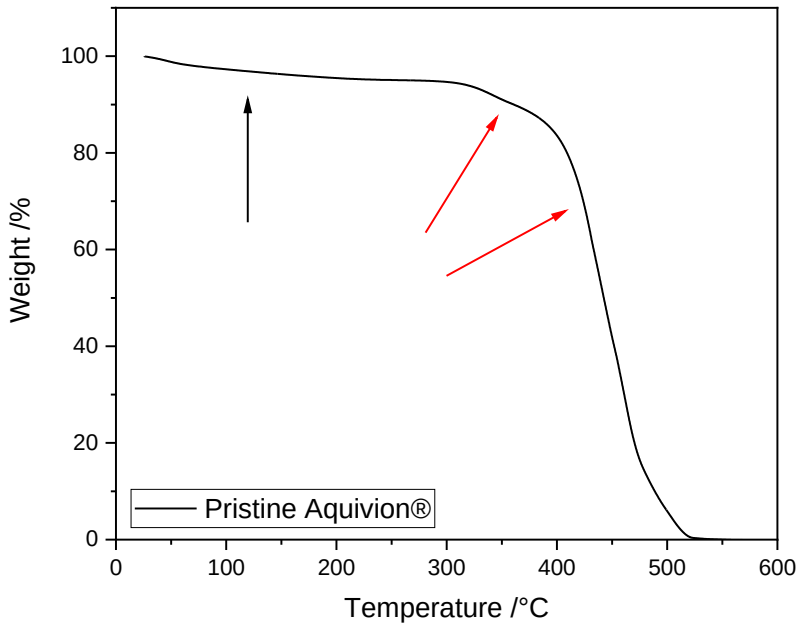


*Figure 2-10 - TGA curve of pristine Aquivion®: the first mass loss and the multi-steps degradation are highlighted with black and red arrows, respectively*

From DSC measurement, non-reversible endothermic peaks were detected at 80 and 175°C due to moisture release. In the cooling scan, a small recrystallization process was detected at 190°C. While in the second heating scan the glass transition (Tg) at 146°C followed by melting process at 190°C were detected according to Solvay data sheet[12].

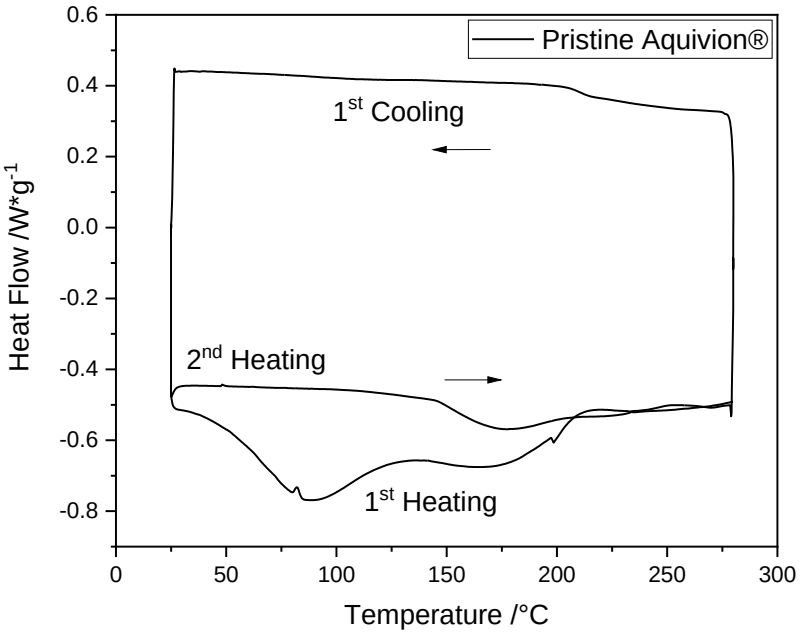


*Figure 2-11 - DSC curve of pristine Aquivion®*

### 2.2.2 – Following the synthesis

I investigated the modification progress by FTIR and solid-state NMR. In the figure 11, the IR spectra of pristine Aquivion®, N,N,2,2-tetramethyl-1,3-propandiamine and the step_3 were reported. The diamines spectrum shows the characteristic N-H stretching at 3390 and 3316 $cm^{-1}$, the C-H stretching of the methyl group at 2970 and 2860 $cm^{-1}$, of the methylene group at 2944 and 2816 $cm^{-1}$, and of the N-$CH_3$ group at 2764 $cm^{-1}$ [7,13,14]. The signals given by the C-H bending of the methyl and methylene groups were detected at 1475, 1455, 1388, 1360, 1315 $cm^{-1}$ as reported in Ref [14]. In the fingerprint zone also the stretching of C-N at 1141 $cm^{-1}$ and the wagging of N-H at 840 $cm^{-1}$ [14] can be observed. In the step_3 spectrum there are the main signals of pristine material such as $CF_2$ in 1400-1100 $cm^{-1}$ zone (see 2.2.1) and also the C-H stretching and bending of alkyl portion. The signal at 1700 $cm^{-1}$ is attributed to the partial carbonation process causing by carbon dioxide which is visible also in $^{13}$C-NMR spectra.

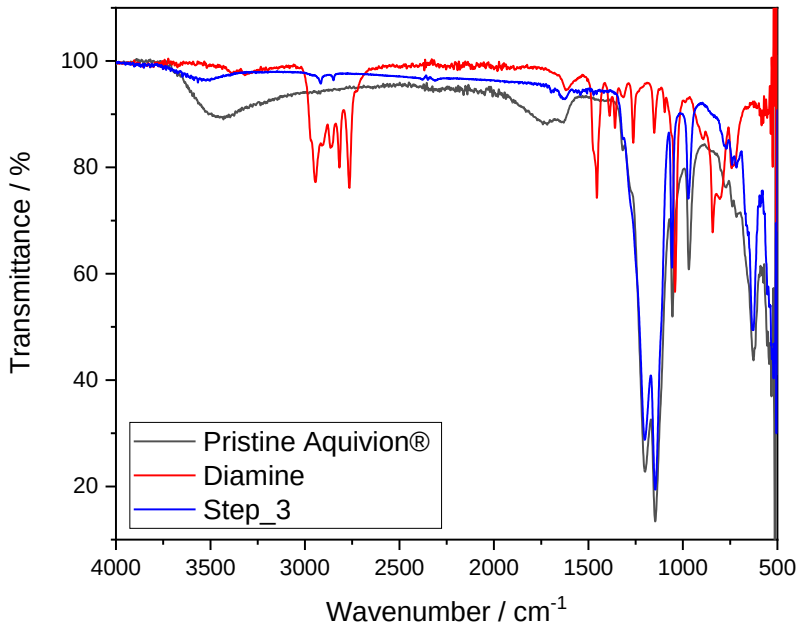


*Figure 2-12 - FTIR spectra of Pristine Aquivion, N,N,2,2-tetramethyl-1,3-propandiamine and functionalized membrane (Step_3)*

The C-H signals of alkyl portion may be used to verify the success of the modification, although they are characterized by low intensity. Luckily, the $SO_3$ stretching gives stronger signal at 1060 $cm^{-1}$ which can shift in function of the cation[11]. In this way, I correlated the signal shift to the counterion changes as happens in step_1a and step_1b.

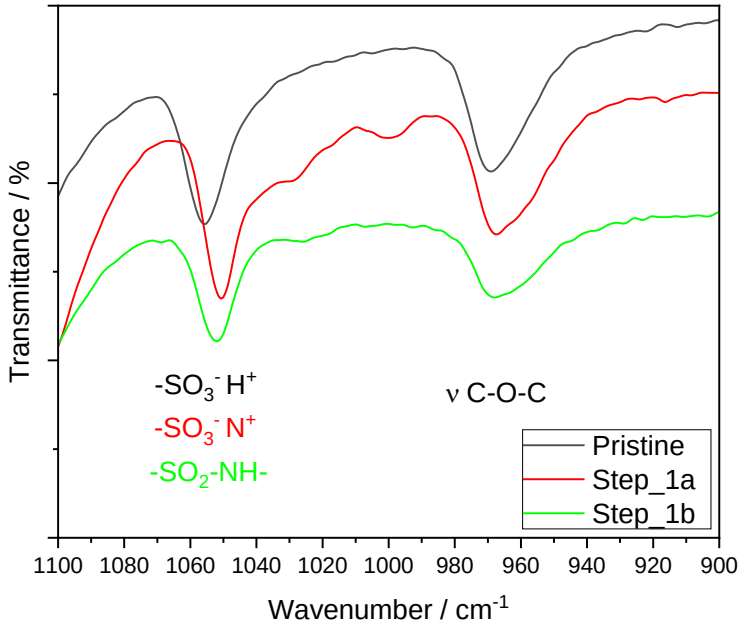


*Figure 2-13 - FTIR spectra of pristine Aquivion®, step_1a and step_1b: zoom from 1100 to 900 cm$^{-1}$*

In figure 13, details of the spectra of pristine Aquivion®, step_1a and step_1b are reported. While the signal of C-O-C stretching is constant at 968 cm$^{-1}$, the sulfonic signal at 1056 cm-1, moves to 1051 cm$^{-1}$ for step_1a and then to 1052 cm$^{-1}$ for step_1b. The first shift is correlated to salt formation, whereas the second one is due to sulfonamide bond formation according to Lee et al. [15].

In figure 14, $^{1}$H-$^{13}$C CPMAS spectra of the reaction steps are reported. In all the spectra there is $CF_2$ signal which is labeled "a" and attributed to Aquivion® backbone. The changes in intensity of this peak is due to unequal efficiency of spectral irradiation, which may be influenced by several physico-chemical properties, including sample crystallinity, polymer viscosity, etc.[16] In the 60-10 ppm zone, the step_1a shows the carbon peak of N,N,2,2-tetramethyl-1,3-propandiamine, labeled from "b" to "f", which are in agreement with the liquid state NMR of pure diamine of AIST database[9]. After step_1b, a small peak in 150 – 160 ppm range is detected and correlated to carbonyl groups originated by reactions with $CO_2$. Moreover, it's possible to notice that signals are shifted upfield confirming the sulfonamide bond formation. In 20-30 ppm zone, the presence of additional peak could be explained considering non-equivalent sites in crystalline and amorphous part of the polymer. In the further steps, the presence of new methyl group induces minor changes in the signal pattern, but only some variation in their intensity.

Actually, the complete assignation of all peak is quite difficult and to address it some additional studies for example Density Functional Theory (DFT) are needed. Consequently, at this point, I can confirm the success of step_1a and step_1b.

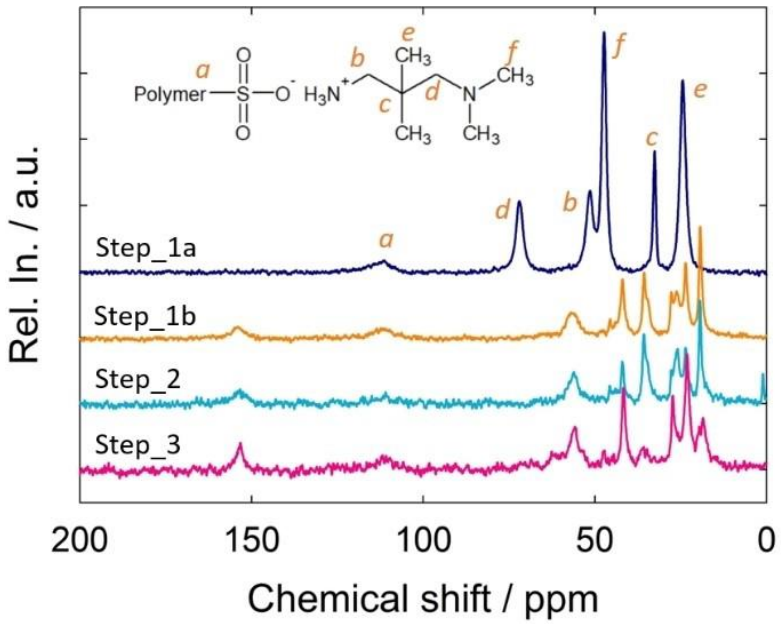


*Figure 2-14 -$^{1}H$ $^{13}C$ CPMAS spectra of all functionalization steps* [16]

The thermogravimetric curves showed an increasing of the thermal stability from 300°C for pristine material, to 350°C after step_1a and then up to 450°C with functionalized membranes (fig. 15). The step_1a curve, that simulates the synthesis heating process of step1b, shows a particular behavior in 30-250°C zone that could be divided in the following four different part (see the insert of fig.15). The part I is from 25°C to 100°C and 0.5 % mass loss is detected and attributed to the moisture. The part II is between 100°C and 130°C and it is a flat zone without losses. The part III is between 130°C and 245°C and 2% mass loss is noticed. The part IV is over 246°C, and 1% mass loss is revealed.

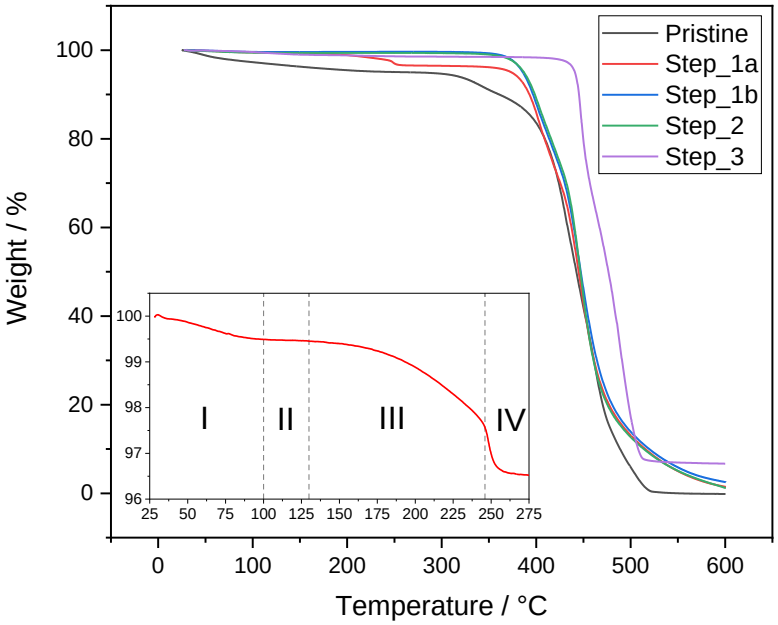


*Figure 2-15 - TGA measurements of all steps: the insertion is the zoom of step1a curve with the four zones*

Thanks to simple stoichiometric calculations, it's possible demonstrate the loss of part III and IV are due to water and diamine, respectively. In step_1a product, the water content is about 2% wt and the diamine content is about 11,8 % wt according to the reaction stoichiometry.

$$\%\ \text{water} = \frac{\text{MM water}\ (\frac{\text{g}}{mol})}{\text{MM step 1a}\ (\frac{\text{g}}{mol})} * 100 = \frac{18\ (\frac{\text{g}}{mol})}{1108\ (\frac{\text{g}}{mol})} * 100 = 1.6\ \% \sim 2\ \%$$

$$\%\ \text{diamine} = \frac{\text{MM diamine}\ (\frac{\text{g}}{mol})}{\text{MM step 1a}\ (\frac{\text{g}}{mol})}) * 100 = \frac{130.26\ (\frac{\text{g}}{mol})}{1108\ (\frac{\text{g}}{mol})} * 100 = 11.76\ \%$$

The water content is in good agreement with part III loss, while the 1% mass loss of diamine reflects a functionalization yield of 88.2%. This value is in excellent agreement with the IEC result (91.4%). To support this data, I performed the TGA-FTIR analysis on step_1a.

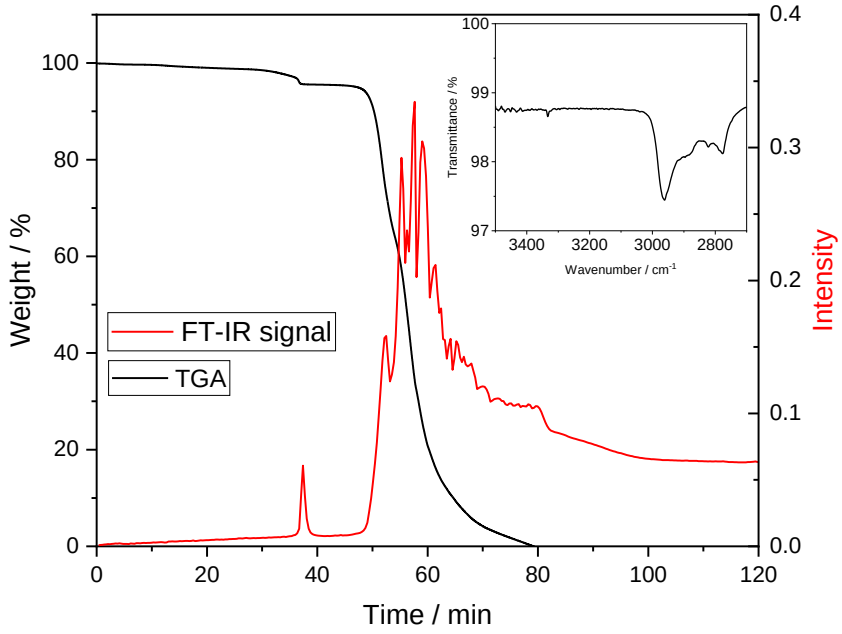


*Figure 2-16- TGA-FTIR signals in function of the time: TGA curve of step_1a (black), the intensity of FTIR signal (red) and the total IR spectrum collected (insertion) are showed*

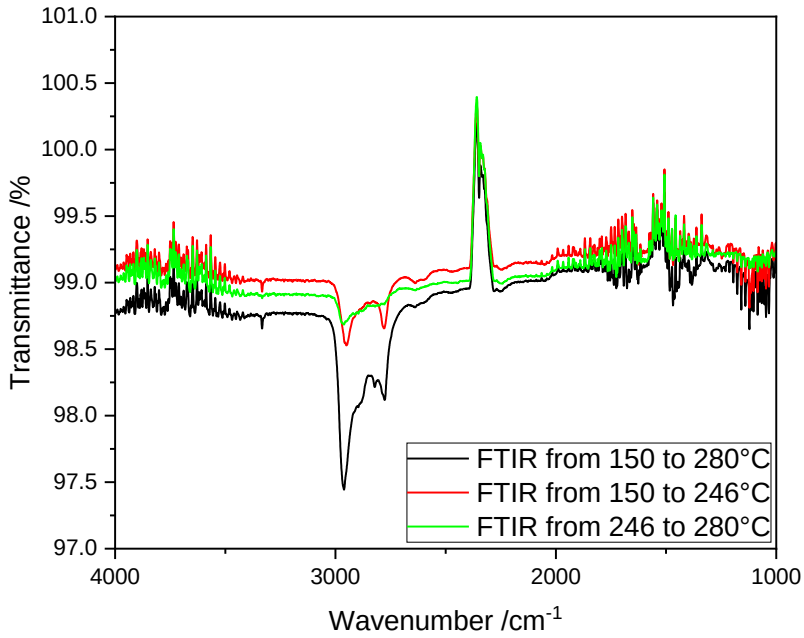


*Figure 2-17 – The FTIR spectra collected in part III (red), part IV (green) and the sum of part III and IV (black)*

In figure 16, the TGA curve and IR signal were reported in function of time. It's possible observe an intense signal at time = 37 minutes corresponding to 246°C TGA stair. To better understand, the IR collected spectra in 150-280°C (part III+IV), 150-246°C (part III) and 246-280°C (part IV) zones were displayed in figure 16. The main signals are C-H stretching of diamine portion in 3000-2800 $cm^{-1}$ zone and the O-H stretching of water at 3300 $cm^{-1}$. In particular, this last signal is only present in 150-246°C (part III) and 150-280°C collected spectra, confirming the calculation and that almost water is formed before 246°C.

In addition, I studied the sulfonamide bond formation by DSC, during step1b measurement. According to TGA analysis it's possible detect two non-reversible endotherms at 50°C and 246°C corresponding to the loss in region I and IV of TGA curve.

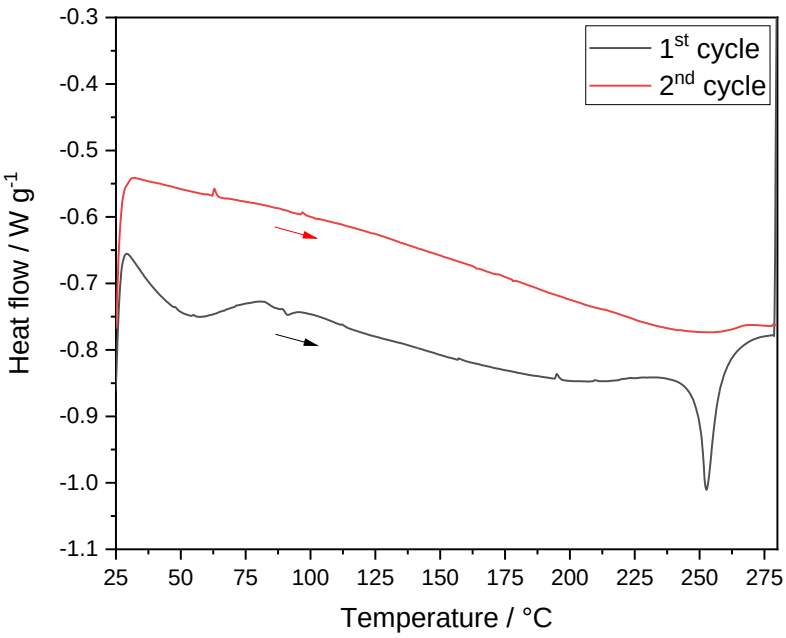


*Figure 2-18 - DSC curve of step_1a: first heating scan (black) and second heating scan (red)*

### 2.2.3 – Functionalized membranes

I investigated the microstructure of functionalized membranes through SEM cross-section and surface images. The cross-sectional images showed the present of some roundish bumps of microstructure which could be attributed to polymer channels. The white lines present in cross-

sectional are caused by the samples preparation which do not depend on the membrane structure. For the surface image, it's possible to notice the same features found in cross-section ones.

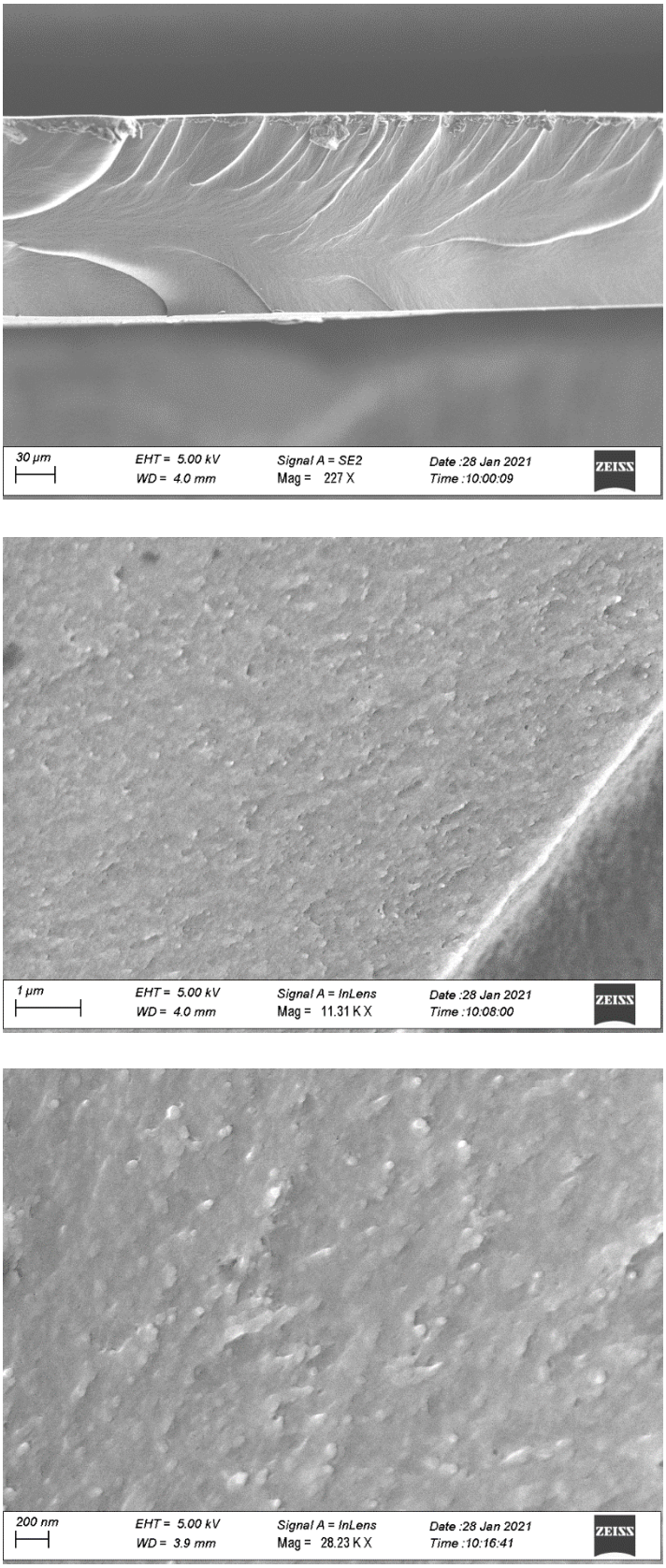


*Figure 2-19 -SEM images of Functionalized Aquivion®: Cross-sectional images (top and middle) and surface image (down)*

Finally, I checked the hydrophilicity level of the membranes surface by using contact angle measurements. Figure 19 reports the frames of pristine and functionalized Aquivion®: the left column represented the beginning situation; the central column gave the instant when the drop touched the surface and the right column reported the situation several second later. Here, FAA-3-50 (Fumatech) membrane is reported as reference material.

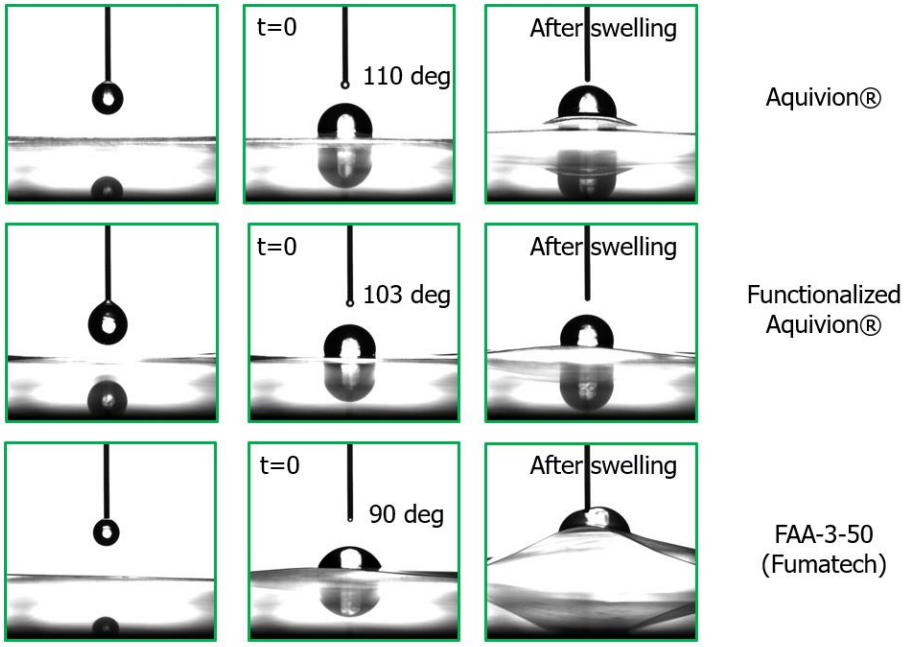


*Figure 2-20 - Contact angle images before and after depositing the drop (left and right column) and "just touched" moment (central column)*

I determined the contact angle values as the angle between the tangent lines of the horizon and the profile of the drop, by using ImaJ software for the measurement. In t=0 moment, the contact angle values were 110, 103 and 90 deg for Aquivion, functionalized Aquivion and FAA-3-50, respectively. At "after swelling" time the changes of polymer swelling, and membranes folding were visible. All samples demonstrate a behavior halfway between hydrophilic and hydrophobic. Thanks to the comparison, it's possible to say that there is no significant change after functionalization for polyfluorinated polymer and these values are in agreement with the literature[17]. The lower value of Fumatech membrane is correlated to the higher hydrophilicity of Poly(p-Phenylene-Oxide) matrix, likely due to the presence of oxygen in backbone.

## 2.3 – Specific characterization

On the pristine and functionalized Aquivion® membranes, I determined the ion exchange capacity (IEC) and ionic conductivity.

For pristine Aquivion® I used acid-basic back-titration, while for the functionalized polymer I applied the Mohr method[15]. The values of IEC were 0.86 meq*$g^{-1}$ for the protonic system and 0.77 meq*$g^{-1}$ for the alkaline version. From these values, I can determinate a global modification yields about 91.4%.

For conductivity measurements, the pristine Aquivion was activated before testing (see 2.2.1) and the anion membranes were in I-form (Step_2) and OH-form (Step_3). In this case, FAA-3-50 membrane (Fumatech) was used as the reference material. The commercial membrane was activated according to the literature[15]. Figure 20 shows the conductivity value in function of the relative humidity at 80°C.

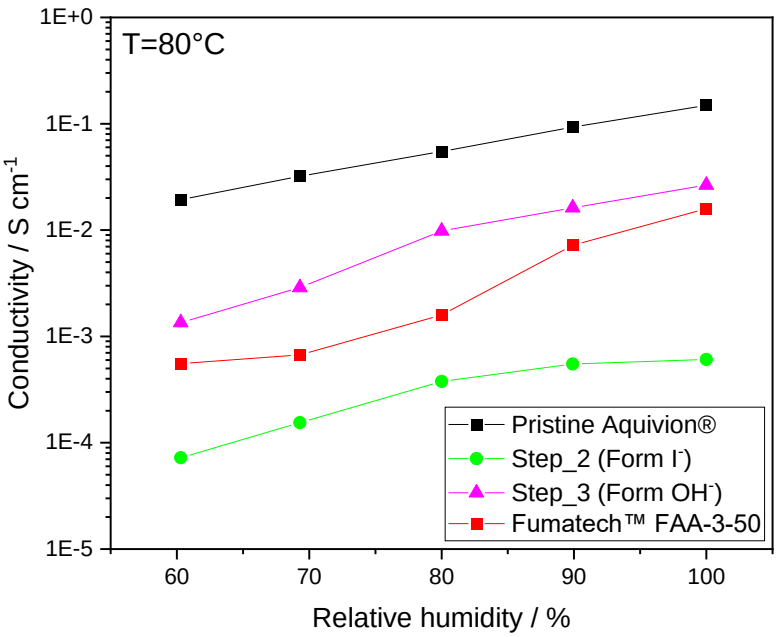


*Figure 2-21 - ionic conductivity in function of relative humidity a 80°C*

At 80°C and 100% RH, the proton exchange Aquivion® achieved 160 mS*$cm^{-1}$ while I-form and OH-form showed 0.6 and 26 mS*$cm^{-1}$, respectively. The FAA-3-50 reference showed about 16 mS*$cm^{-1}$

in the same measurement conditions. As expected both anionic membranes have a lower ionic conductivity that pristine material, however the OH-form showed a better behavior than commercial reference.

## 2.3 – Chemical and electrochemical stability tests

The durability of alkaline system is one of the main goals for AEMFC and AEMEL technologies spread[18]. In this part, I reported the results of accelerating ageing treatments on the functionalized membranes.

In order to study their chemical and electrochemical stability, I used both *ex-situ* and *in-situ* methods[19,20]. For *ex-situ* test the membranes were soaked in KOH solution by varying concentration, temperature and time, while the *in-situ* test membranes were used as separator in water electrolyzer.

### 2.3.1 – Ex-situ tests

The membranes were immersed and stored in KOH solution at constant temperature for different times. To explore their durability, I chose the treatment conditions considering non- and operating electrolyzer and the main degradation mechanism of AEM[21]. I supposed that electrolyzer works discontinuously and that in alkaline exchange membrane water electrolyzer the membrane is always soaked in feed solution. The typically working temperature is about 80°C [22] , indeed I could suppose that the "turn-off" temperature is about the room temperature. Taking into account the degradation processes of AEM, i.e. Hoffman degradation for amines[21], and the organic reaction which involve $OH^-$ anions, i.e. saponification, it is possible to hypothesize a first kinetic order. This means than increasing the concentration of $OH^-$, products are more favorite[23,24]. Evaluating these considerations, I performed *ex-situ* test at room temperature and in temperature using 1M, 3M, 6M KOH solutions.

### Room temperature

For this case, I soaked the membranes in 6M KOH solution at room temperature approximately for 70 days. These conditions are different to those of electrolyzer working in temperature, however the very strong excess of $OH^-$ (over 1200 times than active sites), combined to the long treatment time, may simulate the chemical stress. To point out the ageing effects, I performed impedance measurement after 23, 38, 68 days and, when the treatment was over, I did SEM and FTIR on the aged membrane.

The figure 22 shows the comparison of the trend ionic conductivity at 80°C of the membrane as prepared and after 23, 38 and 68 days.

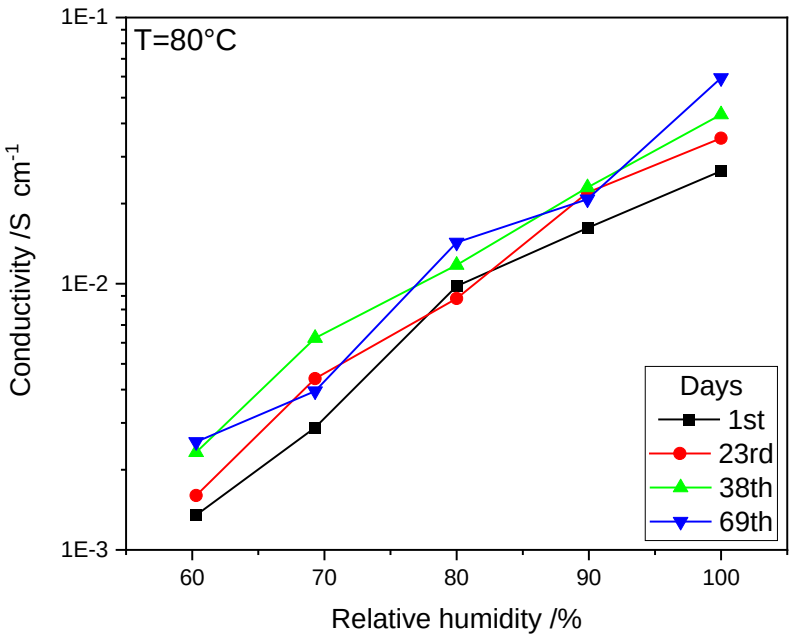


*Figure 2-22- Comparison of ionic conductivity values as prepared and at 23rd, 38th, 69th days*

The as-prepared modified Aquivion® presented an ionic conductivity of 26 mS $cm^{-1}$, while the aged membrane achieved 59 mS $cm^{-1}$ at 80°C and 100% relative humidity. It's possible to observe a monotonous increase during the ageing treatment that may be caused by some microstructure changes. To validate this hypothesis, I did SEM images on the aged membranes. In figure 23, it' possible to observe a more open polymer microstructure after ageing, which could reduce the tortuosity of the system and may justify the conductivity behavior.

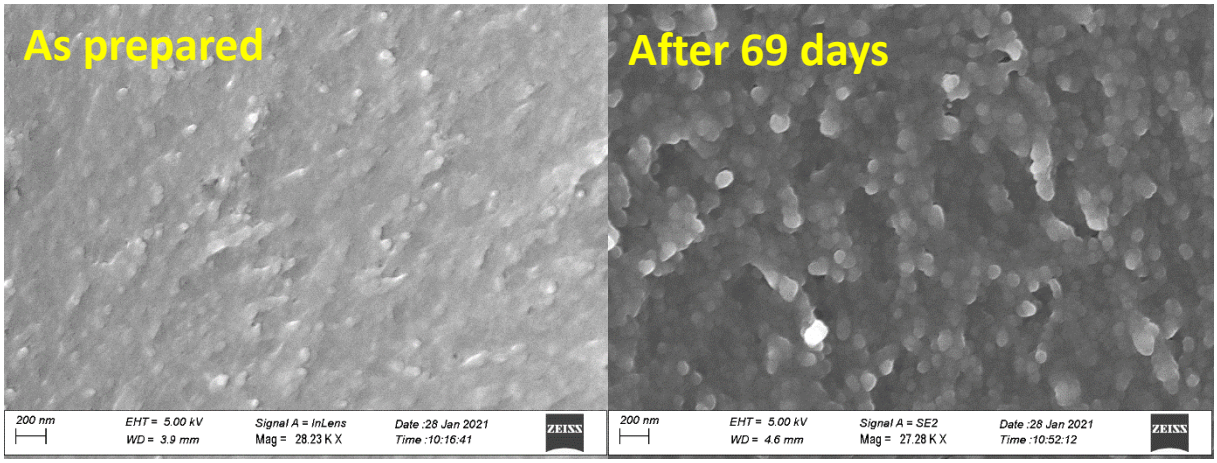


*Figure 2-23 - SEM images of modified Aquivion®: as prepared (top) and aged after 69 days (down)*

## In temperature

For these tests, I worked in similar electrolyzer working condition in order to simulate only the chemical stress effect on the membrane. According to the experimental part (ES11), I applied the light (60°C 1M), medium (80°C 1M) and heavy (80°C 3M) protocols for two and six days. I named the sample according to the following example: if the membrane was aged by heavy treatment for 144 hours, the sample was called "144H". The aged membranes were characterized by impedance spectroscopy, SEM images and IEC.

The figure 24 displays the values of ionic conductivity of aged modified Aquivion® for 50 and 120 µm of thickness.

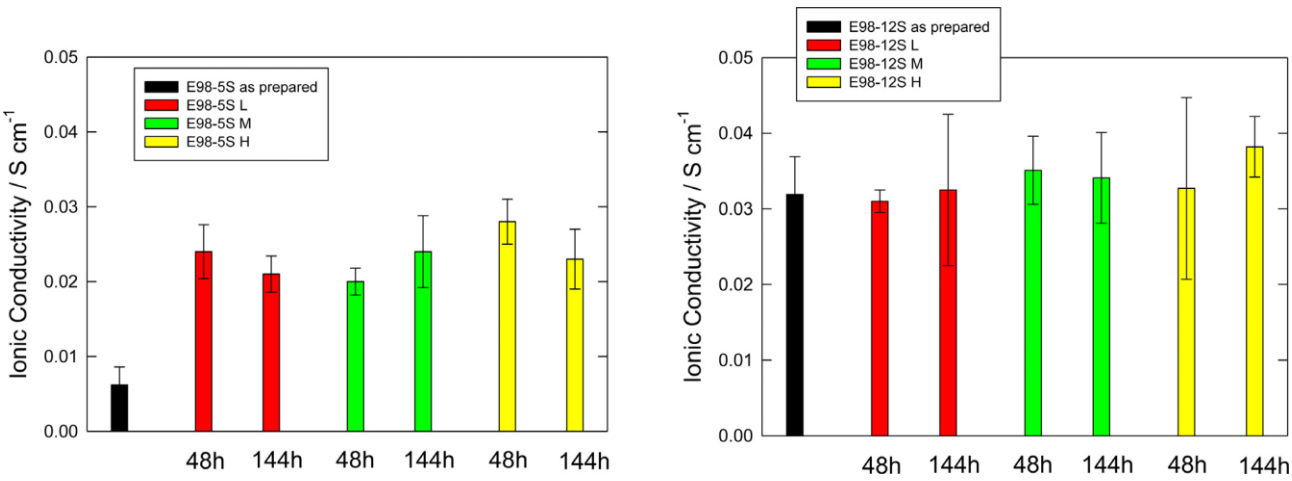


*Figure 2-24 – Ionic conductivity of aged membrane with 50 µm (left) and 120 µm (right) of thichness*

For the 50 µm membrane, the treatments increased the ionic conductivity by a factor of 4, obtaining values between 20-30 mS $cm^{-1}$. Actually, this behavior is not completely clear and it could be due to insufficient ion exchange. The 120 µm membrane showed similar value of conductivity ranging from 30 to 40 mS $cm^{-1}$. Within the experimental error, I can say that the effects of ageing of the conductivity are negligible. The experimental values are in good agreement with those reported by Lee et al. on their Aquivion®-based AEM[15].

Considering other polymer matrices, similar ionic conductivity was reported for PBI and ABPBI-based membranes with 1,4-diazabicyclo (2.2.2) octane as active group[25]. Indeed, our values are lower than those reported by Varcoe for his hydrocarbon-based radiation-grafted membranes[26].

In the tables below the percentage losses of weight and IEC are reported after treatments.

| | 48 hours | | | | |
|---|---|---|---|---|---|
| Ageing treatment | Thickness (µm) | Weight loss (%) | ΔW/time ($g*h^{-1}$) | IEC loss (%) | ΔIEC/time ($meq*h^{-1}$) |
| Light (L) | 50 | 0.17 ±0.13 | $1.23 \times 10^{-5}$ | 15.16 | $2.5 \times 10^{-3}$ |
| | 120 | 0.70 ±0.16 | $1.90 \times 10^{-5}$ | 26.38 | $4.3 \times 10^{-3}$ |
| Medium (M) | 50 | 0.14 ±0.14 | $1.04 \times 10^{-6}$ | 20.51 | $3.3 \times 10^{-3}$ |
| | 120 | 0.73 ±0.16 | $1.83 \times 10^{-5}$ | 30.03 | $4.9 \times 10^{-3}$ |
| Heavy (H) | 50 | 0.97 ±0.13 | $1.25 \times 10^{-6}$ | 22.16 | $3.6 \times 10^{-3}$ |
| | 120 | 0.85 ±0.15 | $1.95 \times 10^{-5}$ | 32.63 | $5.3 \times 10^{-3}$ |

*Table 1 - Weight and IEC losses after ex-situ ageing for 48 hours*

| | 144 hours | | | | |
|---|---|---|---|---|---|
| Ageing treatment | Thickness (µm) | Weight loss (%) | ΔW/time ($g*h^{-1}$) | IEC loss (%) | ΔIEC/time ($meq*h^{-1}$) |
| Light (L) | 50 | 0.84 ±0.12 | 1.08 × 10 −6 | 19.76 | 1.1 × 10 −3 |
| | 120 | 0.76 ±0.15 | 6.25 × 10 −6 | 14.53 | 7.9 × 10 −4 |
| Medium (M) | 50 | 1.47 ±0.18 | 3.83 × 10 −6 | 30.27 | 1.6 × 10 −3 |
| | 120 | 0.71 ±0.16 | 6.83 × 10 −6 | 27.16 | 1.5 × 10 −3 |
| Heavy (H) | 50 | 0.35 ±0.14 | 3.33 × 10 −6 | 31.75 | 1.7 × 10 −3 |
| | 120 | 0.73 ±0.14 | 7.52 × 10 −6 | 29.30 | 1.6 × 10 −3 |

*Table 2 - Weight and IEC losses after ex-situ ageing for 144 hours*

For all samples the weight losses were less than 1%, with the only exception of the 50 µm membrane aged under medium condition for 144 hours. The weight loss rate was always below $2x10^{-5}$ $g*h^{-1}$, irrespective of the ageing conditions and I observed the IEC losses vary from 15 to 30% depending the ageing treatment. These variations might be attributed to the detachment of diamine. I report the calculations considering the diamine as the lost part (158,3 $g*mol^{-1}$), 0.77 $meq*g^{-1}$ as starting IEC and 0.1 g as sample weight.

E.g. the 120 µm- 144H aged-membrane showed a 29.30% IEC loss that means an IEC variation of 0.23 $meq*g^{-1}$.

$$\Delta IEC\ \left(\frac{mmol}{g}\right) = \frac{\Delta n\ (mmol)}{mass\ (g)} \rightarrow \Delta n(mmol) = \Delta IEC\ \left(\frac{mmol}{g}\right) * mass\ (g)$$

$$= 0.23\ \left(\frac{mmol}{g}\right) * 0.1\ (g) = 0.023\ mmol$$

The IEC variation corresponds to 0.023 mmol. If I correlated these mols to the diamine loss, I obtain the following mass difference and percentage variation.

$$\Delta\ mass = \Delta n\ (mol) * MWdiamine\ \left(\frac{g}{mol}\right) = 0.023 * 10^{-3}\ (mol) * 158.3\ \left(\frac{g}{mol}\right) = 0.0036\ g$$

$$\%\ \Delta\ mass = \frac{0.0036\ (g)}{0.1000\ (g)} * 100 = 3.6\ \%$$

Those theorical mass loss values are higher than the experimental ones. Consequently, given the low weight losses and considering the calculation, I can't even exclude that the titration method

used is inadequate to determine the IEC value in these membranes. Although relevant, these losses are not unusual in these membranes. In fact, similar losses were reported for other polymers such as hydrocarbon-based[26] and PBI-based membranes[25].

In figure 25 and 26 the cross-section and surface SEM images of the 120 µ modified Aquivion® are showed. From the comparison between the samples as prepared and after 144 h treatment, there was no significant variation of the morphology and the microstructure of the membrane, in agreement with the physico-chemical results of weight loss and ionic conductivity.

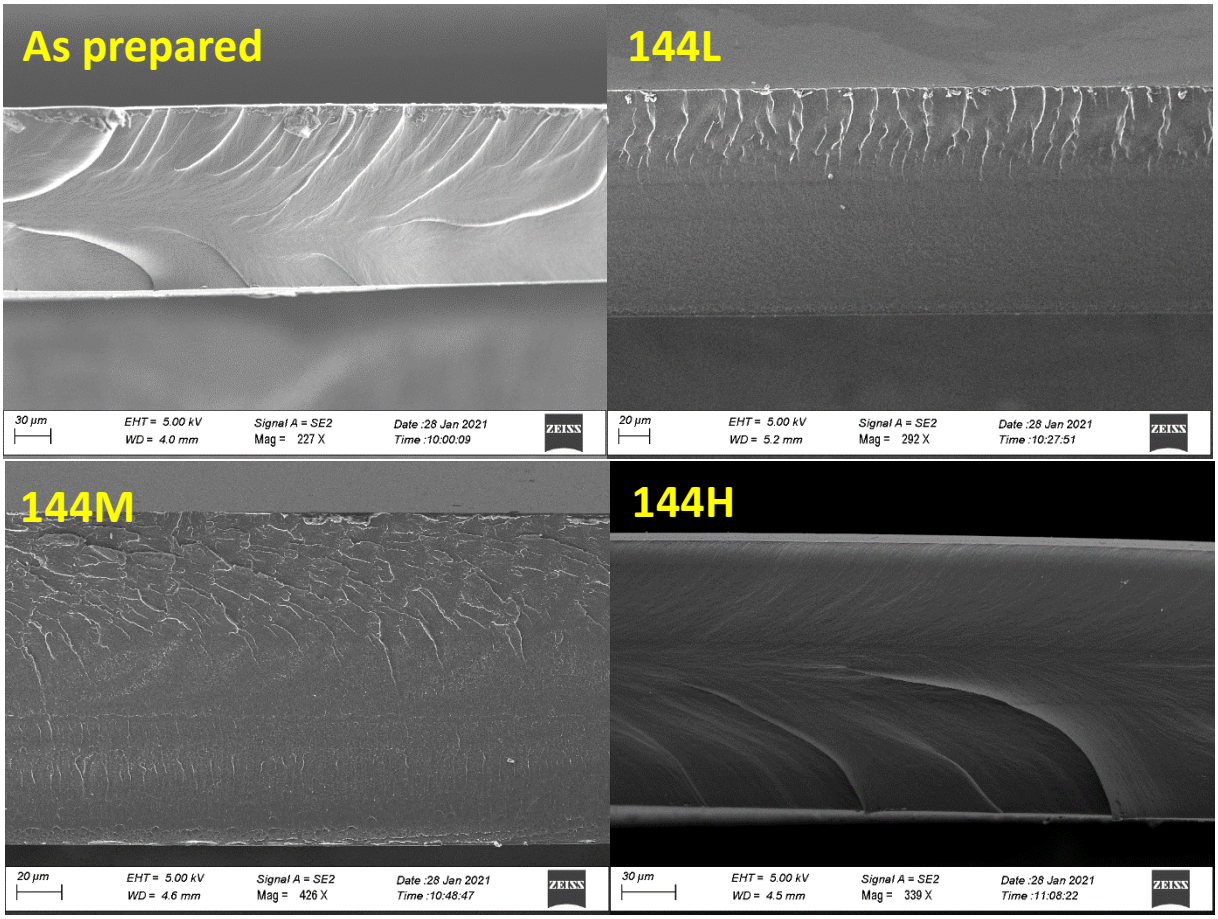


*Figure 2-25 - Cross-section SEM images of modified Aquivion® before and after ageing test*

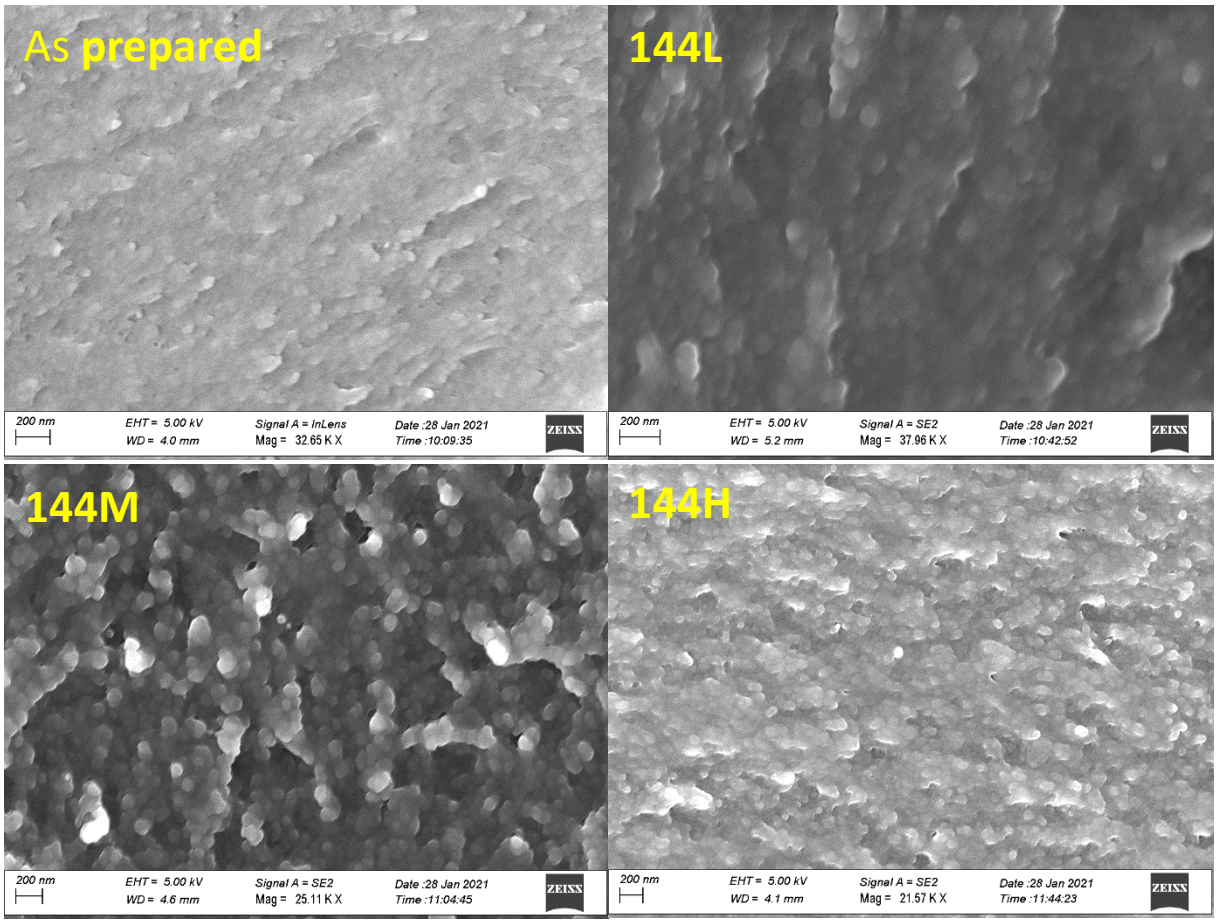


*Figure 2-26 - Surface SEM images of modified Aquivion® before and after ageing test*

Finally, I performed FTIR and elementary analysis on the 144H aged membrane. The comparison reported in figure 27 shows no changes after ageing, the peak assignment is reported in paragraph 2.2.2. The CHNS analysis gives the expected values in agreement with the other physico-chemical results of weight loss and ionic conductivity.

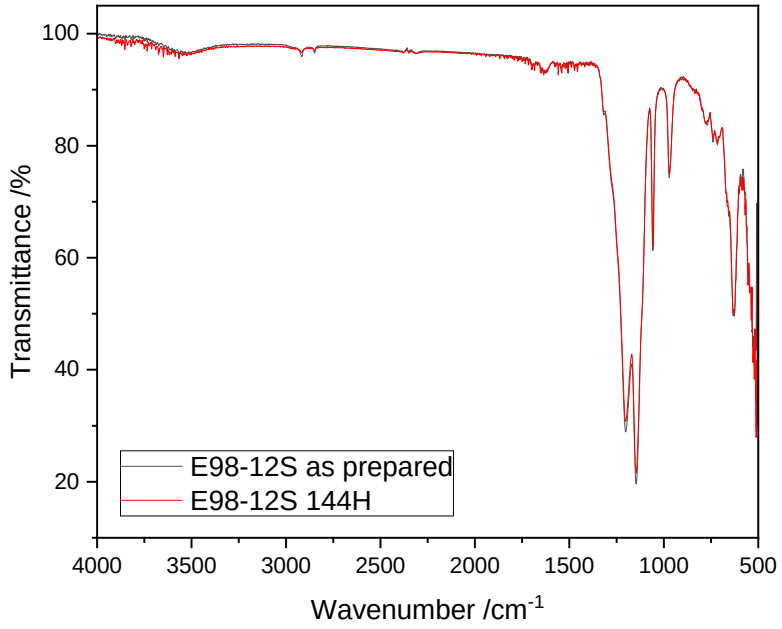


*Figure 2-27 - IR spectra of modified membranes before and after 144H treatment*

| | C (%) | H (%) | N (%) | S (%) | O (%) | F (%) |
|---|---|---|---|---|---|---|
| Calculated | 28.53 | 2.04 | 2.47 | 2.82 | 5.63 | 58.51 |
| As prepared | 27.83 | 1.98 | 2.79 | 2.97 | 5.31 | 59.12 |
| After ageing | 27.56 | 1.94 | 2.85 | 2.93 | 5.40 | 59.32 |

*Table 3 - Value of CHNS analysis of modified Aquivion® before and after 144H treatment*

### 2.3.2 *In-situ*: electrolyzer application

For the *in-situ* tests, I used functionalized membranes in an electrolyzer at fixed potential of 2V, using nickel foam as electrodes and different KOH solution as supply feed. As for *ex-situ* experiments, I tested the membranes at 80°C with 1M KOH (medium) and 3M KOH (heavy). To investigate the ageing effects, I recorded resistance variation of the system and the current overtime. In adding, polarization curves were performed sweeping the potential from 2 to 1.2 V (see experimental part ES11). As reference material, I tested the AEMION membrane (IONOMER) in the same conditions.

## Polarization curve

In figure 28 and 29 the polarization curves for medium conditions were reported. The results showed that during the first cycle the membranes had the same behavior while, during the last cycle, the 50 µm modified Aquivion® was better. Both Aquivion® membranes held constant the maximum current values after ageing.

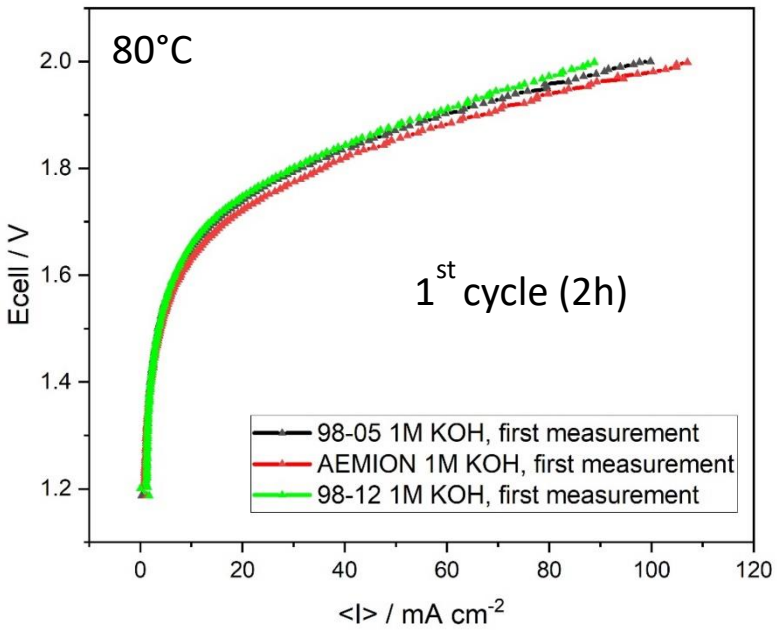


*Figure 2-28 - Polarization curves: 1st cycle of medium conditions*

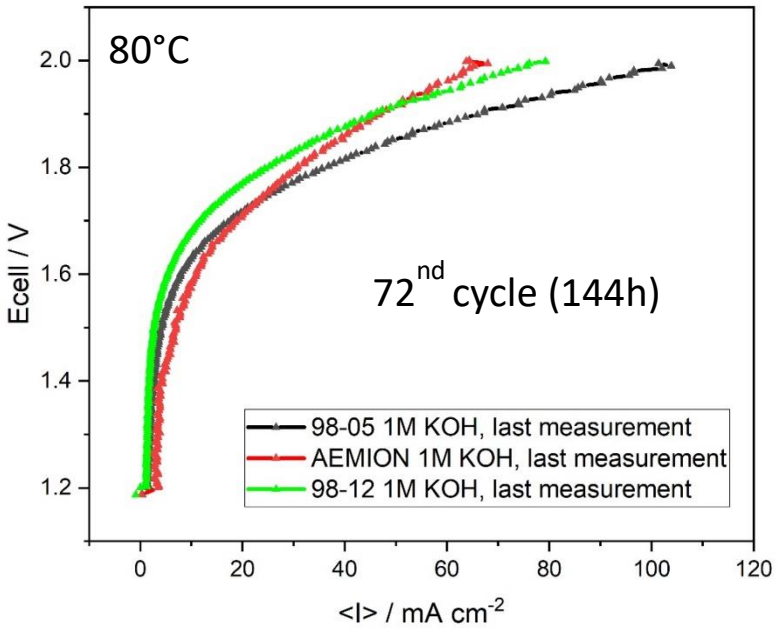


*Figure 2-29 - Polarization curves: 72nd cycle of medium conditions*

The polarization curves for heavy conditions were reported in figures 30 and 31. The results showed that during the first cycle the 50 µm membrane had better behavior while, during the last cycle, the 50 µm modified Aquivion® and AEMION membranes displayed similar performance. In this case, all the membranes showed a decrease of the performance after ageing.

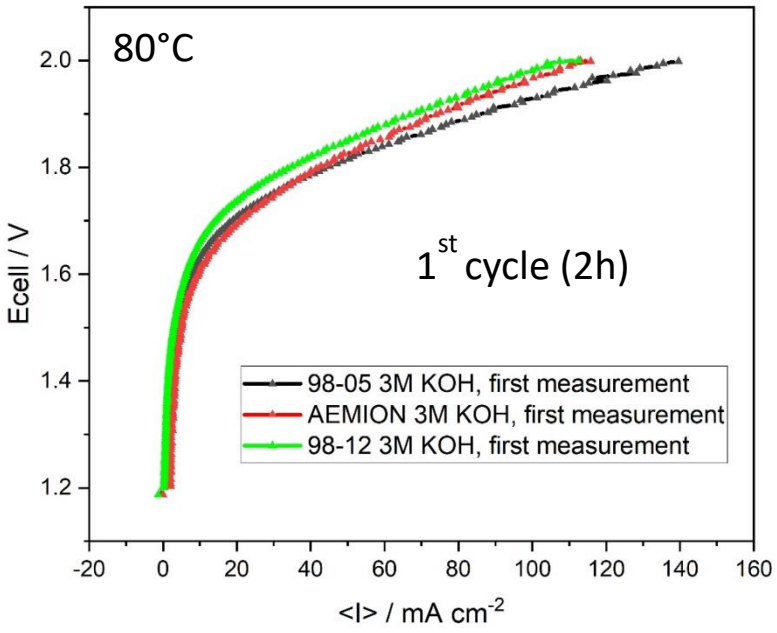


*Figure 2-30 - Polarization curves: 1st cycle of heavy conditions*

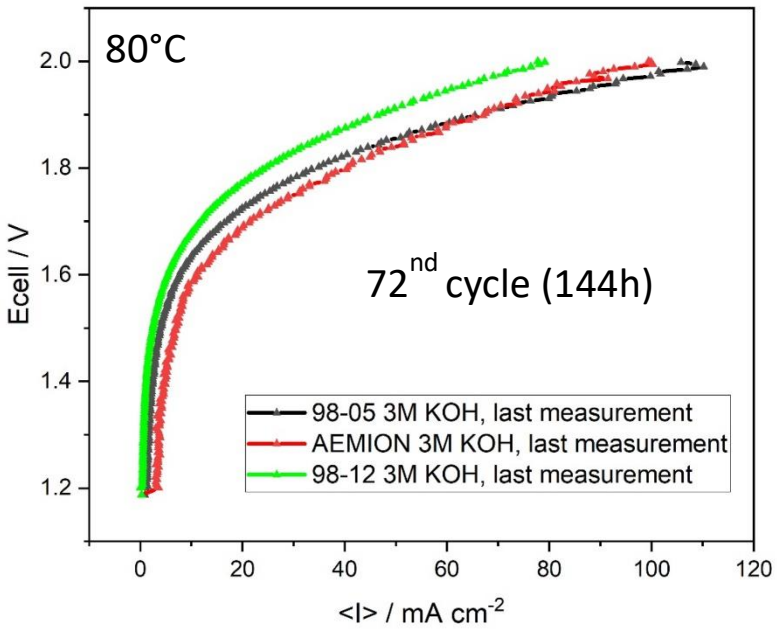


*Figure 2-31 - Polarization curves: 72nd cycle of heavy conditions*

## Resistance overtime

In figure 32 and 33 the resistance overtime for medium and heavy conditions was showed. In case of medium conditions, both Aquivion® membranes kept constant their values. The AEMION membrane, although initially showing lower resistance, increased 7-times its beginning value during the experiment.

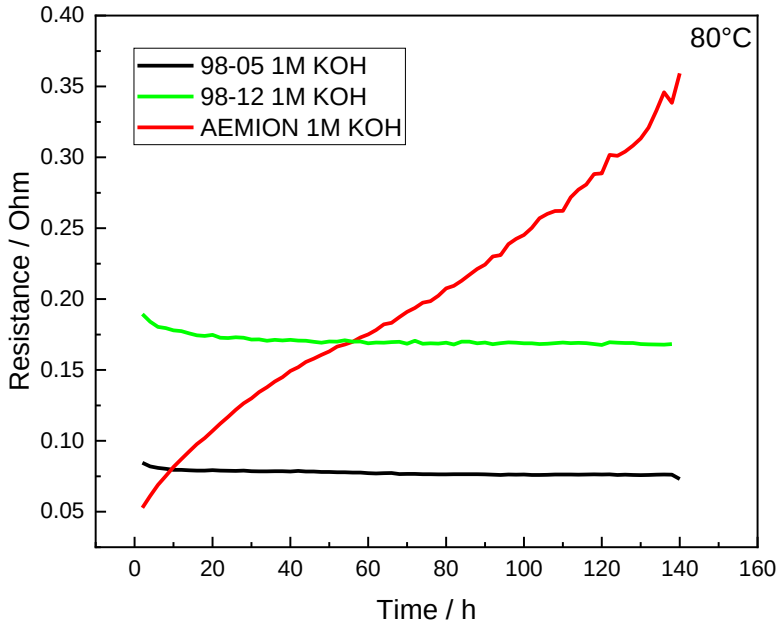


*Figure 2-32 - Resistance overtime for medium treatment*

For heavy treatment, all the membranes hold roughly constant resistance overtime. The modified Aquivion® showed the same values for medium and heavy conditions. I can conclude that the membranes were stable during the measurements.

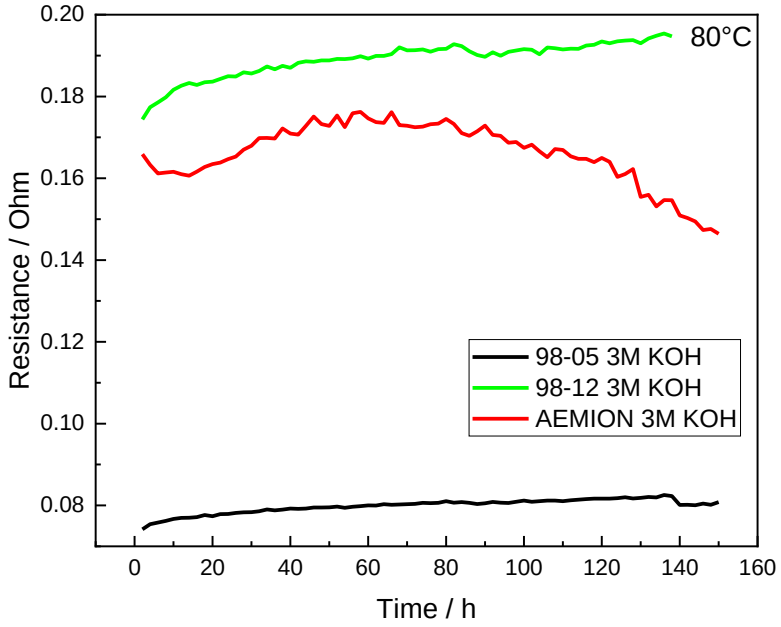


*Figure 2-33 - Resistance overtime for heavy treatment*

Here, I report some EIS spectra of modified membranes before and during these *in-situ* test.

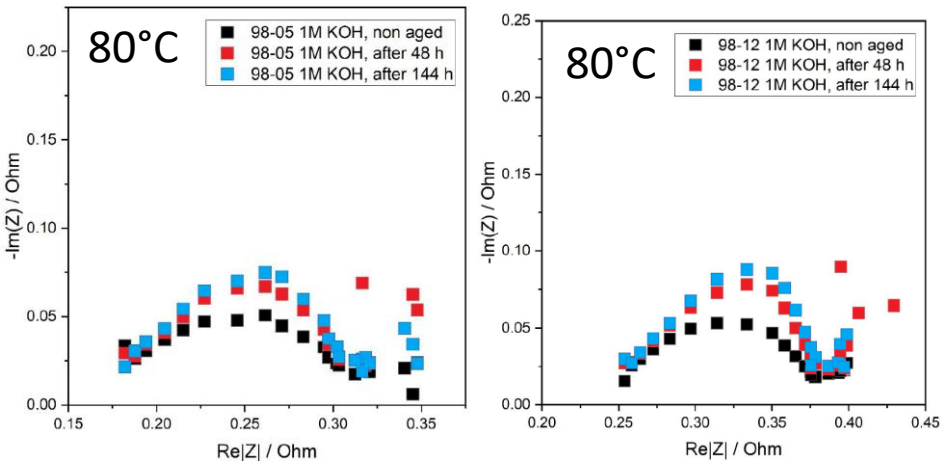


*Figure 2-34 - Impedance spectra of modified Aquivion® before and during the medium ageing*[27]

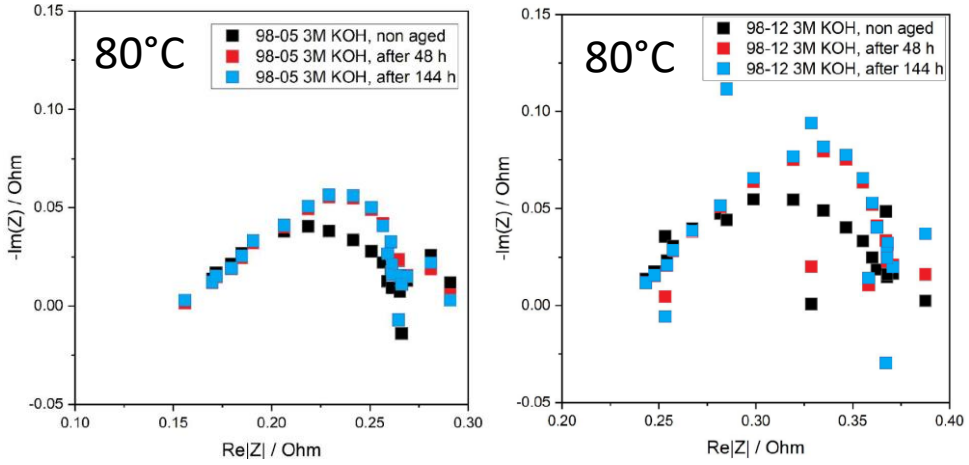


*Figure 2-35 - Impedance spectra of modified Aquivion® before and during the heavy ageing*[27]

## Current overtime

In figures 36 and 37 the current overtime at 2V for the medium and heavy conditions were reported. In both cases, the modified Aquivion® membranes showed a nearly constant current, while the AEMION membrane was better only at the beginning of the medium treatment, but it degraded more rapidly than the Aquivion®-based ones. The initial decrease observed for all the samples during the first 4-5 measurements is attributed to the stabilization of the MEA.

After 144 hours, the membranes showed stable current around 100 mA*cm$^{-2}$ for 50 µm and around 85 mA*cm$^{-2}$ for 120 µm, using 1M KOH concentration. For 3M KOH concentration, they hold constant current around 110 mA*cm$^{-2}$ for the 50 µm and 80 mA*cm$^{-2}$ for the 120 µm. These current values are comparable with others reported in the literature for electrolyzers employing Nickel foam as anodic and cathodic material[28].

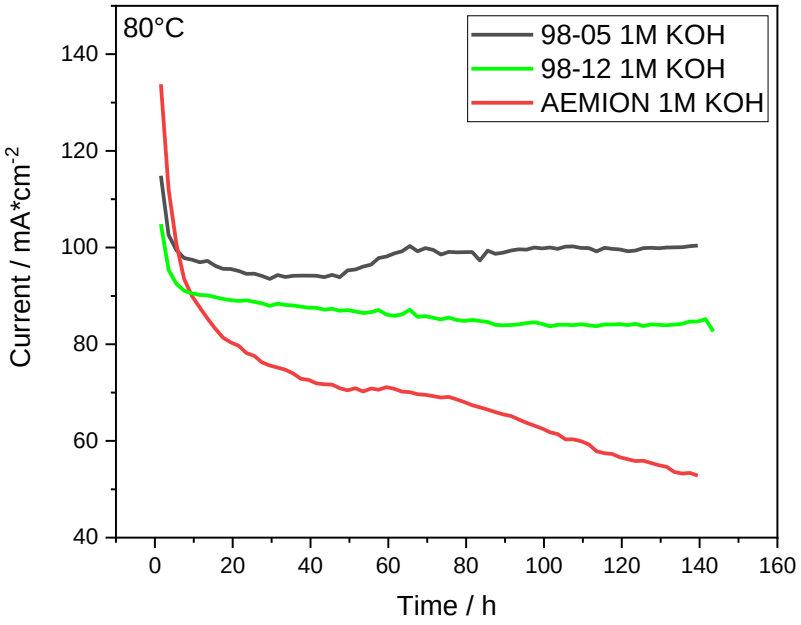


*Figure 2-36 - Current overtime for in-situ test in medium conditions*

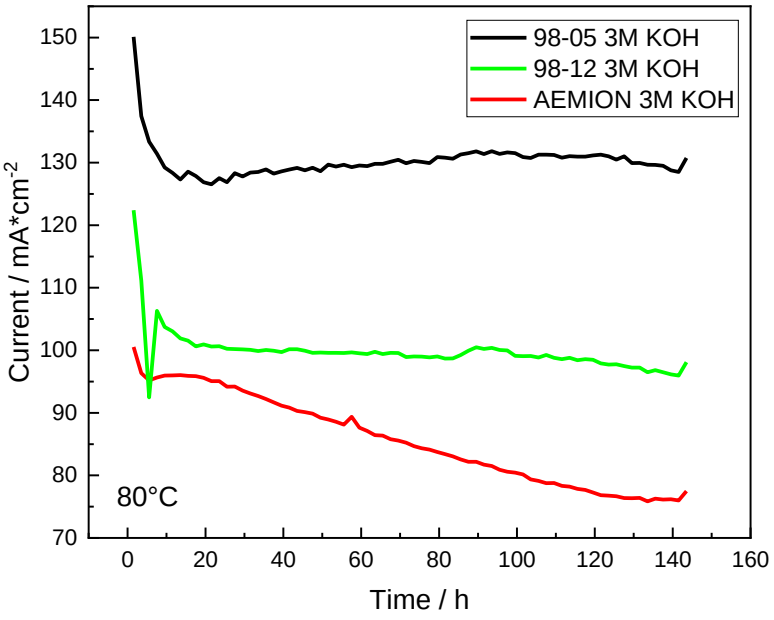


*Figure 2-37 - Current overtime for in-situ test in heavy conditions*

In figure 38 cross-section of functionalized Aquivion® after *in-situ* test were reported. There is not any significant evidence of degradation after ageing, in agreement with the functional results.

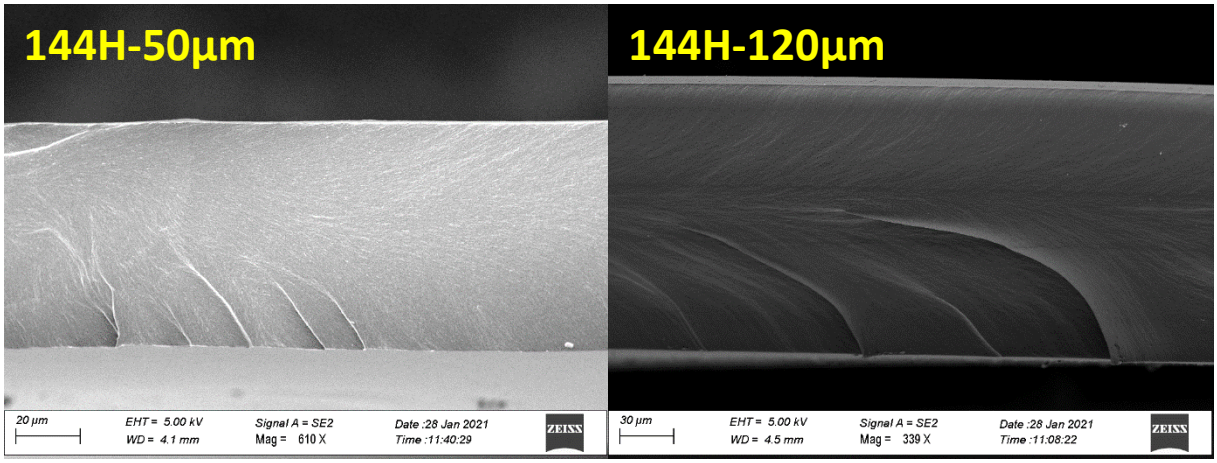


*Figure 2-38 - Cross-section SEM images after in-situ medium (left) and heavy (right) conditions*

## 2.4 – Chapter conclusions

I modified a commercial proton-exchange membrane to obtain an anionic conducting membrane. The Aquivion® membranes were functionalized by reaction with aqueous diamine solution to obtain sulfonamide AEM. This allows to maintain the same mechanical and chemical resistance of the pristine material but at the same time, it increases the thermal stability thanks to the formation of sulfonamide bonds. In addition, this functionalization was carried out in an aqueous media, which is clearly advantageous from the environmental point of view. The synthesis was confirmed by using several techniques i.e. IR and NMR spectroscopies and TGA and DSC measurements. The modified membranes showed an ionic conductivity of 26 mS*cm$^{-1}$ at 80°C and 100% relative humidity, with IEC of 0.77 meq*g$^{-1}$. I investigated the chemical and electrochemical stability using *ex-situ* and *in-situ* methods. As *ex-situ* treatments, I checked the durability of membranes by soaking them in KOH solution by varying the concentration, temperature and duration of the tests. The results demonstrated that the membranes were stable in alkaline environment and the changes of physical-chemical properties (i.e., conductivity) were negligible. For *in-situ* test, the membranes were used in electrolyzer using nickel foam as electrode, 1M and 3M KOH solutions as supply feed at 80°C. The best results, in terms of current, were obtained with the 50 µm modified Aquivion® at 2V after 144 hours obtaining 100 mA*cm$^{-2}$ and 130 mA*cm$^{-2}$ for 1M and 3M KOH solution, respectively.

This new Aquivion®-based anion exchange membranes showed excellent durability in alkaline environment making them promising materials for AEMFC and AEMWE.

## Bibliography


1. Di Noto V, Zawodzinski TA, Herring AM, Giffin GA, Negro E, Lavina S. Polymer electrolytes for a hydrogen economy. *Int J Hydrogen Energy*. 2012;37(7):6120-6131. doi:10.1016/j.ijhydene.2012.01.080

2. Weber AZ, Mench MM, Meyers JP, Ross PN, Gostick JT, Liu Q. Redox flow batteries: A review. *J Appl Electrochem*. 2011;41(10):1137-1164. doi:10.1007/s10800-011-0348-2

3. Spiegel C. *Designing and Building Fuel Cells*.; 2007.

4. Oldani C, Merlo L. Ionomer Membranes and Dispersions. 2016:1-35.

5. Pujiastuti S, Onggo H. Effect of various concentration of sulfuric acid for Nafion membrane activation on the performance of fuel cell. *AIP Conf Proc*. 2016;1711(February 2016). doi:10.1063/1.4941639

6. Mazzapioda L, Panero S, Navarra MA. Polymer electrolyte membranes based on Nafion and a superacidic inorganic additive for fuel cell applications. *Polymers (Basel)*. 2019;11(5). doi:10.3390/polym11050914

7. Hine J, Shyong L. Internal Hydrogen Bonding and Positions of Protonation in the Monoprotonated Forms of Some 1,3- and 1,4-Diamines. *J Org Chem*. 1975;40(12):1795-1800. doi:10.1021/jo00900a026

8. Petricci S, Guarda PA, Oldani C, Marchionni G. Liquid compositions of fluorinated anion exchange polymers. 2012.

9. Spectral Database for Organic Compounds SDBS. https://sdbs.db.aist.go.jp/sdbs/cgi-bin/cre_index.cgi.

10. Danilczuk M, Lin L, Schlick S, Hamrock SJ, Schaberg MS. Understanding the fingerprint region in the infra-red spectra of perfluorinated ionomer membranes and corresponding model compounds: Experiments and theoretical calculations. *J Power Sources*. 2011;196(20):8216-8224. doi:10.1016/j.jpowsour.2011.05.067

11. Lowry SR, Mauritz KA. An Investigation of Ionic Hydration Effects in Perfluorosulfonate Ionomers by Fourier Transform Infrared Spectroscopy. *J Am Chem Soc*. 1980;102(14):4665-

4667. doi:10.1021/ja00534a017

12. Polymers SS. Aquivion ® PFSA Functional Polymers Dev't Group Solvay Specialty Polymers. 2019.

13. Krueger PJ. Intramolecular hydrogen bonds in ethylenediamines and other aliphatic diamines. *Can J Chem*. 1967;45. doi:https://doi.org/10.1139/v67-348

14. Hine J, Li W-S. Synthesis of Some cis- and trans-2-Dimethylaminomethy1.CycliAc mines and Related Diamines. *J Org Chem,*. 1975;Vol. 40:1-4.

15. Lee S, Lee H, Yang TH, et al. Quaternary ammonium-bearing perfluorinated polymers for anion exchange membrane applications. *Membranes (Basel)*. 2020;10(11):1-13. doi:10.3390/membranes10110306

16. Bonizzoni S, Stilli P, Lohmann-Richters F, et al. Facile Chemical Modification of Aquivion® Membranes for Anionic Fuel Cells. *ChemElectroChem*. 2021;8(12):2231-2237. doi:10.1002/celc.202100382

17. Goswami S, Klaus S, Benziger J. Wetting and Absorption of Water Drops on Nafion Films. 2008;51(Nafion 112):8627-8633. doi:doi.org/10.1021/la800799a

18. Varcoe JR, Atanassov P, Dekel DR, et al. Anion-exchange membranes in electrochemical energy systems. *Energy Environ Sci*. 2014;7(10):3135-3191. doi:10.1039/c4ee01303d

19. Mustain WE, Chatenet M, Page M, Kim YS. Durability challenges of anion exchange membrane fuel cells. *Energy Environ Sci*. 2020;13(9):2805-2838. doi:10.1039/d0ee01133a

20. Lin C, Gao Y, Li N, et al. Quaternized Tröger's base polymer with crown ether unit for alkaline stable anion exchange membranes. *Electrochim Acta*. 2020;354. doi:10.1016/j.electacta.2020.136693

21. Cheng J, He G, Zhang F. A mini-review on anion exchange membranes for fuel cell applications: Stability issue and addressing strategies. *Int J Hydrogen Energy*. 2015;40(23):7348-7360. doi:10.1016/j.ijhydene.2015.04.040

22. Scheepers F, Stähler M, Stähler A, et al. Temperature optimization for improving polymer electrolyte membrane-water electrolysis system efficiency. *Appl Energy*. 2021;283(June). doi:10.1016/j.apenergy.2020.116270

23. Loudon M. *Chimica Organica*.; 2010.

24. Clayden J, Greeves N, Warren S. *Organic Chemistry*. Second edi. (Press O university, ed.).

25. Coppola RE, Herranz D, Ming N, Abuin GC. Polybenzimidazole-crosslinked-poly ( vinyl benzyl chloride ) as anion exchange membrane for alkaline electrolyzers. 2020;157:71-82. doi:10.1016/j.renene.2020.04.140

26. Wang L, Peng X, Mustain WE, Varcoe JR. Radiation-grafted anion-exchange membranes: The switch from low- to high-density polyethylene leads to remarkably enhanced fuel cell performance. *Energy Environ Sci*. 2019;12(5):1575-1579. doi:10.1039/c9ee00331b

27. Stilli P, Bonizzoni S, Lohmann-Richters F, Beverina L, Papagni A, Mustarelli P. Aquivion®-based anionic membranes for water electrolysis. *Electrochim Acta*. 2022;405:139834. doi:10.1016/j.electacta.2022.139834

28. Su X, Gao L, Hu L, et al. Novel piperidinium functionalized anionic membrane for alkaline polymer electrolysis with excellent electrochemical properties. *J Memb Sci*. 2019;581(January):283-292. doi:10.1016/j.memsci.2019.03.072

# Chapter 3: Polyketones-based anion exchange polymer

Aliphatic polyketones are usually synthesized by co-polymerization reaction between carbon monoxide and an olefin. In general, these materials show good mechanical, thermal properties, high chemical resistance [1–3] and, when the monomers are cheap e.g. ethylene, they are also low-cost polymers[3,4]. Moreover, polyketones could be easily functionalized thanks to the high versatility of carboxyl group, making them very interesting material[5]. In fact, their properties are compatible with those required by membranes for fuel cell and electrolyzer applications[6].

In this chapter, I reported my initial studies and investigations of a commercial poly(ethyl-ketone) and its functionalization by Pall-Knorr reaction in order to obtain anion exchange polymer for AEMFC and AEMWE.

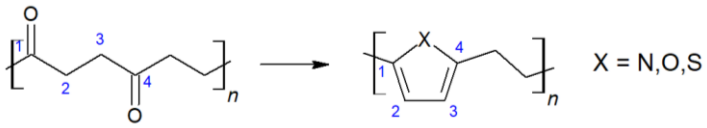


*Figure 3-1 Pall-Knorr reaction of poly(ethyl-ketone*

## 3.1 – Pristine poly(ethyl-ketone)- (PK) - AKROTEK® PK-HM natural (7536)

For this work, I used the PK-HM 7536 sold by AKROTEK® (Germany), a commercial terpolymer of carbon monoxide, ethylene and propylene[1]. The addition of small quantities of propylene helps to improve the workability of this material in the industrial manufacture[2,3]. I referred to this material simply as “poly(ethyl-ketone)” of “polyketones” of “PK”.

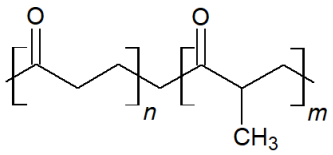


*Figure 3-2 – Structure of PK-HM 7536*

This polymer was characterized by IR and NMR spectroscopies, elementary and thermal analysis.

### *Structure investigation*

The figure 3 shows the IR spectra of the polymer.

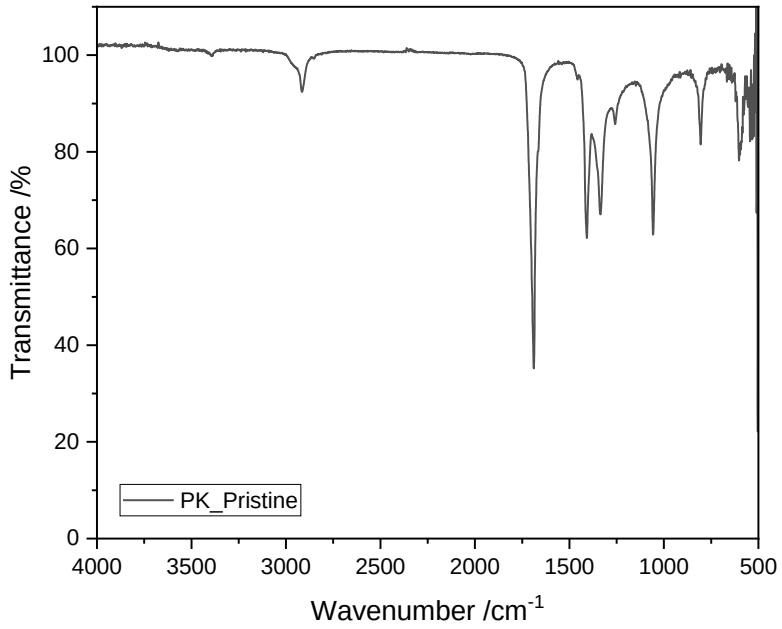


*Figure 3-3 - IR spectrum of PK*

In 3000-2800 $cm^{-1}$ zone were detected the C-H asymmetric and symmetric stretching of $-CH_2-$ at 2913, 2851 $cm^{-1}$ and also a small shoulder at 2971 $cm^{-1}$ attributed to methyl group of propyl portion[7,8]. The signals C=O stretching were reveled at 1690 and 1663 $cm^{-1}$ [2]. The signals at 1407, 1334, 1259 $cm^{-1}$ were identified as bending, wagging and twisting deformation of $-CH_2-$[5,9,10]. At 1057 $cm^{-1}$ there was the stretching of $CH_2$-CO-$CH_2$ system[11] while the peak at 809 $cm^{-1}$ was assigned to carbon backbone vibration [11,12].

The $^{13}$C-NMR spectrum allows to investigate the polymer structure and its changes during the functionalization and, in this case, I also used quantitively $^{13}$C-NMR to determinate the stoichiometric ratio. The figures 4 and 5 show the CP-MAS and high-power decoupling (HPDEC) experiments.

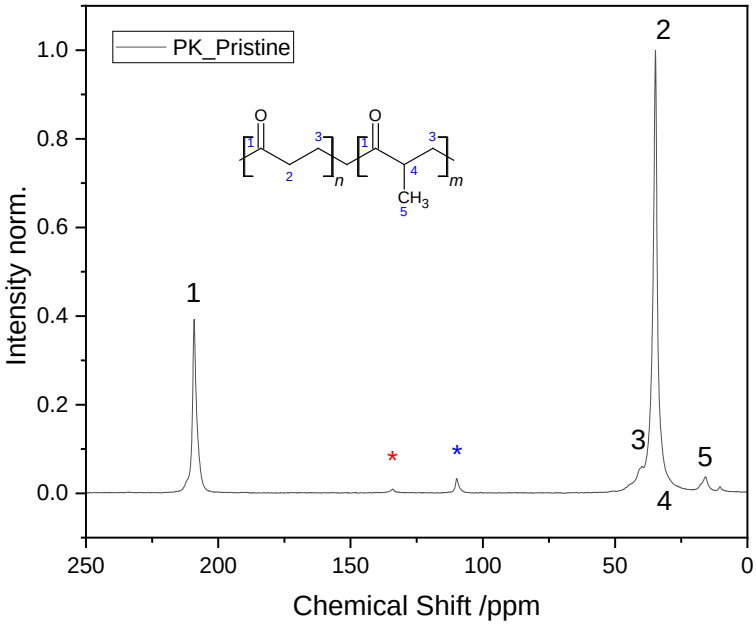


*Figure 3-4 – $^{13}$C-CPMAS spectrum of PK*

In figure 4 it's possible to notice two intense peaks of -$CH_2$- and C=O at 34 and 210 ppm, respectively[13]. There also smaller peaks at 16 and 40.5 ppm due to -$CH_3$ and -CH- of propyl group. The signals marked with star were identified as spinning sideband of carboxyl and methylene signals. This NMR experiment did not give quantitative information of the functional groups, consequently, the HPDEC experiment was also done. I obtained quantitative information following these steps: at first, I adjusted the baseline of HPDEC data and then I used the best fitting procedure to simulate the experimental profile. From the area of simulated peaks, I evaluated the carbons concentration. As support, I had also generate theorical spectrum using NMRDB.org website[14–16].

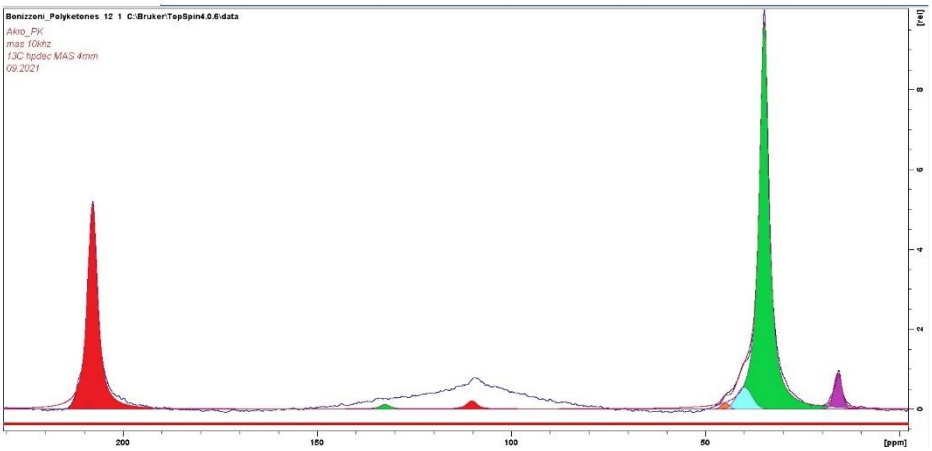


*Figure 3-5 - $^{13}$C-HPDEC of polyketones with the following signals: C=O (red), -$CH_2$- ethyl (green) and -$CH_3$ (purple), -CH- (light blue) and -$CH_2$- propyl (orange)*

From the best fitting, I produced the following data.

| N° signals | Chemical shift (ppm) | Area |
|---|---|---|
| 1 | 207,9 | 2,44E+09 |
| 2 | 209,2 | 2,50E+07 |
| 3 | 34,9 | 4,54E+09 |
| 4 | 15,9 | 2,40E+08 |
| 5 | 40,0 | 2,83E+08 |
| 6 | 45,0 | 4,01E+07 |

$$\%\ CO\ signal = \frac{Sum\ of\ CO\ signals}{Sum\ of\ all\ signals} * 100 = 32.6\ \%$$

$$CO/C_2H_4\ ratio = \frac{Sum\ of\ CO\ signals}{Sum\ of\ CH_2\ signals} = 0.48$$

$$\%\ propyl\ signal = \frac{Signal\ of\ CH_3}{Sum\ of\ CH_2\ signals} * 100 = 4.7\ \%$$

From % CO signal, I could calculate a pseudo “polymer mols” as:

$$n\ (polymer) = n\ (CO) = \frac{\%\ CO\ signal}{PM\ (CO)} = \frac{32.6\ \%}{28.01\ \left(\frac{g}{mol}\right)} = 1.16\ \frac{mol}{g}$$

Then, I could calculate the mol ratio of propyl in the polymer, using the molecular weight ratio.

$$mol\ ratio\ (propyl-\ polymer)\ = \frac{\frac{\%\ prolyl\ signal}{PM\ C_3H_6}}{n\ (polymer)} = \frac{\frac{4.7\ \%}{42.08\ \left(\frac{g}{mol}\right)}}{1.16\ \left(\frac{mol}{g}\right)} = 0.084$$

From the calculation the content in mol of propyl is about 8.4%.

### *Thermal properties*

In figure 6, the TGA curve in air was reported.

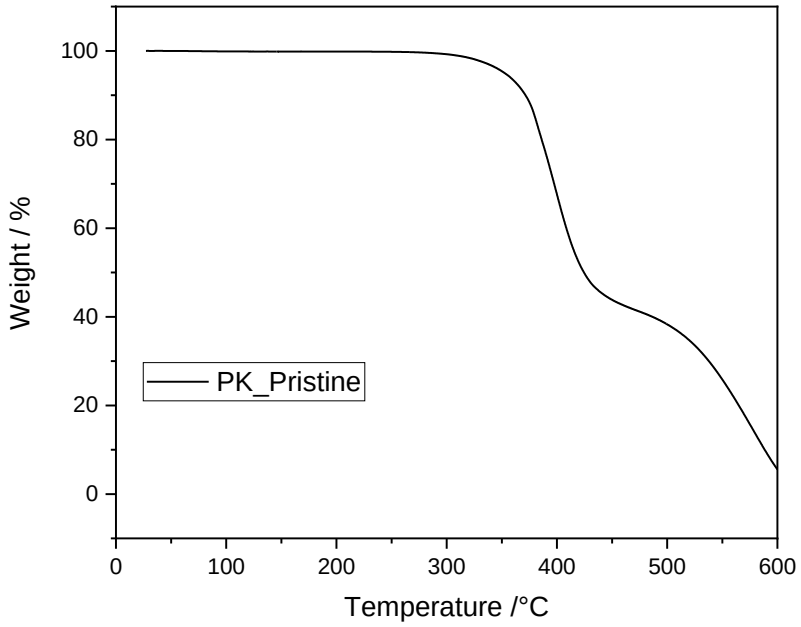


*Figure 3-6 - TGA curve of PK (black) and simultaneous DSC curve (red)*

The curve showed two mass losses of 56.4% at 300°C and about 40% at 450°C. The first mass loss could be attributed to carboxyl degradation, while the second one to the backbone[17].

$$\Delta mass\ CO\ theorical = \frac{PM\ CO}{PM\ polymer} * 100 = \frac{28.01\left(\frac{g}{mol}\right)}{56.06\left(\frac{g}{mol}\right)} * 100 = 50.0\ \%$$

$$\Delta mass\ (300-450) = (99.9-42.8)\% = 56.4\ \%$$

This means that in the first step the polymer loses the CO content with something else. In order to better understand the degradation processes, I performed TGA-IR experiment in air.

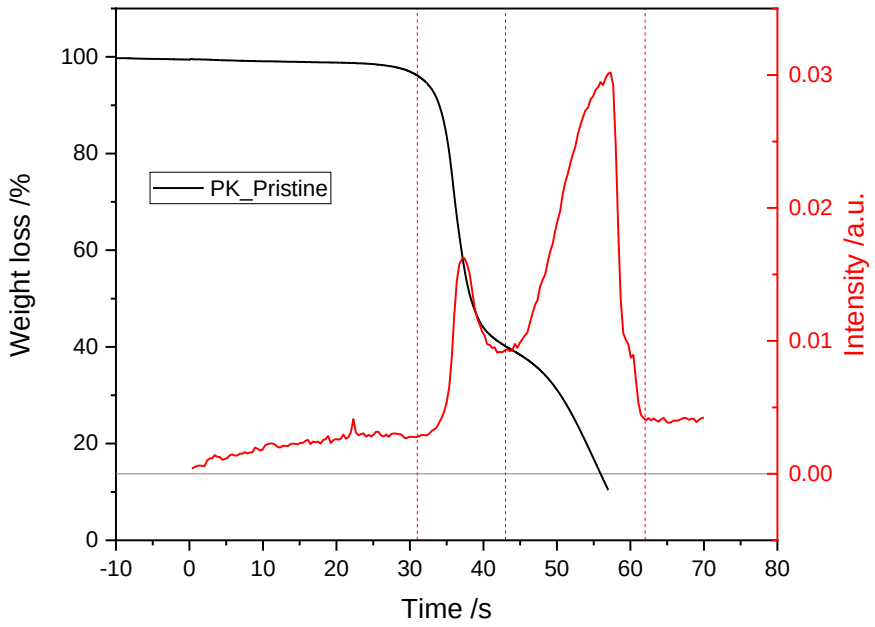


*Figure 3-7 - TGA-IR curve: in black the TGA curve and in red the intensity of FTIR signal: the dashed lines indicate the reference times*

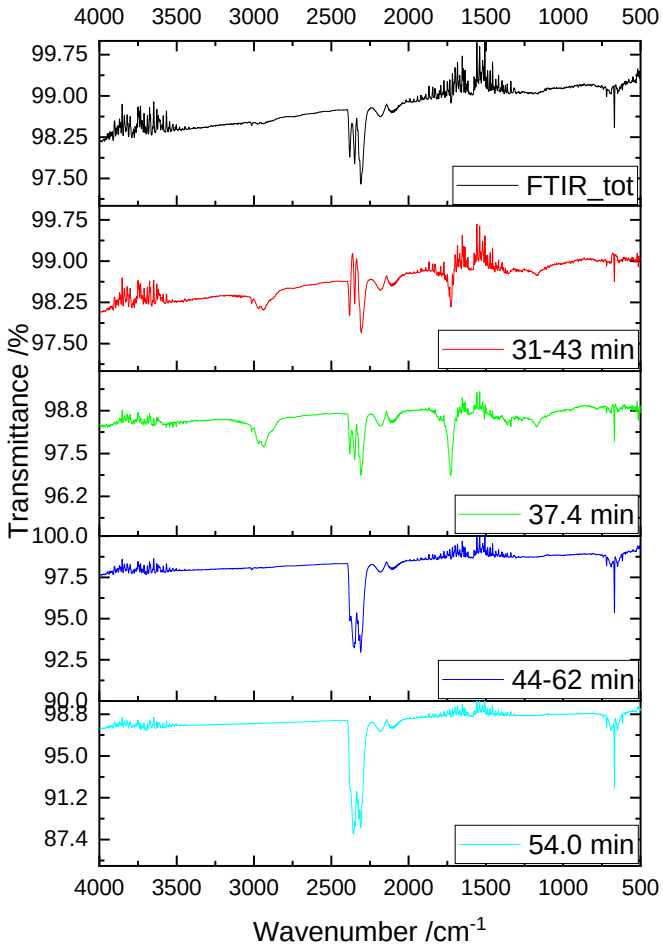


*Figure 3-8 - IR spectra of TGA-IR analysis*

In figure 8, were reported the IR spectra collected from 31 to 43 minutes and from 44 to 62 minutes, corresponding to the period when TGA degradations occurred. The IR spectra at time=37.4 min and time=54.0 min were those recorded at the maximum points of the signals (Fig. 7). In 31-43 and 37.4 spectra, the C-H stretching at 3015, 2934 and 2934 $cm^{-1}$ were attributed to aromatic system, methyl and methylene group, respectively[7,11,18]. The signal of C=O stretching was detected at 1723 $cm^{-1}$ and carbon dioxide signals were observed at 2382, 2343, 2308 and 668 $cm^{-1}$ [8,19]. Further small signals of C=C stretching at 1595 $cm^{-1}$, C-H bending at 1356 $cm^{-1}$ and C-O deformation at 1163 $cm^{-1}$ were noticed[11]. In 44-62 and 54.0 spectra, only the carbon dioxide signals were observed at 2382, 2343, 2308 and 668 $cm^{-1}$. The results showed the formation of carbon dioxide with some unsaturated and carboxy systems in 300-450°C zone and only carbon dioxide starting from 450°C. These phenomena could be explained by thermal and radical degradation of carboxyl groups[17] followed by carbon backbone oxidation and, at the same time, they could explain the TGA results.

The figure 9 shows the DSC curve in which the main phenomena are the α-β glass transition (Tg) [20,21] and the melting/solidification of the polymer, according to company data sheet[1,22]. In the first heating cycle, the Tg and the melting point were detected in 80-110 °C zone and at 208 °C, respectively. In the cooling scan, solidification peak and glass transition were detected at 188°C and 110-90°C while, in the second heating cycle, only the polymer melting at 203 °C was detected.

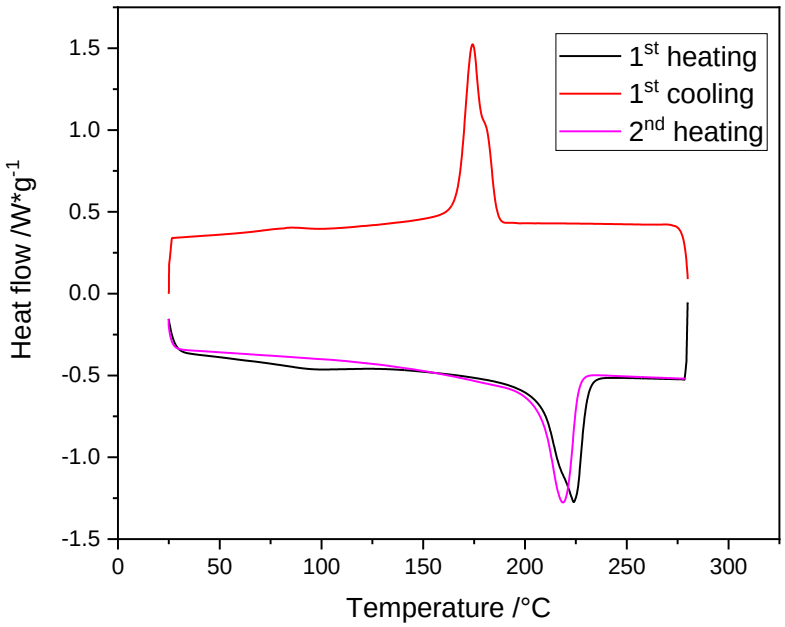


*Figure 3-9 - DSC curve of PK*

From the elementary analysis, I obtain the following data and then I calculated the % propyl and % CO content.

| CHNS | % C | % H | % N | % S | % O |
|---|---|---|---|---|---|
| PK_Pristine | 66,01 | 7,098 | 0,00 | 0,140 | 26,75 |
| Poly(ethyl-ketone) | 64,27 | 7,192 | 0,00 | 0,000 | 28,54 |
| Poly(propyl-ketone) | 85,69 | 10,788 | 0,00 | 0,000 | 28,54 |

$$ratio\ (propyl-polymer) = \frac{\%\ sample - \%\ PK(ethyl)}{\%\ PK(Propyl) - \%\ PK(ethyl)} * 100 = \frac{(66.01 - 64.27)\%}{(85.69 - 64.27)\%} = 0.081$$

Considering the % propyl content, I could calculate the new stoichiometry index of carbon for a general formula $C_xN_xO_1$.

$$New\ C\ index = n\ PK(ethyl - ketone) * (1 - 0.081) + n\ PK(propyl - ketone) * 0.081 =$$
$$= 3 * 0.919 + 4 * 0.081 = 3.08$$

$$\%\ CO = \frac{\%\ C\ * PM\ CO\ \left(\frac{g}{mol}\right)}{PA\ \left(\frac{g}{mol}\right) * 3.08} = \frac{66.01\ \%\ * 28.01\ \left(\frac{g}{mol}\right)}{12.01\ \left(\frac{g}{mol}\right) * 3.08} = 50.0\ \%$$

The content in mol of propyl was 0.081 and the content of carbonyl group was 50% wt, both in excellent agreement with NMR and TGA results.

### *Workability of the material*

The AKRO_PK is sold as pellet but its high impact resistance avoids all milling procedure to reduce the dimensions. In order to facilitate the functionalization of the AKRO_PK, I used two approach to improve the workability of this materials: chemical and thermal. The first approach was the use using the right solvent combination to perform the modification in solution. Indeed, the second was to obtain thin films around 100 µm by hot-pressing at 210°C and then, to cut them reducing the size to less than 1 $mm^2$. This polymer is not soluble in the mostly common solvent but in few solvents with strong polarization such as 1,1,1,3,3,3-Hexafluoro-2-propanol[23] and its mixture with dichloromethane[24], Trifluoroacetic acid[2], m-cresol, benzoic acid[25] and resorcinol and water mixture[26].

## 3.2- Pall-Knorr modification

Thanks to Pall-Knorr reaction, an 1,4-diketones unit forms a 5-member ring including a heteroatom such as nitrogen, oxygen, sulfur, creating the corresponding pyrrole, furan and thiophene derivates[23,27,28].

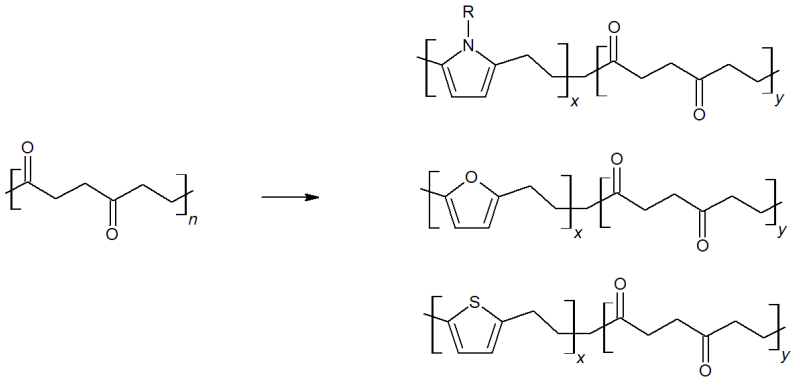

*Figure 3-10 - Pall-Knorr reaction products*

These reactions are very attractive because allowed to insert a heteroatomic ring inside the backbone of poly(ethyl-ketone). The main advantages were related to the introduction of an aromatic rings which could increase the mechanical and thermal stability of the polymers [12,29]. Moreover, these reactions generate aromatic precursors from which it is possible to obtain anionic polymers with a few steps[9,22]. This aspect, in addition to the PK low-cost, is more important for the scalability of these synthesis.

During my PhD period, I worked on the synthesis of pyrrole, furan and thiophene derivates. Here, I reported the initial works for pyrrole-based and furan-based conducting polymers.

### 3.2.1 – Poly(ethyl-pyrrole-ketone)

The pyrrole derivatives can be produced by reacting 1,4-diketones unit with a primary amine[23,30,31].

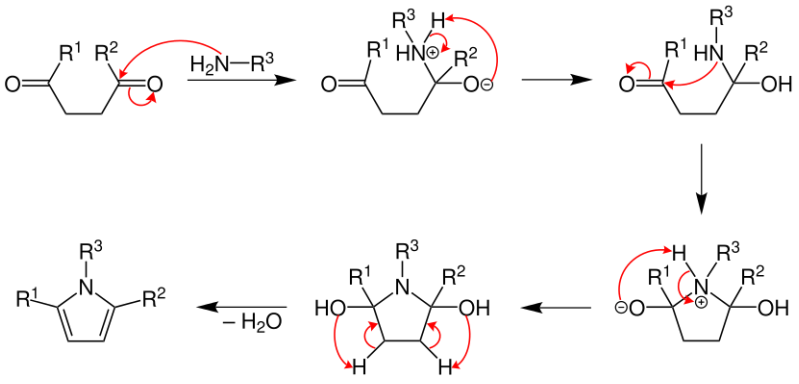

*Figure 3-11 - Pall-Knorr mechanism for pyrrole derivates [32]*

The advantage of this reaction was in the choice of a suitable amine: the primary amine must be connected to positively chargeable groups. In this way you can choose the active group to be introduced into the polymer but also generate an anionic conduction polymer in just two steps. I reported the functionalization of PK with N,N,2,2-tetramethyl-1,3-propandiamine.

### *3.2.1.1 – Synthesis overview*

The anion conducting polymers were prepared in two steps, using a primary-ternary diamine: the first one was the Pall-Knorr reaction between the PK and the primary amine (Step_1) while second was the methylation process of the ternary amine to obtain a quaternary ammonium group (Step_2). This diamine usually showed a low reactive for the Pall-Knorr reaction, so, It was necessary the application of a catalyst such as $Bi(NO_3)_2$ [33,34].

#### *Step_1*

The step_1 was the Pall-Knorr reaction between the PK and the N,N,2,2-tetramethyl-1,3-propandiamine. The polyketones and $Bi(NO_3)_2$ were soaked in a 1:3 wt mixture of 1,1,1,3,3,3-Hexafluoro-2-propano (HFIP) and dichloromethane (DCM) and let to dissolve under stirring[24]. Then, three washing nitrogen-vacuum were performed to reduce the moisture and carbon dioxide in the reaction environment. After that, the N,N,2,2-tetramethyl-1,3-propandiamine was added and let react for a precise time at 35°C and under stirring. The products were recovered by precipitation in ethyl ether, washed with ethyl ether and water and dried in vacuum at 100°C.

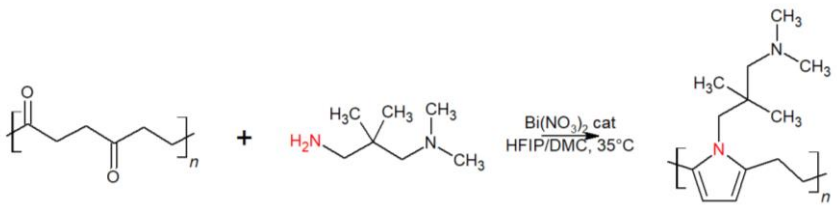


*Figure 3-12 - Scheme of Step_1*

Step_2

The step_2 is the methylation process of the ternary amine to obtain a quaternary ammonium group. The step_1 product was placed in a balloon with a condenser and then, three washing nitrogen-vacuum were performed to reduce the moisture and carbon dioxide in the reaction environment. After that, the iodomethane is added to cover the powder and let react for 15 hours at 40°C in reflux condition and under slowly stirring. Later the products were covered by filtration, washed with abundant water and dried in vacuum at 100°C for 2 hours.

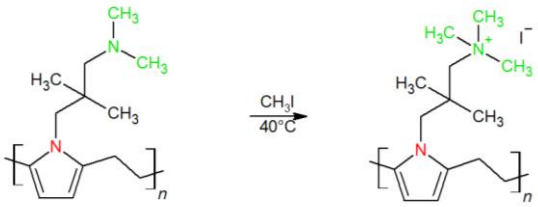


*Figure 3-13- Scheme of Step_2*

### *3.2.1.2 - Following the synthesis*

In order to understand the reactivity of step_1, I did an exploratory test leaving the reaction for 11 days, using 10% excess in mol of diamine compared to the polymer dimer unit moles. Each 2 days, a small amount of reacting solution was taken and precipitated with ethyl ether, recovering the polymer. On these samples, I performed FTIR in order to monitor the reaction progress.

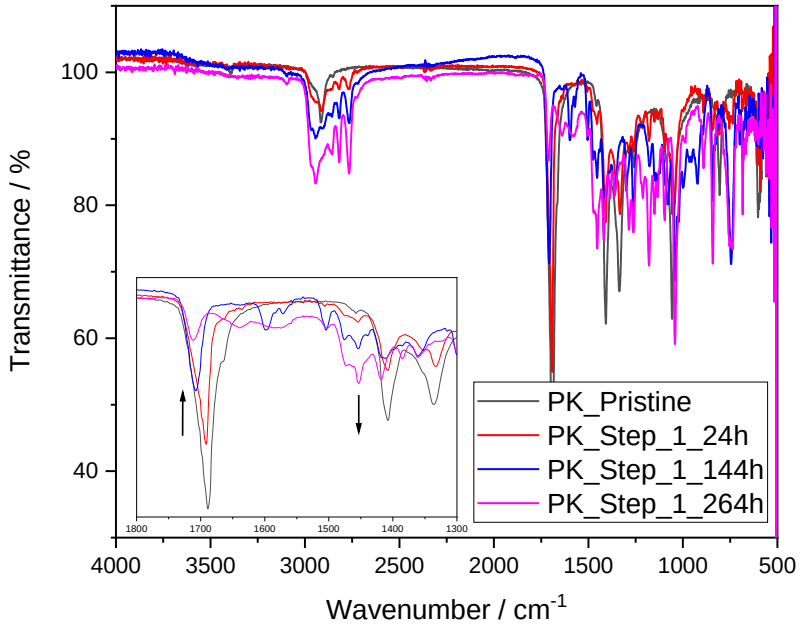


*Figure 3-14 - IR spectra of PK_pristine and Step_1 at 24h, 144h and 264h*

During the reaction the carboxyl groups were converted into pyrrole ring. Consequently, the C=O stretching at 1690 cm-1 decreased while the pyrrole ring and diamine signals appeared. In 3000-2800 $cm^{-1}$ zone were detected the C-H of the polymer at 2913, 2851 $cm^{-1}$ , the C-H stretching of pyrrole and the C-H stretching of $-CH_2-$, $N-CH_3$ of the diamine [7,8,35,36]. In the 1800-1300 $cm^{-1}$ zone, the C=O stretching at 1690 $cm^{-1}$ and the of $-CH_2-$ bending of the polymer were relevated[9]. Further diamine signals as N-C and C-H bending were found at 1475, 1455, 1388 $cm^{-1}$. The pyrrole signals were detected at 3100 cm-1 (C-H stretching) and at 1491 cm-1 (ring stretching)[25].

I could estimate the progress of the reaction observing the CO signal decreasing, so, I made the integrals of C=O peak for each spectrum. The values were reported below.

| Sample | Time (h) | Area CO |
|---|---|---|
| PK_pristine | 0 | 7680,7 |
| PK_Step_1_20h | 20 | 6745,2 |
| PK_Step_1_96h | 96 | 5840,1 |
| PK_Step_1_120h | 120 | 5016,6 |
| PK_Step_1_144h | 144 | 4959,3 |
| PK_Step_1_192h | 192 | 4583,5 |
| PK_Step_1_264h | 264 | 4500,6 |

In figure 15, I reported the intensity of CO signal in function of the time.

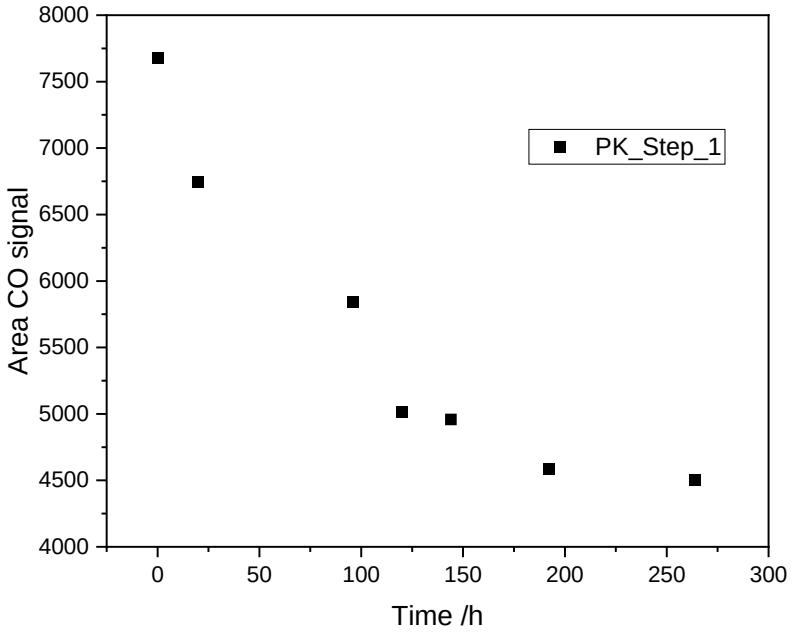


*Figure 3-15 - Area of CO signal of PK_Step_1*

As reported in literature, the good mechanical and thermal properties of this polymer is due to the content of carboxyl group[2]. In addition, higher functionalization degree means, in the end of modification, much charged groups in the polymer which could get worse the mechanical properties of the modified material [37]. So, considering the IR trend and the operating time, I decided to investigate the step_1 fixing at 6 days the experimental duration and varying the molar ratio of diamine. I used 0.6, 0.8 and 1.0 as molar ratio between the diamine and 1,4-diketones units. The samples were called PK_Step_1_n, where n was the diamine stoichiometry used.

In figure 16, the spectra of Step_1 were reported. As expected, increasing the concentration of diamine, the intensity of the C=O stretching peaks was reduced and, at the same time, the signals of pyrrole at 1500 $cm^{-1}$ and the diamine at 1450 $cm^{-1}$ were increased.

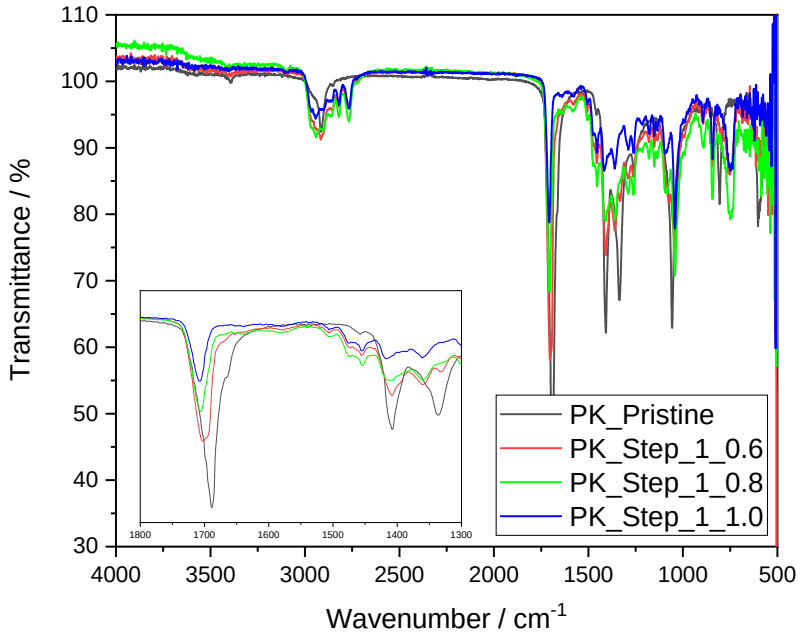


*Figure 3-16 - IR spectra of Step_1 with different ratio*

The figure 17, the NMR spectra of Step_1 were reported. The signals of pyrrole ring were detected at 152 ppm and 124 ppm, while the signals at 89, 69, 59, 44 ppm were attributed to diamine structure according the literature[8,19,38]. Only in the step_1_0.6 the signal at 37 ppm, correlated to $CH_2$ of poly(ethyl-ketone), was remained after functionalization. As expected, increasing the concentration of diamine, the intensity of the C=O peak at 210 ppm was reduced. It' possible notice non-significant changes in intensity between the samples for the pyrrole and diamine signals.

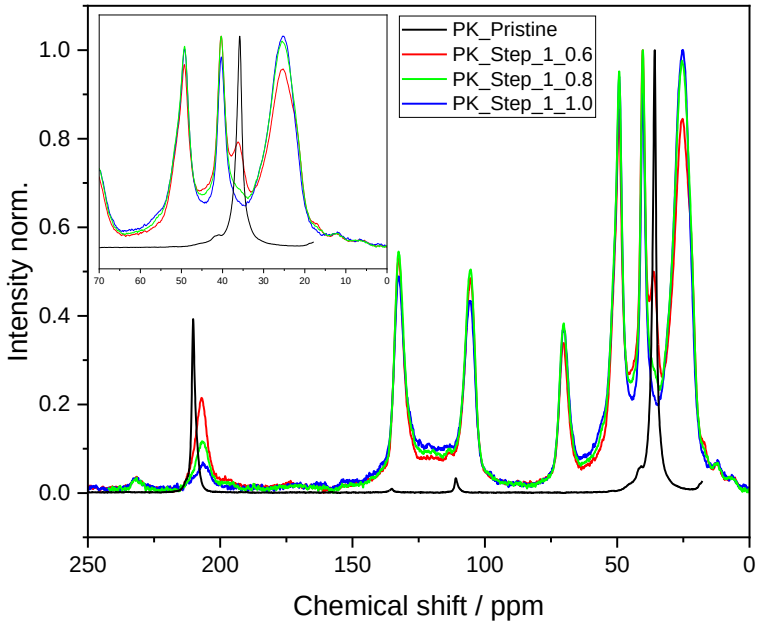


*Figure 3-17 - $^{13}$C-CP-MAS of step_1 product*

As example, I reported the comparison of IR and $^{13}$C-CPMAS NMR spectra for the Step_1_0.8 and Step_2_0.8.

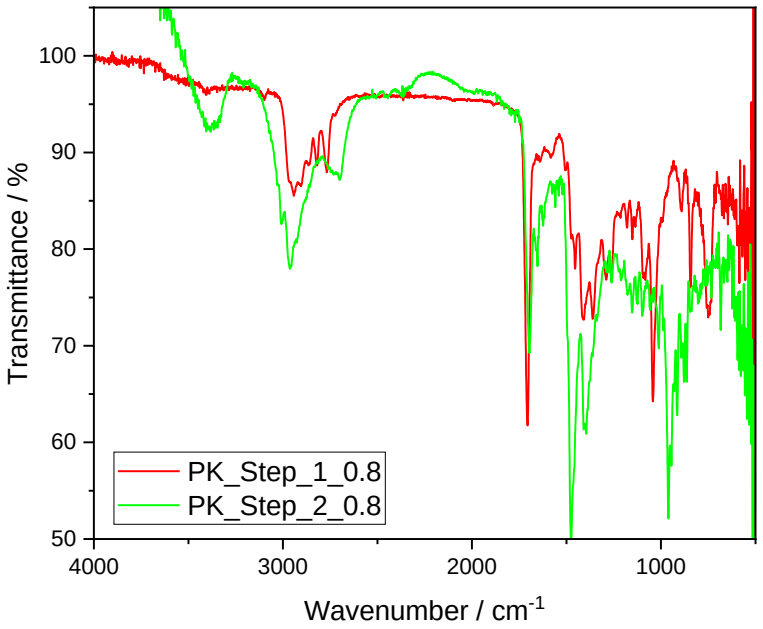


*Figure 3-18 – IR spectra of step_1_0.8 and step_2_0.8*

In Step_2 some changes in 3000-2700 $cm^{-1}$ zone were observed (fig. 18). The new peak at 2700 $cm^{-1}$ could be attributed to the C-H stretching with a charged nitrogen as the quaternary ammonium[7]. In addition, the O-H stretching of water at 3400 $cm^{-1}$ could be related to more hydrophilic system[36,39]. Both signals suggested the reaction was successful. The changes in intensity of the other peak could be related to experimental measurement factors.

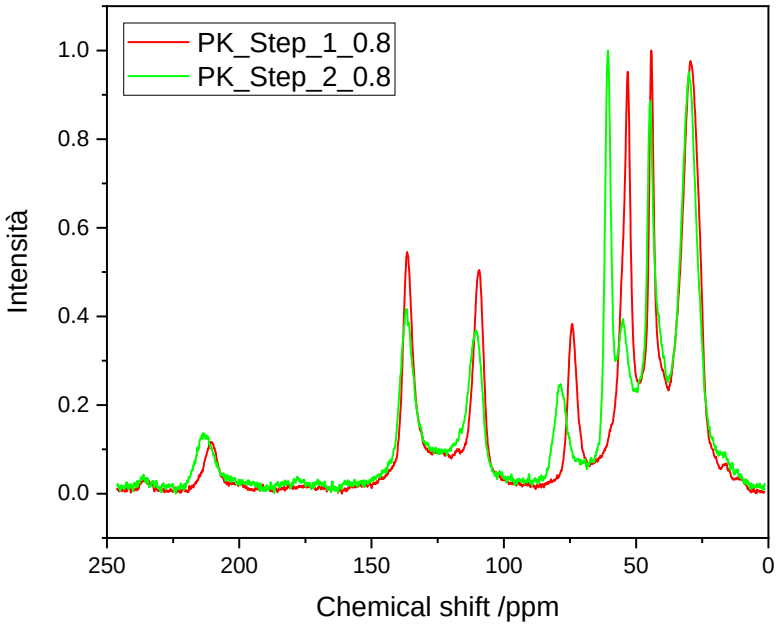


*Figure 3-19 - $^{13}$C-CP-MAS of step_1_0.8 and step_2_0.8*

The figure 19, the NMR spectra of Step_1_0.8 and Step_2_0.8 were reported. The main changes were detected in 100-10 ppm zone: a left-shift to higher magnetic fields of the diamine signals were noticed. This fact was compatible with the formation of quaternary ammonium group in the structure, confirming the success of the reaction[40]. The change in intensity of pyrrole signals was probably due to a different efficiency in $^{1}$H-$^{13}$C cross-polarization experiments[38].

The figure 20 showed the comparison of TGA curves in air of PK_pristine, Step_1_0.8 and Step_2_0.8.

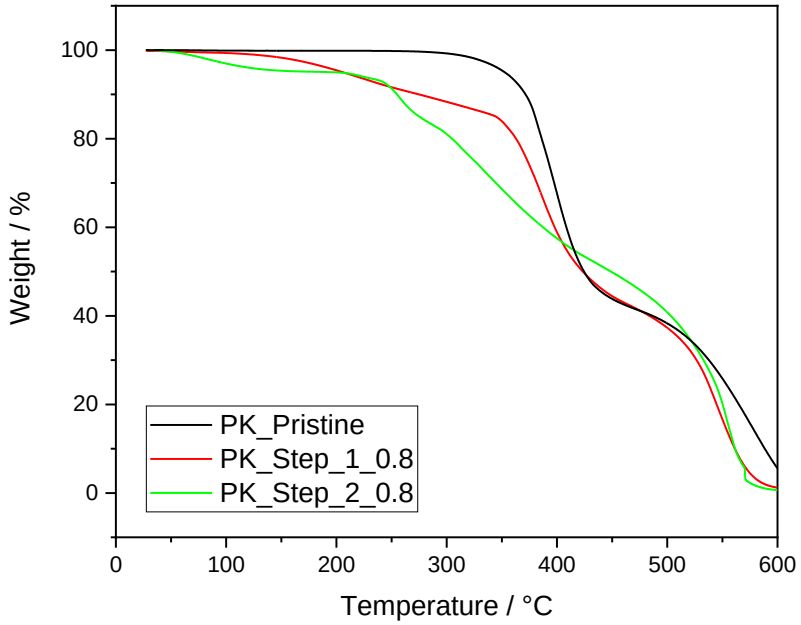


*Figure 3-20 – TGA curves of step_1_0.8 and step_2_0.8*

The step_1 showed a flat zone below 100°C, then a first loss of 14.5% from 100°C to 340°C followed by a multi-step degradation similar to PK profile. The first loss could be correlated to diamine degradation. In step_2 showed a first loss below 100°C and a flat zone since to 206°C. After that, a first degradation step was detected between 200°C and 400°C, probably due to the degradation of the amine, while the subsequent step was attributed to the oxidation of the polymer chains as for the PK thermal profile. It's possible notice that after completely functionalization the ammine-based system increased the thermal stability[38].

The figure 21 and 22 showed the DSC experiments for Step_1_0.8 and Step_2_0.8.

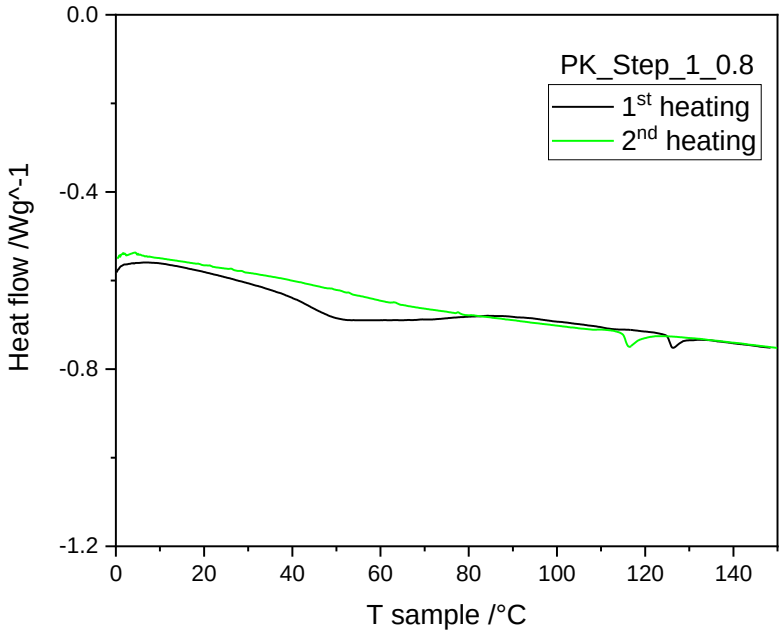


*Figure 3-21 - DSC curve of Step_1_0.8*

In the first heating cycle of step_1, there were a very wide endothermic signal from 20°C to 80°C followed by a net variation of baseline at 125°C that was attributed to the glass transition of the polymer. During the second heating cycle, the glass transition was detected at 115°C. In the first heating cycle of step_2, there was a very wide endothermic signal from 20°C to 140°C that could be correlated to the coordinating water of the quaternary ammonium. During the second heating cycle, a glass transition was detected at 120°C. These value of glass transition were in line with similar system in literature[22,23].

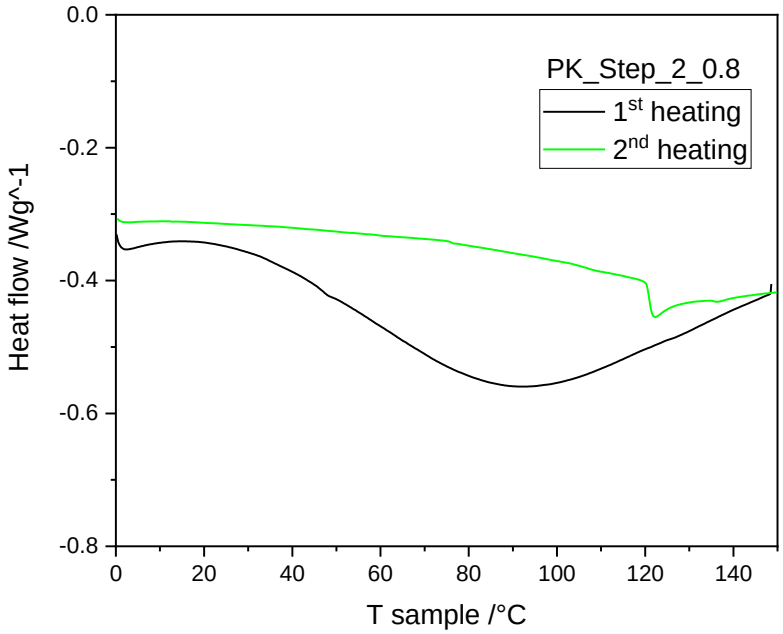


*Figure 3-22 - DSC curve of Step_2_0.8*

On the three methylated polymers (step_2), I determinate the IEC and then calculated the functionalization yield.

| | PK_Step_2_0.6 | PK_Step_2_0.8 | PK_Step_2_1.0 |
|---|---|---|---|
| IEC (mmol*g$^{-1}$) | 1,56 | 1,65 | 1,67 |
| Theorical IEC (mmol*g$^{-1}$) | 3,98 | 3,36 | 2,90 |
| % functionalization | 39,3 | 49,2 | 57,4 |

$$Maximun\ IEC = \frac{n\ (mmol)}{mass\ (g)} = \frac{\frac{mass\ (g)}{MW\ (g\ mol^{-1})} * 1000}{mass\ (g)} = \frac{1000}{MW\ (g\ mol^{-1})}$$

$$= \frac{1000}{297.8\ (g\ mol^{-1})} = 3.36\ \frac{mmol}{g}$$

$$\%\ functionalization = \frac{1.65\ (\frac{mmol}{g})}{3.36\ (\frac{mmol}{g})} * 100 = 49.2\ \%$$

The values obtained were good and promising for fuel cell and electrolyzer applications. These values were similar to those reported for pyrrole-based system[9,25,31]. I could conclude that this functionalization allows to obtain anionic conducting polymers with good IEC values which were potentially useful for applications in AEMFC and AEMWE. In addition, these materials could be generated in few steps, working in mild conditions and with a relative low-cost material.

### 3.2.2 – Poly(ethyl-furan-ketone)

The furan derivatives could be produced by reacting 1,4-diketones unit with an acid or a dehydrating agent. The acid charges the carbonyl group's oxygen making its carbon more electrophilic, facilitating the ring closure while, the dehydrating agent helps to eliminate the water that was formed as a secondary product[12,29].

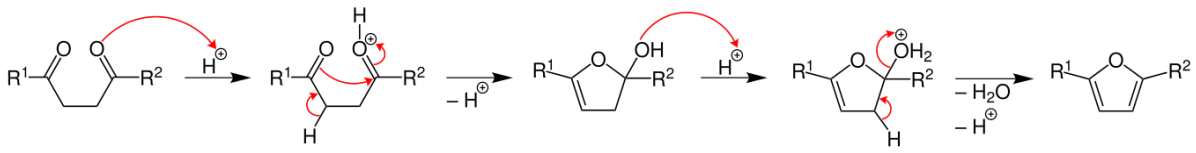


*Figure 3-23 - Pall-Knorr mechanism for furan derivates*[41]

The advantage of this modification is due to the introduction of the furan unit in the polymer backbone[42]. This ring has an intermediate thermal stability between pyrrole and thiophene and, in addition, its slightly aromatic behavior makes its double bonds available for further functionalization e.g. the cycloaddition[12,43]. As in the case of pyrrole, if the appropriate combination of reagents is chosen, I could create an anionic conducting polymer in a few steps.

I reported the exploration and the improvement of a new synthesis method of Poly(ethyl-furan-ketone) and then, I showed my initials functionalization of furan-based derivates thank to Diels-Alder reaction.

#### *3.2.2.1 – Synthesis of Furan derivates*

##### 3.2.2.1.1 - Synthesis overview

The reaction was performed by using several methods which involve phosphoric anhydride ($P_2O_5$) as dehydrating agent combined with different organic solvent[28] and also sulfuric acid. The combinations showed were $P_2O_5$ in dichlorobenzene (Step_1_DCB), $P_2O_5$ in m-cresol (Step_1_mC) and concentrated sulfuric acid (Step_1_$H_2SO_4$). The Step_1_DCB and Step_1_$H_2SO_4$ were heterogenous processes in which the poly(ethyl-ketone) was used as small pieces, while for the Step_1_mC, the polymer was dissolved before the modification.

*Step_1_DCB*

The polyketones pieces and 125 % mole excess of $P_2O_5$ were placed in a balloon, ortho-dichlorobenzene was added[28] and three washing nitrogen-vacuum were performed to reduce the moisture in the reaction environment. After that, the reaction mixture was heated up to 110°C under magnetic stirring for 24 hours. The polymer was recovered by filtration and washed with 5% $NaHCO_3$ solution to remove the acidity of the phosphoric acid produced during the process. Finally, the polymer was dried in vacuum at 100°C.

*Step_1_mC*

The polyketones pieces and m-cresol were placed in a balloon and heated up to 50°C under stirring until the completely polymer dissolution. Then sequentially, 125 % mole excess of $P_2O_5$ was added, three washing nitrogen-vacuum were performed and, after that, the reaction mixture was heated up to 110°C under magnetic stirring and let to react for 24 hours. The resulting reaction mixture was placed into a separating funnel and washed with 5% $NaHCO_3$ solution to remove the acidity of the phosphoric acid. This operation was carried out until the neutrality of the aqueous washing solution was reached. Then, the organic phase was dripped into diethyl ether and centrifuged (9000 rpm for 5 minutes) in order to recover the product. Finally, the polymer was recovered and dried in vacuum at 100°C.

*Step_1_ $H_2SO_4$*

The polyketones pieces were placed in a balloon and then sulfuric acid was added to cover the sample. The solution was kept under magnetic stirring at room temperature for 24 hours. After that,

the reacting solution was poured in water and the product was recovered and washed with 5% $NaHCO_3$ solution basic water to eliminate excess of acid. Finally, the polymer was dried in vacuum at 100°C. I chose the sulfuric acid because it is dehydrating strong acid and could be removed easily by water washing.

#### 3.2.2.1.2 – Following the synthesis

*Step_1_DCB*

As exploratory analysis, I performed FTIR and NMR spectroscopies on the PK_Step_1_DCB.

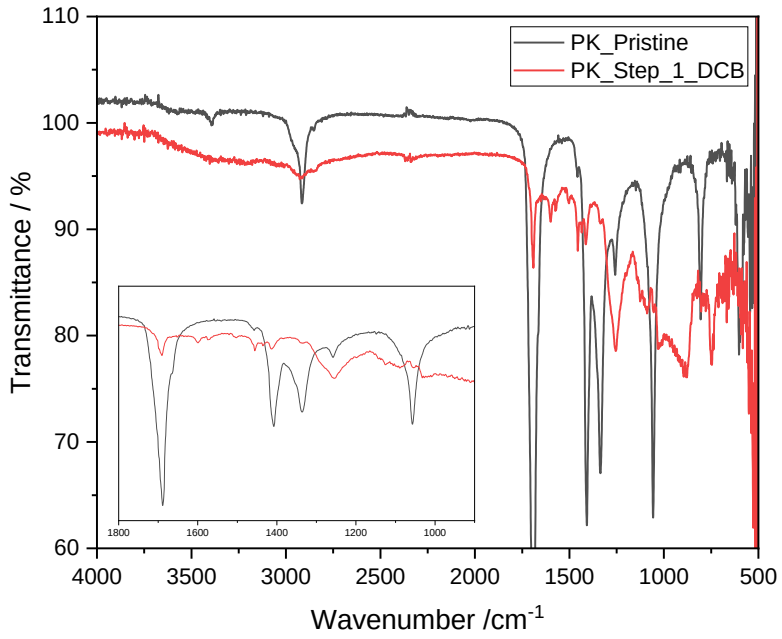


*Figure 3-24 - IR spectra PK and Step_1_DCB*

In figure 24, step_1_DCB showed the main PK peaks and also new signals. The signal at 1602, 1503, 1575 and 1458 $cm^{-1}$ were attributed to the aromatic rings: the first two correspond to the stretching of C=C whereas, the others were assigned to the bending of C=C-C[8,11]. At 1412 $cm^{-1}$ the bending of $CH_2$ groups was detected, while the signal at 1255 $cm^{-1}$ was the overlap of the twisting of $CH_2$ groups of PK and the in-plane deformation of the C-H of furan ring[42]. The signals of C-O-C symmetrical stretching at 1124 $cm^{-1}$, the out-of-plane deformation of the C-H of the aromatic ring at 947 $cm^{-1}$ and the C-Cl bond of the solvent at 753 $cm^{-1}$ were detected[7]. The CO signal at 1670 $cm^{-1}$ reduced after reaction. From these data, the reaction was carried out but traces of solvent were confirmed.

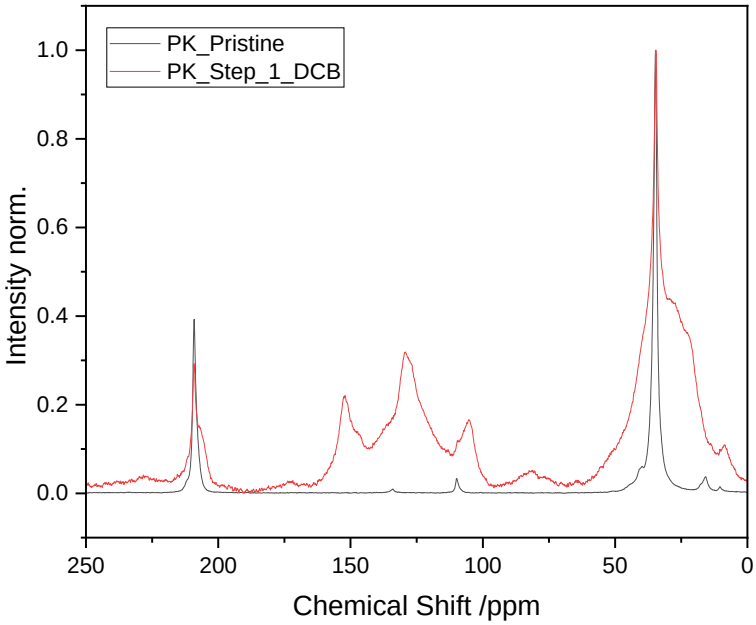


*Figure 3-25 - NMR spectra of PK and PK_Step_1_DCB*

The $^{13}$C-CPMAS NMR spectrum showed the PK signals at 210 and 35 ppm but also three new peaks in the 180-100 ppm zone. The signals at 105 and 152 ppm could be attributed to the carbon atoms of the furanic units, while the central signal at 129 ppm to the dichlorobenzene. In fact, the solvent generated three signals at 128.6, 128.3 and 130 ppm as reported in literature[19]. In addition, the changes of C=O signal at 210 ppm were negligible. This suggested that the reaction occurred, but, unfortunately, in the outer layers due probably to the low solvent permeation in the polymer. For these, I stopped this synthesis route.

*Step_1_mC*

I performed FTIR and NMR spectroscopies on the PK_Step_1_mC.

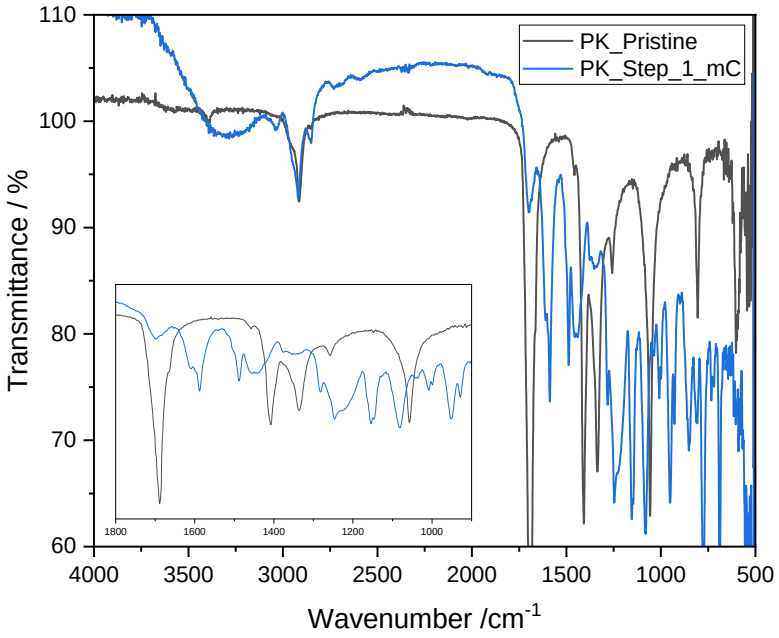


*Figure 3-26 - IR spectra PK and Step_1_mC*

In the figure 26, the step_1_mC showed the main signals of PK, e.g. C-H stretching and bending. The O-H stretching at 3300 $cm^{-1}$, the C-H stretching at 3030 $cm^{-1}$ and the C-O stretching at 1250 $cm^{-1}$ were associated to the m-cresol[19]. In adding, the peaks observed at 1612, 1588 and 1486 $cm^{-1}$ could be correlated to C=C stretching bonds of the solvent or to furanic units[11]. Finally, the C-O-C stretching of the furanic ring and the C-H out-of-plane bending were found at 1150 and 852 cm-1, respectively[7]. The CO signal at 1670 $cm^{-1}$ reduced, but a large quantity of solvent were found inside the sample.

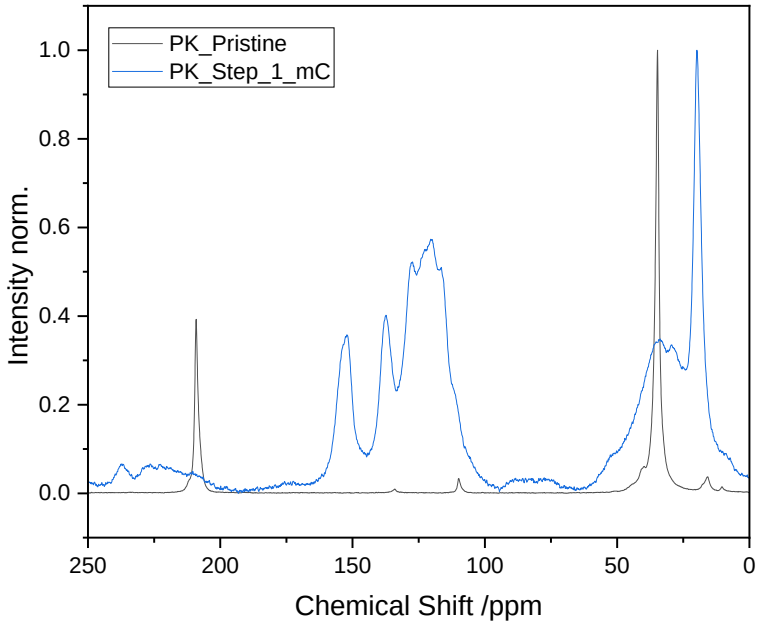


.

*Figure 3-27 – NMR spectra of PK and PK_Step_1_mC*

The $^{13}$C-CP MAS spectrum showed the presence of new signals in 180-100 ppm and 50-10 ppm zones. The peaks at 20 and 29 ppm were assigned to the methyl group of m-cresol and to the $CH_2$ group near the new furanic units, respectively. The expected peaks of furan at 150 and 105 ppm were partially covered by those of m-cresol, confirming the not negligible presence of solvent in the products. The NMR spectrum showed a significant decrease of polyketones signals but the solvent was still inside the polymers. After several treatments, I was unable to eliminate the traces of solvent, so, I decided to stop this synthesis route.

*Step_1_ $H_2SO_4$*

I performed FTIR and NMR spectroscopies on the PK_Step_1_ $H_2SO_4$.

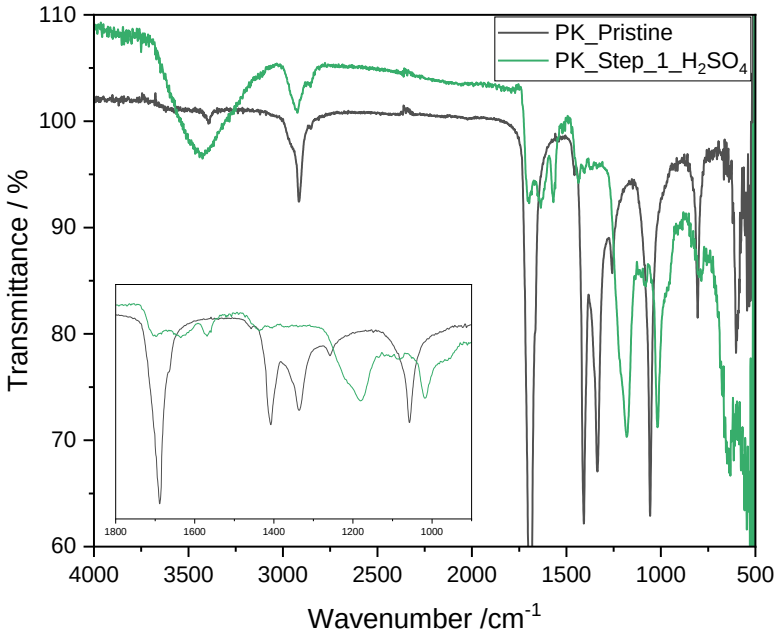


*Figure 3-28 - IR spectra PK and Step_1_$H_2SO_4$*

The IR spectra showed the main PK signals C-H stretching of -$CH_2$- at 2923 $cm^{-1}$ and the C=O stretching at 1690 $cm^{-1}$ [7,8]. The new peaks at 1637 and 1505 $cm^{-1}$ were attributed to C=C stretching, while those at 1567 and 1435 $cm^{-1}$ were attributed to bending modes. The stretching of C-O-C and the "breathing" of the furanic ring were observed at 1182 and 1015 $cm^{-1}$, respectively[8,42]. This spectrum was clearer than others step_1 spectrum. Also in this case, The reduction of CO signal at 1670 $cm^{-1}$ was revelated.

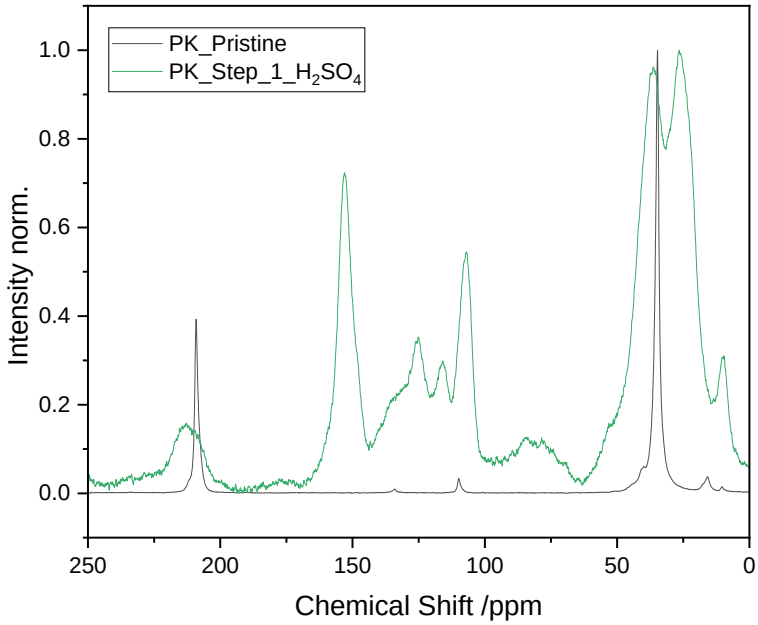


*Figure 3-29- NMR spectra of PK and PK_Step_1_$H_2SO_4$*

In the $^{13}$C-CP-MAS showed the signals of PK at 34 and 209 ppm and new signal in 180-100 ppm and 50-10 ppm zones due to furan formation[19]. There was also detected a wide signal at about 85 ppm. The signals of furan were visible at 150 and 105 ppm and the reduction of CO signal at 210 ppm was reelevated. Considering the IR and NMR spectra obtained, this step seemed much more promising than the others, consequently, I performed a more accurate NMR attributions and also quantitative $^{13}$C-NMR analysis. As support, I generated the theorical spectrum using NMRDB.org website[14–16].

To better understand the structure and its signals, I generated three possible theorical structure. Usually the stability of a furan increases with the degree of substitution, consequently, I could hypothesize that the 8% of propyl portion in the polymer could react better than ethyl one. Another consideration was that the oxygen of the furan could be protonated by the sulfuric acid.

Considering the theorical structure 1 (fig. 30), two signals were obtained: one at 148 ppm, corresponding to carbon 2 and 5 and the other at 110 ppm, corresponding to carbon 3 and 4.

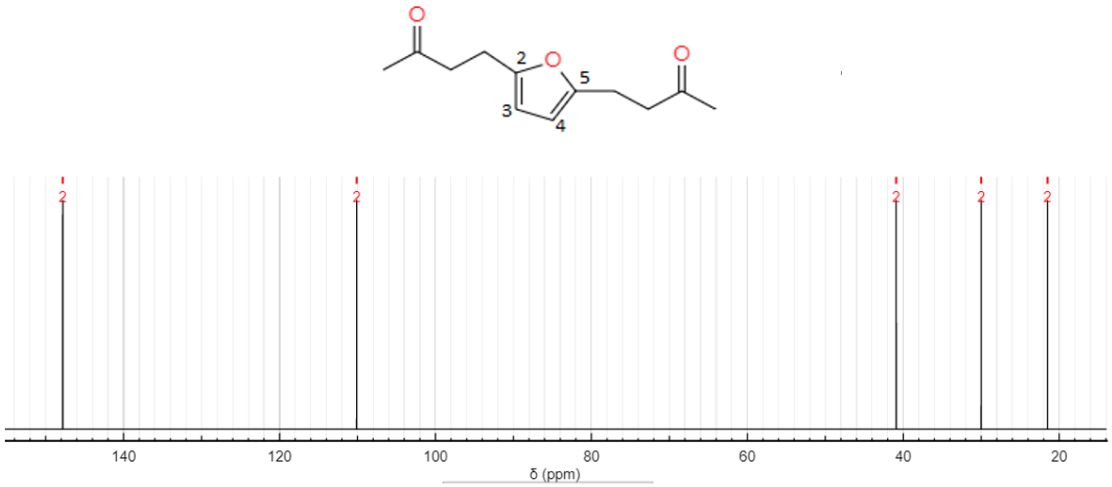


*Figure 3-30 – Poly(ethyl-furan-ketone), theorical structure 1 and its $^{13}C$ spectra*

Considering the theorical structure 2 (fig. 31), the splitting of the signals of the furan units was caused by the methyl group introduction (labeled as Me). Considering the following structure, four signals were obtained: carbon 2 at 152 ppm, carbon 3 at 115 ppm, carbon 4 at 110 ppm and carbon 5 at 153 ppm. The carbon signal of the CH3 group falls instead to 10 ppm, as in the spectrum obtained. The methyl group increased the splitting of the carbon in position 2-5 an 3-4 in the unsaturated zone.

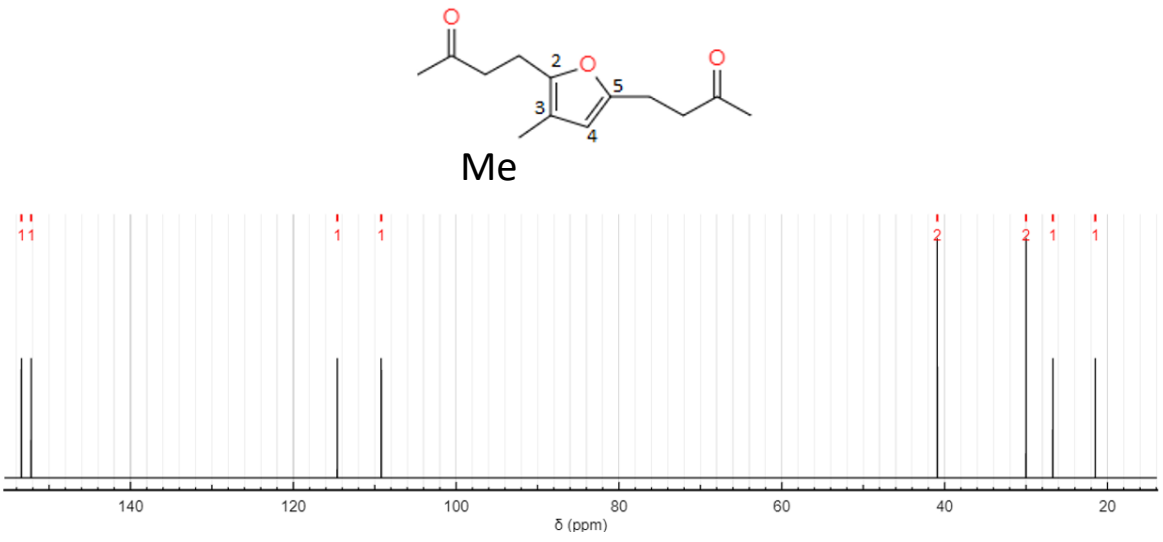


*Figure 3-31 -Poly(ethyl-furan-ketone), theorical structure 2 and its $^{13}C$ spectra*

Considering the theorical structure 3 (fig. 32), The signal at 77 ppm could be explained the acid environment in which the reaction takes place and the presence of a non-delocalized doublet on the furan oxygen that could be protonated. In this case, the carbon 2 and 5 generated the signals at 72 ppm, while the carbon 3 and 4 generated the signals at 124 ppm. So, the effect of the proton presence was the right-shift of the furan signal at lower magnet field[44].

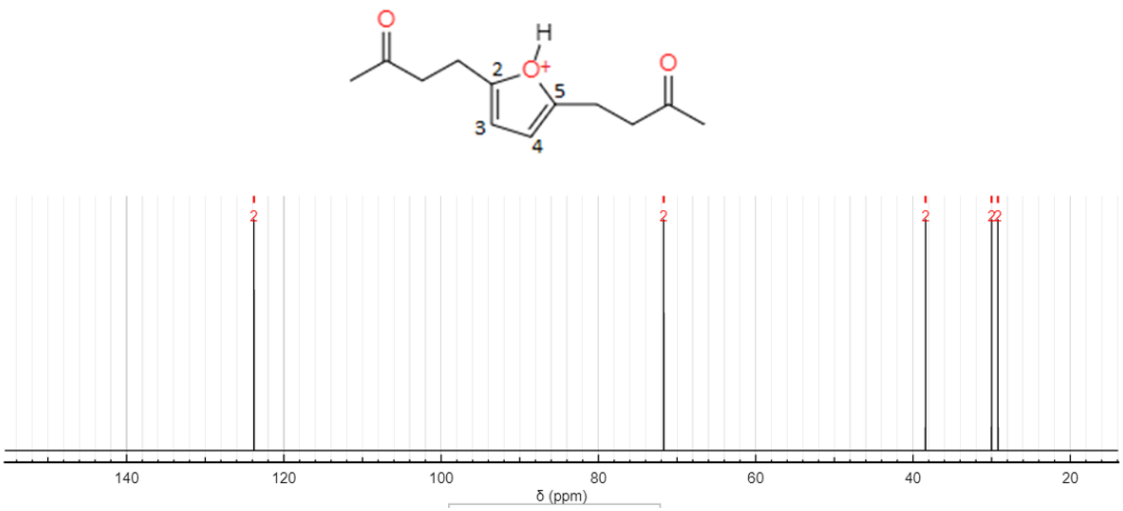


*Figure 3-32 - Poly(ethyl-furan-ketone), theorical structure 3 and its $^{13}C$ spectra*

From the High-Power Decoupling (HPDEC) experiment, I obtained the quantitative information following these steps: at first, I adjusted the baseline of HPDEC data and then I used the best fitting procedure to simulate the experimental profile. From the area of simulated peaks, I evaluated the carbons concentration.

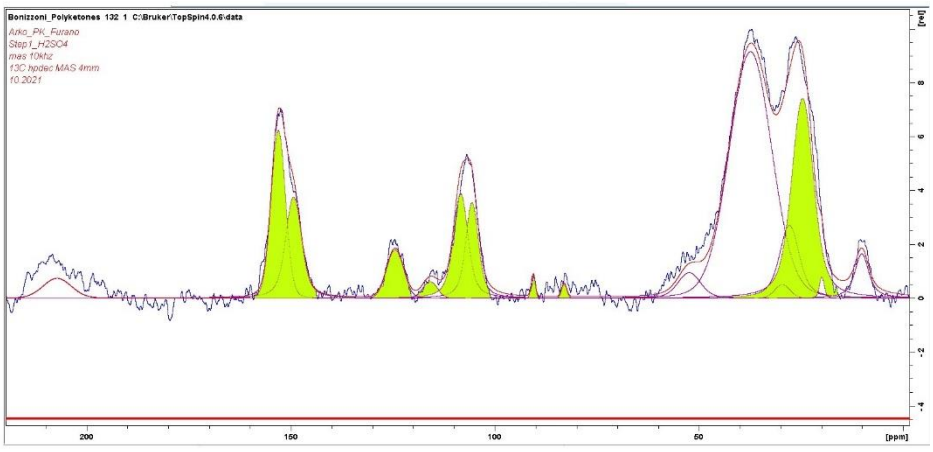

*Figure 3-33 - $^{13}$C-HPDEC of PK_Step_1_$H_2SO_4$ with highlighted in green the main furan signals*

From the best fitting, I produced these data.

| N° | Chemical shift (ppm) | Area |
|---|---|---|
| 1 | 37,4 | 1,12E+09 |
| 2 | 10,1 | 8,49E+07 |
| 3 | 27,9 | 1,80E+08 |
| 4 | 206,6 | 5,84E+07 |
| 5 | 153,0 | 2,51E+08 |
| 6 | 149,3 | 2,05E+08 |
| 7 | 105,6 | 1,55E+08 |
| 8 | 108,4 | 1,91E+08 |
| 9 | 115,9 | 2,45E+07 |
| 10 | 124,4 | 8,35E+07 |
| 11 | 90,6 | 9,34E+06 |
| 12 | 52,4 | 7,18E+07 |
| 13 | 29,6 | 2,35E+07 |
| 14 | 24,6 | 5,32E+08 |
| 15 | 19,9 | 1,26E+07 |
| 16 | 83,0 | 7,73E+06 |

$$\%\ propyl\ signal = \frac{Signal\ at\ 10.1}{Sum\ of\ CH_2\ signals} * 100 = 4.2\ \%$$

$$\%\ protonated\ = \frac{Signal\ at\ 124.4\ and\ 90.6}{Sum\ of\ aromatic\ signals} * 100 = 10.1\ \%$$

The % propyl signal was about 4.2% in good agreement with the one calculated from poly(ethyl-ketone) NMR spectra. I calculated the fraction on protonated ring as the ratio between the signals correlated to charged structure and the total signals for 180-90 ppm zone. This value obtained was 10.1 % that was in line with CHNS result. In addition, the reaction yield was estimated about 60% in good agreement with CHNS.

I continued the characterization of Step_1_ $H_2SO_4$, using TGA, DSC and CHNS analysis.

The TGA curve showed the four degradation steps in air (Fig. 34). The first loss was about 3%, in 30-150°C zone, and could be attributed to the evaporation of the moisture trapped inside the polymer. The second was about 6%, in 150-300°C zone and could be correlated to the decomposition of the aromatic ring. The third and the fourth losses were from 300°C and showed a similar profile to PK curve, so, I could relate them to polyketone degradation. The mass loss in from 300°C to 430°C is about 14%.

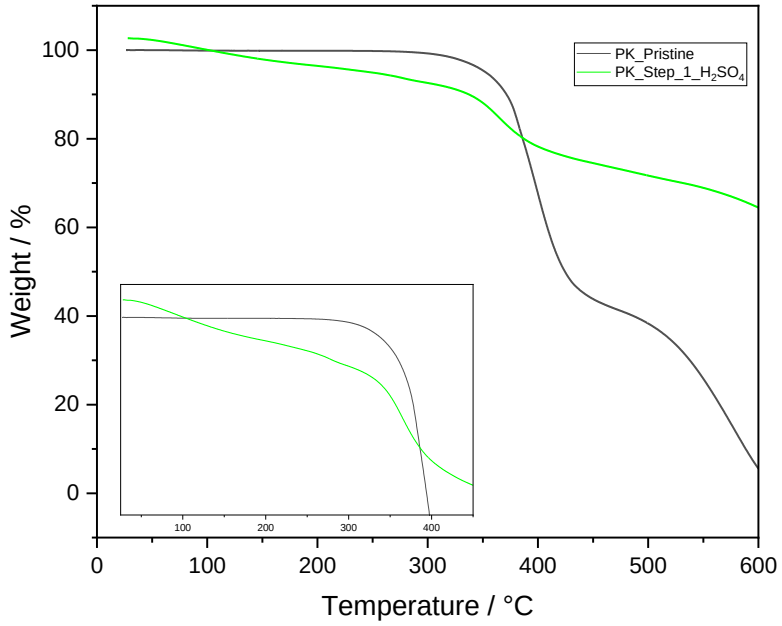


*Figure 3-34 - TGA curves of PK and Step_1_$H_2SO_4$*

In the figure 35, the DSC curve was reported. In the first heating cycle there was a very wide and weak endothermic signal from 40°C to 100°C and then a net variation of baseline was visible at 140°C that was attributed to the glass transition of the polymer. During the second heating cycle, the glass transition was detected at 110°C. This glass transition values were well-known for this poly(ethyl-ketone) derivates. In fact for similar pyrrole-based derivates the Tg were about 70 -80 °C[23,25].

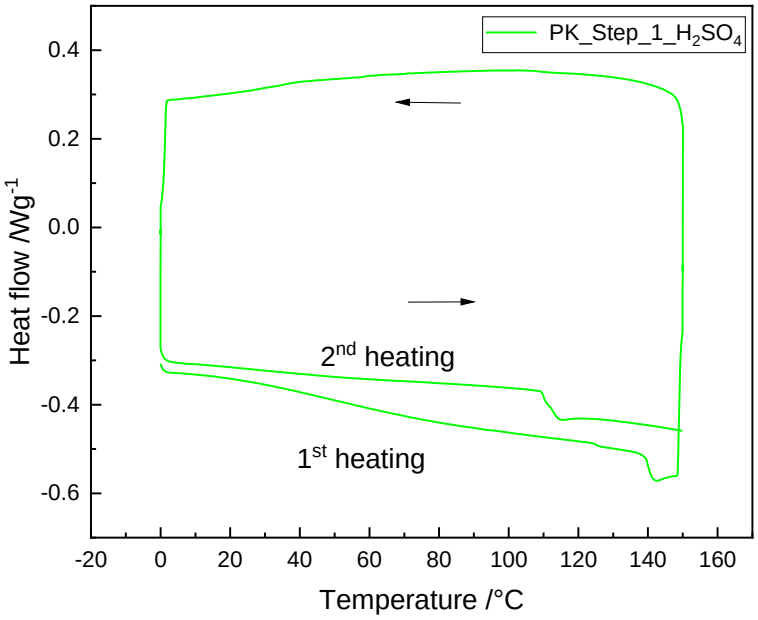


*Figure 3-35 – DSC curve of Step_1_$H_2SO_4$*

From the CHNS analysis, I calculated the yield of Step_1_ $H_2SO_4$ and it was 54.3%.

| CHNS | % C | % H | % N | % S | % O |
|---|---|---|---|---|---|
| Step_1_H2SO4 | 55,51 | 5,231 | 0,00 | 7,185 | 32,07 |
| Step_1_$H_2SO_4$_recalculated | 70,95 | 6,686 | 0,00 | 9,184 | 41,00 |
| Poly(ethyl-ketone) | 64,27 | 7,192 | 0,00 | 0,000 | 28,54 |
| Furan unit | 76,57 | 6,427 | 0,00 | 0,000 | 17,00 |

The data showed a sulphur content of 7.185 % that could be explained with the presence of $HSO_4^-$ as counterion of protonated furan ring according the NMR results. So, I recalculated the percentage of carbon, hydrogen and oxygen removing the % S as $HSO_4$ ion. Then I calculated the yield of this step_1.

$$\%\ yield\ step_1 = \frac{\%\ sample - \%\ PK(ethyl)}{\%\ Furan\ unit - \%\ PK(ethyl)} * 100 = \frac{(71.95 - 64.27)\%}{(76.57 - 64.27)\%} * 100 = 54.3\%$$

This value was in excellent agreement with NMR results. I could conclude that the Step_1_ $H_2SO_4$ could convert the 60% of PK into furan derivates. I used this product the furan derivate modifications, called it simply “step_1”.

### *3.2.2.2 – Furan derivates modification*

In generally, the furan ring has a lower aromatic behavior than pyrrole and thiophene[42]. This fact makes the double bonds present in the ring more available for specific reactions, e.g. Diels-Alder reactions (DA). The DA procedure are 4+2 cycloaddition reactions between a diene and a dienophile, that generate a 6-membered ring with a new double bond[45,46].

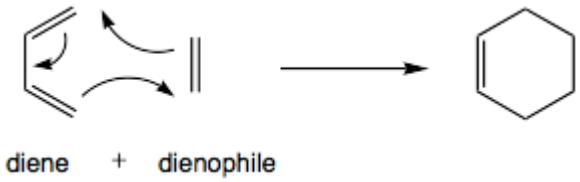


*Figure 3-36 - General scheme or Diels-Alder reactions*[43]

For this modification, I explored the DA reactions to modify the poly(ethyl-furan-ketone) in order to introduce an active site for the anion conducting properties[45,47]. Here, I reported the initials modifications with 1-vinylimidazole thanks to DA reaction.

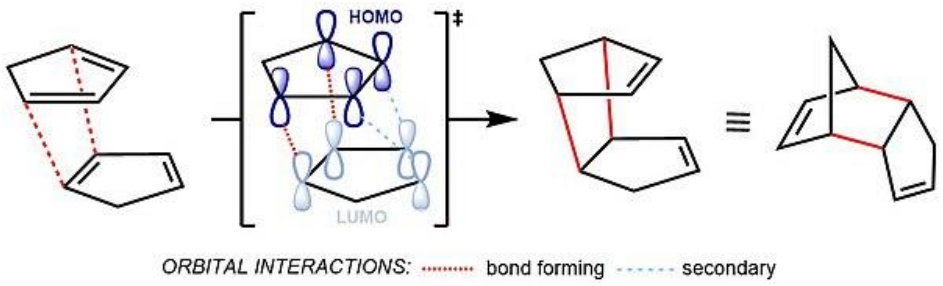


*Figure 3-37 - General scheme or Diels-Alder reactions between two aromatic rings* [43]

#### 3.2.2.2.1 - Synthesis overview

*Step_2*

The step_2 is the Diels-Alder reaction between the poly(ethyl-furan-ketone) with 1-vinylimidazole. The products of Step_1 was placed in a pressurized reaction testing tube and then, 1-vinylimadazole was add to cover the polymer. The tube was closed, heated to 130°C for 3 days. After that, the products were recovered by filtration and washed with ethanol and then dried in vacuum at 80°C.

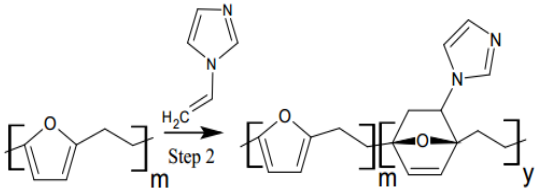


*Figure 3-38 - Scheme of Step_2*

*Step_3*

The step_3 is the methylation process of the free-nitrogen of imidazole ring to obtain charge it giving the anion conducting properties to the polymers. The products of Step_2 was placed in a balloon with a condenser and then, three washing nitrogen-vacuum were performed to reduce the moisture and carbon dioxide in the reaction environment. After that, the iodomethane is added to cover the powder and let react for 15 hours at 40°C in reflux condition and under slowly stirring. Later the products were covered by filtration, washed with abundant water and dried in vacuum at 100°C for 2 hours.

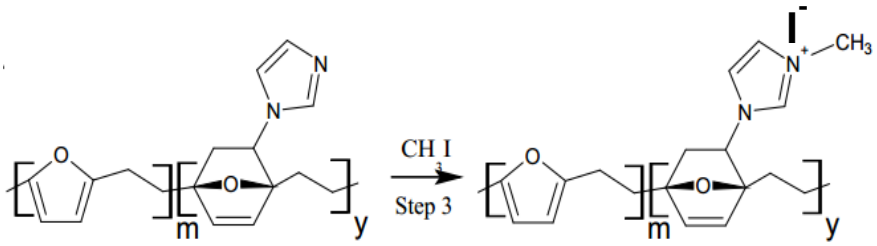


*Figure 3-39 - - Scheme of Step_3*

### 3.2.2.2.2 - Following the synthesis

In order to explore the Diels-Alder, I did the following DSC curves in the thermal stability range of step_1 (below 150°C), with a scan rate of 5°C for minutes. I chose this temperature rate because these conditions were quite similar to the working conditions in the laboratory. The experiments were performed on PK_step_1, 1-vinylimidazole and their mixture 1:2 in moles to guarantee the contact among the chemicals.

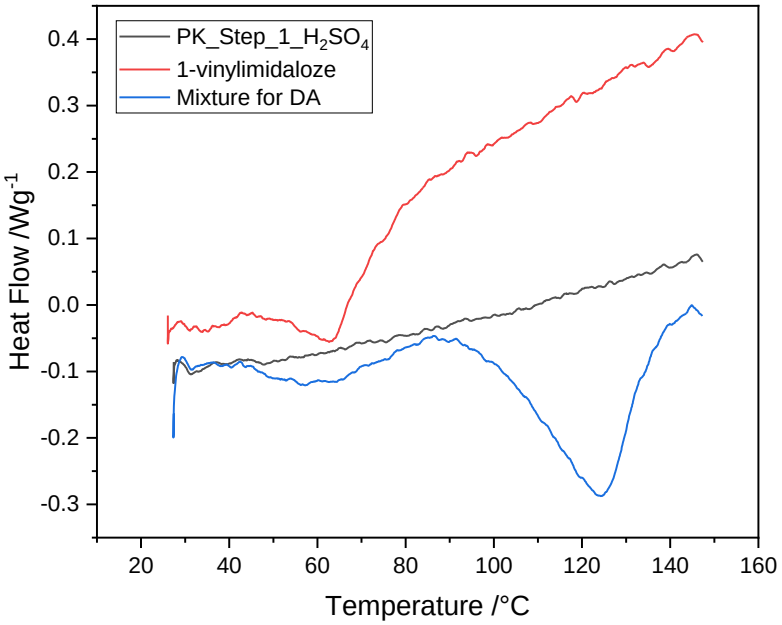


*Figure 3-40 – DSC curve of Step_1, 1-vinylimidazole and the mixture*

The polymer DSC remained quite constant during the experiment while the curve of 1-vinylimidazole showed an endothermic peak from 40°C to 80°C, correlated to moisture. In the mixture, there were the same peak of 1-vinylimidazole followed by a large and more intense endothermic signal from 90°C to 140°C, which could be attributed to the energy variation resulting from the rearrangement of the bonds during the Diels-Alder reaction[46]. From these results, I decided to perform the DA reaction at 130°C corresponding the maximum temperature of the DSC signal.

In figure 41 and 42 the IR spectra of step_2 and step_3 were reported.

In the Step_2 spectrum appeared the characteristic signals of polyketone and furan and, also, new peaks at 3111, 1491, 1223, 1081 and 810 $cm^{-1}$. The signals at 3111 and 1223 $cm^{-1}$ were correlated to the C-H and C-N stretching of the imidazole, while at 1491 $cm^{-1}$ was attributed to the imidazolic ring stretching [19,48]. The peaks at 1081 and 810 $cm^{-1}$ were associated to the bending of the imidazolic ring. Moreover, considering the reduction of the intensity of the furan signals and the absence of the C=C signals of the vinyl group of 1-vinylimidazole at 1647 $cm^{-1}$, I could hypnotize that the successful of reaction.

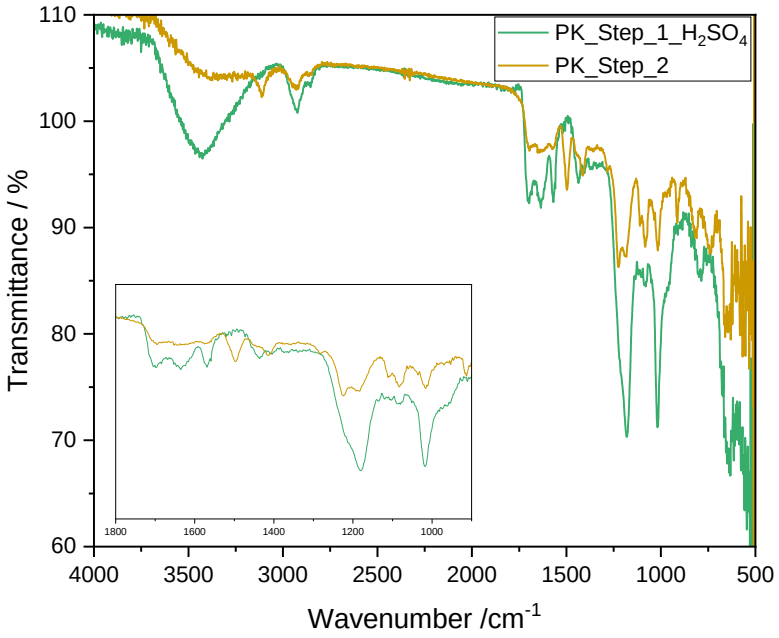


*Figure 3-41 - IR spectra of Step_1 and Step_2*

In the Step_3, it's possible observe peaks of the Diels-Alder product and a new signal at 2963 $cm^{-1}$ that could be attributed to the methylation process of imidazole ring. In adding, there was a more intense water band at 3400 $cm^{-1}$ that also correlated to more hydrophilic structure[7].

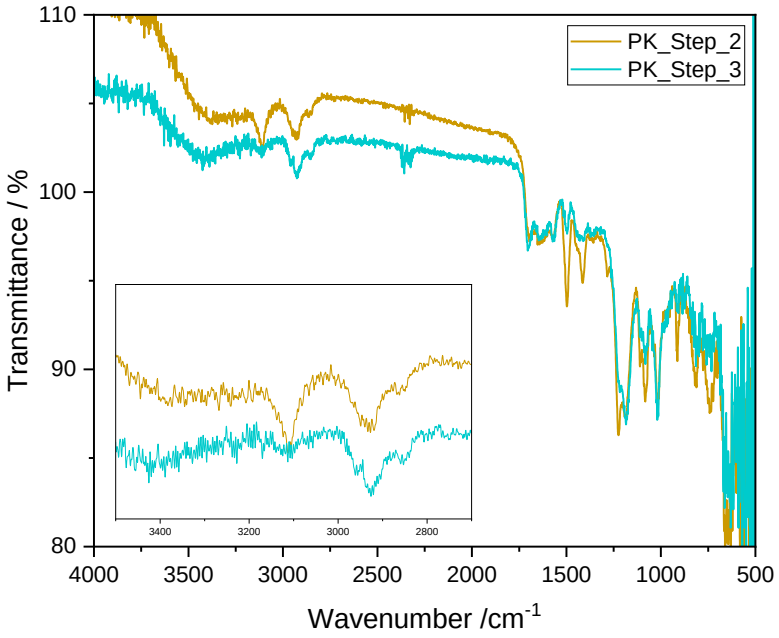


*Figure 3-42 - IR spectra of Step_2 and Step_3*

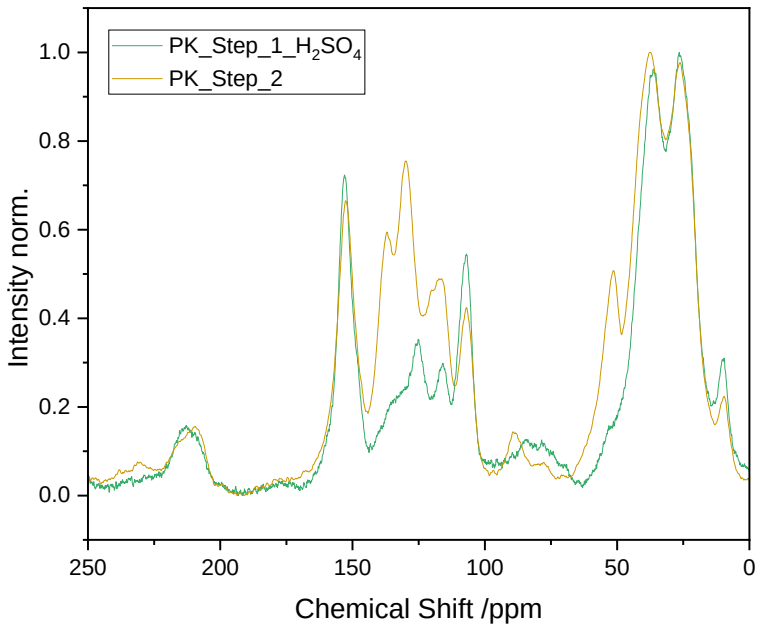


*Figure 3-43 - $^{13}$C-CPMAS NMR spectra of Step_1 and Step_2*

The comparison in figure 43 the NMR spectrum showed the present of new signals at 52, 89, 129 and 136 ppm. The global signal at 34 ppm was more intense, while the furan signals in 180-90 zones were less intense than the step_1. This fact was compatible with the Diels-Alder product because, considering the theorical structure and its spectrum (Fig.44), the step_2 process generated a sp3 carbon (carbon 6) at 31 ppm, new C-N (carbon 5) at 52 ppm and two quaternary carbon (1 and 4) at 89 ppm. The signals at 136, 130, 119 ppm could be correlated to the carbon 9,8,7 of the imidazole, while the carbons 2 and 3 generated at signals about 160 ppm.

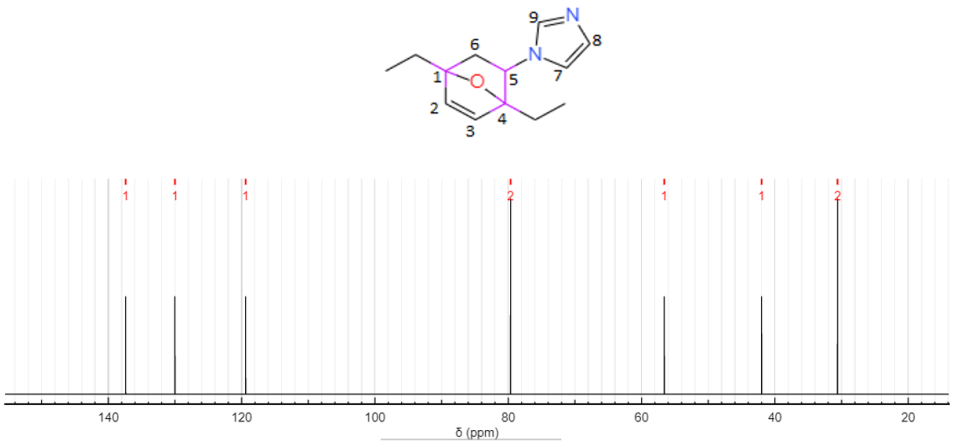


*Figure 3-44 – Structure of the step_2*

In addition, the characteristic signal of the vinyl group at 101 ppm was absent[19,48]. I could conclude that imidazole was connected with the furan-based derivate.

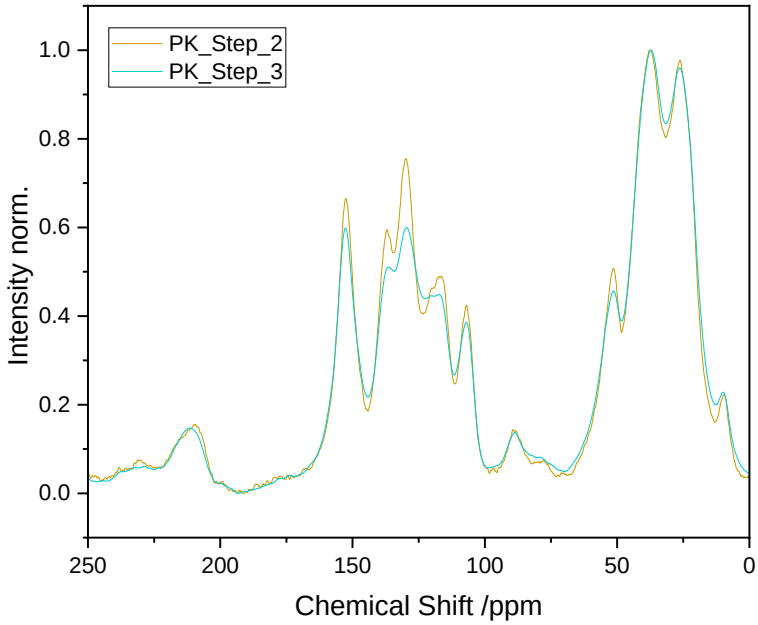


*Figure 3-45 $^{13}$C-CPMAS NMR spectra of Step_2 and Step_3*

The methylation process could generate some chemical shift in in the signals of imidazole due to the insertion of a positive charge. The Step_3 showed the same signals of step_2. The only different in intensity were found for the peak at 50 ppm and in the zone from 150 ppm to 100 ppm. This different could be attributed to methylation process, but to confirm the successful of the process, I needed further results.

The TGA curves in air were reported in figure 46.

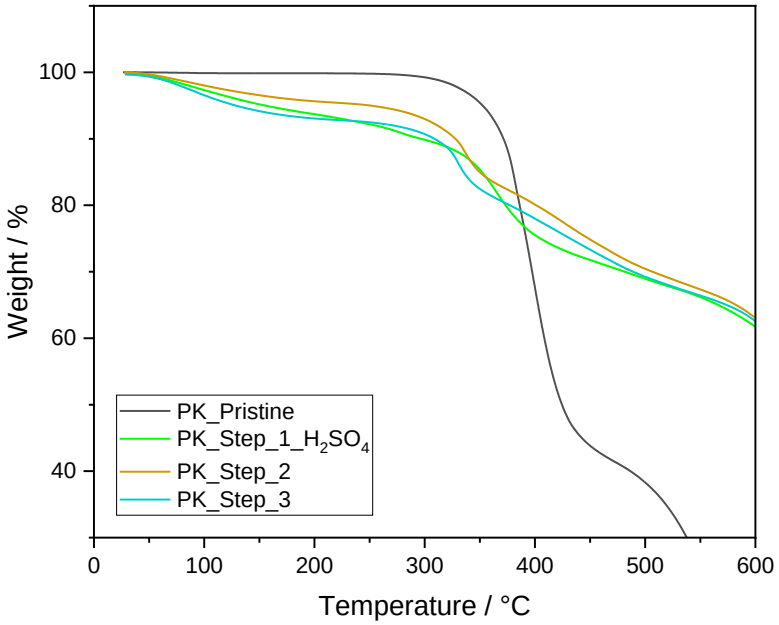


*Figure 3-46 - TGA curves of Step_1 products*

The three TGA curve showed the same behavior and, unfortunately, with these data, I couldn't to determine the success of the processes. However, it is possible observe some changes in the thermal stability of the polymer during the steps in the 250-350°C zone[49].

In figure 47 and 48 the DSC curves of step_2 and step_3.

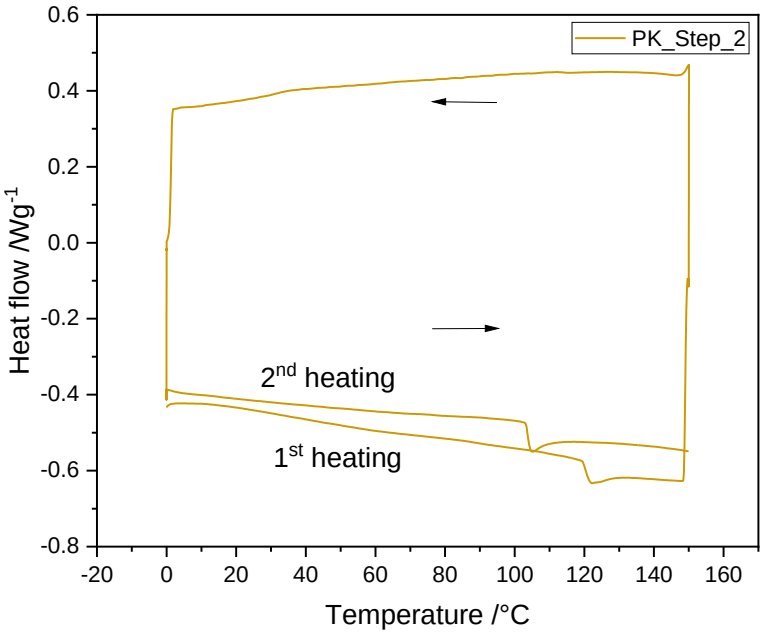


*Figure 3-47 - DSC curve of Step_2*

The step_2 curve showed a glass transition at 120°C in the first cycles and at 105°C in the second heating cycle. Indeed, the step_3 showed in the first heating scan a very broad not-reversible endothermic peak from 20 to 140°C and a small variation in the profile that could be correlated to a glass transition. In the second scan, the Tg was noticed at 105°C. These value of glass transition were in line with similar system in literature[22,23].

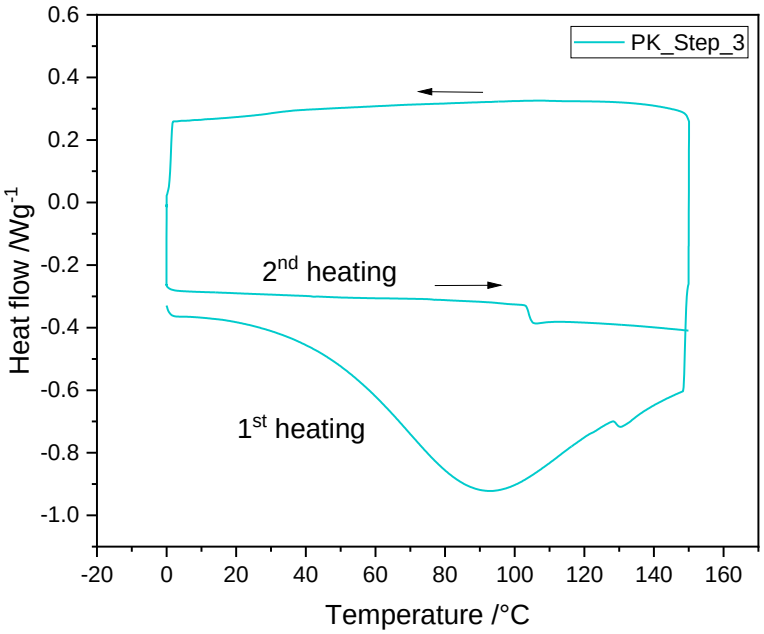


*Figure 3-48 DSC curve of Step_3*

The final product IEC was 0.08 meq*g$^{-1}$, with a global functionalization yield of 2.7%.

$$Maximun\ IEC = \frac{n\ (mmol)}{mass\ (g)} = \frac{\frac{mass\ (g)}{MW\ (g\ mol^{-1})} * 1000}{mass\ (g)} = \frac{1000}{MW\ (g\ mol^{-1})}$$

$$= \frac{1000}{300.1\ (g\ mol^{-1})} = 3.03\ \frac{mmol}{g}$$

$$\%\ functionalization = \frac{0.08\ (\frac{mmol}{g})}{3.03\ (\frac{mmol}{g})} * 100 = 2.7\ \%$$

This value of IEC explained the minimum variation between the step_2 and step_3 IR and NMR spectra.

Although this IEC value is very low and not suitable for fuel cell applications, this demonstrates the feasibility of this synthesis route. For this procedure the bottleneck step was the Diels-Alder

reaction. To improve this step, it's possible use a dienophile which had more electrophilic groups. This consideration will be investigated in further works.

## 3.3 – Chapter conclusion

I reported my initial functionalization of a commercial polyketones thanks to the Pall Knorr reaction in order to obtain anionic conducting polymer for fuel cell and electrolyzer application. This reaction allows to introduce a heteroatom aromatic ring inside the polymer chain, modifying for example its mechanical and thermal properties. Here, I reported my initial investigation and studies of pyrrole-based and furan-based polymer systems.

For pyrrole-based polymer, the synthesis procedure involved the reaction of polyketone with a primary-ternary diamine. In the first step, the primary nitrogen was used for the formation of the pyrrole ring thanks to the Pall Knorr reaction, and then, in the secondary step, the ternary nitrogen was methylated in order to obtain a quaternary ammonium conductive polymer. In the first phase, I investigated the effect of time on the reaction yield to identify an optimal process duration and then I studied the effect of the different diamine stoichiometry and the properties of the pyrrole-derivates. The best result was for the 57,4 % functionalized pyrrole-based polymers with an IEC of 1.67 meq*$g^{-1}$. The advantages of this reaction are related to the possibility of obtaining a conductive polymer in only two steps, working in mild conditions and with a relative low-cost material.

For furan-based polymers, the synthesis procedure involved two steps. In the first, furan-based derivatives were obtained by reaction of Pall-Knorr, then, in secondary step, I functionalized them through the Dials-Alder reaction, introducing the active site with an appropriate dienophilic. In the first phase I studied and developed a new method for obtaining funanic derivatives, using sulfuric acid. This procedure doesn't employ of organic solvents making it more sustainable and greener. In the second phase, I investigated the functionalization of the furanic derivate thanks to Diels-Alder reaction, using 1-vinylimidazole. In step_2 the DA product was prepared and then, in the step_3, the imidazole ring was methylated making the polymer conductive. The obtained polymer showed an IEC of 0.08 meq*$g^{-1}$ and, although it was low, it demonstrated the feasibility of this synthesis route. The advantages of this process are related to the possibility of using low-cost reagents that can be recycled (e.g. by distillation), making it an economic and potentially scalable process. Although the development of these polymers was still under development, both methods were

interesting and offered potentially useful advantages for the development of anion exchange polymers for fuel cell and electrolyzer applications. Further studies will be carried out in the future in order to optimize these processes.

## Bibliography


1. AKRO-PLASTIC. *AKROTEK® PK-HM Natural (7536)*.; 2022.
2. Sommazzi A, Garbassi F. Olefin-carbon monoxide copolymers. *Prog Polym Sci*. 1997;22(8):1547-1605. doi:10.1016/S0079-6700(97)00009-9
3. Nozaki K, Ito S. *Alkene/CO Copolymerization*. Vol 3. Elsevier B.V.; 2012. doi:10.1016/B978-0-444-53349-4.00086-8
4. Data RUSA. United States Patent (19). 1996;(19).
5. Shkrabo DM, Zhizhin GN, Kuzik LA, Garbuzova IA. Ethylene - carbon monoxide copolymer ('Carilon') vibrational spectra and study of nanometer films on gold covered substrate. *Vib Spectrosc*. 1998;17(2):155-162. doi:10.1016/S0924-2031(98)00023-X
6. Couture G, Alaaeddine A, Boschet F, Ameduri B. Polymeric materials as anion-exchange membranes for alkaline fuel cells. *Prog Polym Sci*. 2011;36(11):1521-1557. doi:10.1016/j.progpolymsci.2011.04.004
7. Millipore Sigma. IR Spectrum Table. *Millipore Sigma*. 2020:1-18. https://www.sigmaaldrich.com/technical-documents/articles/biology/ir-spectrum-table.html.
8. Spectral Database for Organic Compounds SDBS. https://sdbs.db.aist.go.jp/sdbs/cgi-bin/cre_index.cgi.
9. Ataollahi N, Girardi F, Cappelletto E, et al. Chemical modification and structural rearrangements of polyketone-based polymer membrane. *J Appl Polym Sci*. 2017;134(44):1-8. doi:10.1002/app.45485
10. Cho S, Lee JS, Jang H, Park S, An JH, Jang J. Comparative studies on crystallinity, thermal and mechanical properties of polyketone grown on plasma treated cvd graphene. *Polymers (Basel)*. 2021;13(6):1-15. doi:10.3390/polym13060919
11. Silverstein RM, Webster FX, J. Kiemle D. *Identificazione Spettrometrica Di Composti Organici*.
12. Loudon M. *Chimica Organica*.; 2010.
13. Koenig JL. *Spectroscopy of Polymers*. Elsevier Science doi:https://doi.org/10.1016/B978-0-

444-10031-3.X5000-2

14. Banfi D, Patiny L. www.nmrdb.org: Resurrecting and processing NMR spectra on-line. *Chimia (Aarau)*. 2008;62(4):280-281. doi:10.2533/chimia.2008.280

15. Castillo AM, Patiny L, Wist J. Fast and accurate algorithm for the simulation of NMR spectra of large spin systems. *J Magn Reson*. 2011;209(2):123-130. doi:10.1016/j.jmr.2010.12.008

16. Aires-de-Sousa J, Hemmer MC, Gasteiger J. Prediction of 1H NMR chemical shifts using neural networks. *Anal Chem*. 2002;74(1):80-90. doi:10.1021/ac010737m

17. De Vito S, Ciardelli F, Benedetti E, Bramanti E. Thermal phase transitions of carbon monoxide-ethylene alternating copolymer: An FT/IR study. *Polym Adv Technol*. 1997;8(2):53-62. doi:10.1002/(SICI)1099-1581(199702)8:2<53::AID-PAT616>3.0.CO;2-T

18. Ohsawa O, Lee KH, Kim BS, Lee S, Kim IS. Preparation and characterization of polyketone (PK) fibrous membrane via electrospinning. *Polymer (Guildf)*. 2010;51(9):2007-2012. doi:10.1016/j.polymer.2010.02.045

19. National Institute of Standards and Technology. NIST Chemistry WebBook.

20. Lagaron JM, Powell AK, Davidson NS. Characterization of the structure and crystalline polymorphism present in aliphatic polyketones by Raman spectroscopy. *Macromolecules*. 2000;33(3):1030-1035. doi:10.1021/ma990302p

21. Chukanova OM, Shul'Ga YM, Belov GP. Alternating copolymerization of ethylene with carbon monoxide on a supported palladium catalyst. *Polym Sci - Ser B*. 2009;51(7-8):283-290. doi:10.1134/S1560090409070112

22. Nawn G, Vezzù K, Cavinato G, et al. Opening Doors to Future Electrochemical Energy Devices: The Anion-Conducting Polyketone Polyelectrolytes. *Adv Funct Mater*. 2018;28(29):1-10. doi:10.1002/adfm.201706522

23. Ataollahi N, Vezzù K, Nawn G, et al. A Polyketone-based Anion Exchange Membrane for Electrochemical Applications: Synthesis and Characterization. *Electrochim Acta*. 2017;226:148-157. doi:10.1016/j.electacta.2016.12.150

24. Zhou YC, Zhang ZM, Zhou L, et al. Imidazole-functionalized polyketone-based polyelectrolytes with efficient ionic channels and superwettability for alkaline polyelectrolyte fuel cells and

multiple liquid purification. *J Mater Chem A*. 2021;9(26):14827-14840. doi:10.1039/d1ta03460j

25. Nawn G, Vezzù K, Cavinato G, et al. Opening Doors to Future Electrochemical Energy Devices: The Anion-Conducting Polyketone Polyelectrolytes. *Adv Funct Mater*. 2018;28(29). doi:10.1002/adfm.201706522

26. Jung YS, Canlier A, Hwang TS. An efficient and facile method of grafting Allyl groups to chemically resistant polyketone membranes. *Polymer (Guildf)*. 2018;141:102-108. doi:10.1016/j.polymer.2018.03.007

27. Zehetmaier PC, Vagin SI, Rieger B. Functionalization of aliphatic polyketones. *MRS Bull*. 2013;38(3):239-244. doi:10.1557/mrs.2013.49

28. Jiang Z, Sanganeria S, Sen A. Polymers incorporating backbone thiophene, furan, and alcohol functionalities formed through chemical modifications of alternating olefin–carbon monoxide copolymers. *J Polym Sci Part A Polym Chem*. 1994;32(5):841-847. doi:10.1002/pola.1994.080320505

29. Clayden J, Greeves N, Warren S. *Organic Chemistry*. Second edi. (Press O university, ed.).

30. Vezzu K, Maes AM, Bertasi F, et al. Interplay Between Hydroxyl Density and Relaxations in Membranes for Electrochemical Applications Interplay Between Hydroxyl Density and Relaxations in poly ( vi- nylbenzyltrimethyl ammonium ) - b -poly ( methylbutylene ) Membranes for Electrochemical Appl. 2018. doi:10.1021/jacs.7b10524

31. Zhou YC, Zhou L, Feng CP, et al. Direct modification of polyketone resin for anion exchange membrane of alkaline fuel cells. *J Colloid Interface Sci*. 2019;556:420-431. doi:10.1016/j.jcis.2019.08.086

32. Wollrab A. *Organische Chemie*.

33. Zhou YC, Zhang ZM, Zhou L, et al. Imidazole-functionalized polyketone-based polyelectrolytes with efficient ionic channels and superwettability for alkaline polyelectrolyte fuel cells and multiple liquid purification. *J Mater Chem A*. 2021;9(26):14827-14840. doi:10.1039/d1ta03460j

34. Samples EM, Schuck JM, Joshi PB, Willets KA, Dobereiner GE. Synthesis and Properties of N-

Arylpyrrole-Functionalized Poly(1-hexene- alt-CO). *Macromolecules*. 2018;51(22):9323-9332. doi:10.1021/acs.macromol.8b01629

35. Krueger PJ. Intramolecular hydrogen bonds in ethylenediamines and other aliphatic diamines. *Can J Chem*. 1967;45. doi:https://doi.org/10.1139/v67-348

36. Hine J, Li W-S. Synthesis of Some cis- and trans-2-Dimethylaminomethy1.CycliAc mines and Related Diamines. *J Org Chem,*. 1975;Vol. 40:1-4. doi:https://doi.org/10.1021/jo00891a005

37. Cheng J, He G, Zhang F. A mini-review on anion exchange membranes for fuel cell applications: Stability issue and addressing strategies. *Int J Hydrogen Energy*. 2015;40(23):7348-7360. doi:10.1016/j.ijhydene.2015.04.040

38. Bonizzoni S, Stilli P, Lohmann-Richters F, et al. Facile Chemical Modification of Aquivion® Membranes for Anionic Fuel Cells. *ChemElectroChem*. 2021;8(12):2231-2237. doi:10.1002/celc.202100382

39. Hine J, Shyong L. Internal Hydrogen Bonding and Positions of Protonation in the Monoprotonated Forms of Some 1,3- and 1,4-Diamines. *J Org Chem*. 1975;40(12):1795-1800. doi:10.1021/jo00900a026

40. Duer MJ. *Solid-State NMR Spectroscopy Principles and Applications*.

41. Kürti L, Czakó B. *Strategic Applications of Named Reactions in Organic Synthesis*.

42. Grigg R, Knight JA, Sargent M V. 1131. Studies in furan chemistry. Part I. The infrared spectra of 2,5-disubstituted furans. *J Chem Soc*. 1965:6057-6060. doi:10.1039/JR9650006057

43. Allouche A. Software News and Updates Gabedit — A Graphical User Interface for Computational Chemistry Softwares. *J Comput Chem*. 2012;32:174-182. doi:10.1002/jcc

44. Fitzgerald JJ, DePaul SM. Solid-state NMR spectroscopy of inorganic materials: An overview. *ACS Symp Ser*. 1999;717:2-133. doi:10.1021/bk-1999-0717.ch001

45. Viswanathan T, Jethmalani J. The aqueous ring-opening metathesis polymerization of furan-maleic anhydride adduct: Increased catalytic activity using a recyclable transition metal catalyst. *J Chem Educ*. 1993;70(2):165-167. doi:10.1021/ed070p165

46. Toncelli C, De Reus DC, Picchioni F, Broekhuis AA. Properties of reversible diels-alder furan/maleimide polymer networks as function of crosslink density. *Macromol Chem Phys*.

2012;213(2):157-165. doi:10.1002/macp.201100405

47. Widstrom AL, Lear BJ. Structural and solvent control over activation parameters for a pair of retro Diels-Alder reactions. *Sci Rep*. 2019;9(1):1-8. doi:10.1038/s41598-019-54156-4

48. Kuba AG, Smolin YY, Soroush M, Lau KKS. Synthesis and integration of poly(1-vinylimidazole) polymer electrolyte in dye sensitized solar cells by initiated chemical vapor deposition. *Chem Eng Sci*. 2016;154(Ii):136-142. doi:10.1016/j.ces.2016.05.007

49. Martins JN, Klohn TG, Bianchi O, Fiorio R, Freire E. Dynamic mechanical, thermal, and morphological study of ABS/textile fiber composites. *Polym Bull*. 2010;64(5):497-510. doi:10.1007/s00289-009-0200-6

# Chapter 4: Styrene-base anion exchange polymers

The styrene-based polymers, e.g. polystyrene, are used for wide applications such as packaging or as structure materials[1–3]. However, after their utilization these materials are considered non-recyclable waste and actually, few commodities have some recycling protocol[4]. From the point of view of materials science, these materials show excellent thermal stability, good chemical resistance in acid and alkaline environments and also interesting mechanical properties due mainly to aromatic portions[2–4]. These characteristics are compatible with those ideally required for an AEMFC and AEMWE[5] and, in accordance with this, styrene-base polymer waste must be considered as a resource. For these considerations, I tried some functionalization processes on common styrene-base polymers. In my Aquivion® functionalization, I used the N,N,2,2-tetramehyl-1,3-propandiamine to generate a anionic conducting sulfonamide[6]. The advantage on its employment is due to the absence of beta-hydrogen near quaternary ammonium groups that avoid the Hoffmann degradation, giving very stable polymers [7,8]. My idea is to combine the good properties of styrene-based materials with the high alkaline durability of this diamine, obtaining a styrene-based N-(quaternary ammonium)alkylsulfonamide as in the figure below.

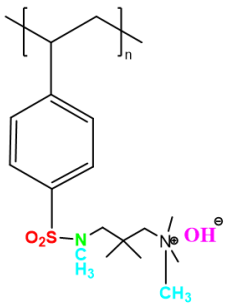


*Figure 4-1 - Proposal styrene unit functionalization*

In this chapter, I reported my initials results of the functionalization of styrene-based polymer.

## 4.1 – Synthesis

### 4.1.1 – Synthesis Overview

This process was aimed to explore the synthesis of styrene-based N-(quaternary ammonium) alkylsulfonamide. The general scheme is showed in figure 2. The step_1 was the sulfonation process of aromatic rings, then, in step_2, sulfonic groups were converted into sulfonamide by reactions with diamine. Finally, in step_3 the polymers were methylated, generating a quaternary ammonium group.

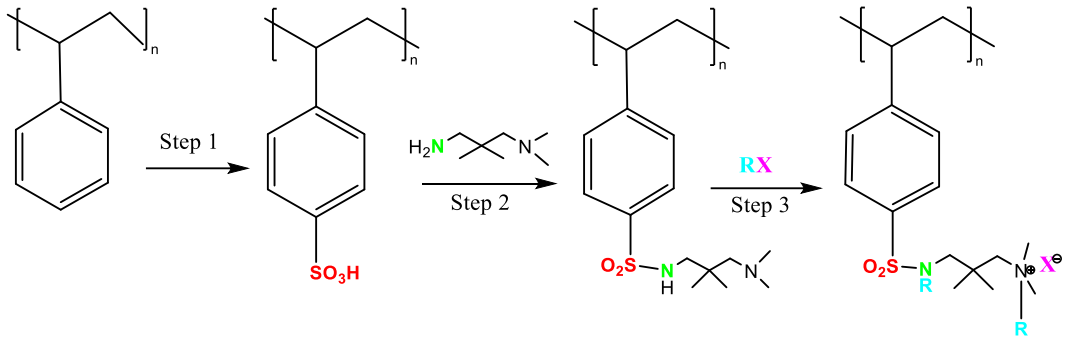


*Figure 4-2 - General scheme of the synthesis process*

I choose poly(4-styrenesulfonic acid) (PSA), polystyrene (PS) and acrylonitrile-butadiene-styrene terpolymer (ABS) as starting materials. In the initial phase, I explored the modification of poly(4-styrenesulfonic acid) and then I focused the study of the effects of sub-stoichiometry sulfonation degree (SD) on styrene-based matrix. For polystyrene, I varied the stoichiometry ratio of sulfonating agent in order to generate different sulfonated polystyrene (SPS). Indeed, for ABS I explored the synthesis of full-sulfonated polymer because, the content of styrene unit is just 47.5% wt, so, I could already considerate it as “diluted” system.

## Step_1

The step_1 is the sulfonation process of the aromatic ring of styrene units. This reaction is classified as electrophilic aromatic substitution and, in this case, it gives the para substitution[9,10]. For this step, I followed two methods which applied chlorosulfuric acid and fuming sulfuric acid, called them step_1a and step_1b, respectively. Both chemicals react energetically with water but only chlorosulfuric acid could be dissolved in chlorinated solvent allowing a stoichiometry control[11].

The step_1a was carried out in anhydrous condition due to the instability of chlorosulfuric acid with the moisture[9,10,12]. I used a double neck balloon equipped with mechanical stirrer, dropping funnel

and Ice bath. The polymers and chlorosulfuric acid were dispersed separately in anhydrous dichloromethane and then the acid solution was added dropwise slowly to polymer dispersion under mechanical stirring and let to react for two hours at room temperature. During the reaction, the sulfonated product separates from the reaction environment. The product was poured in water, recovered, and dried in vacuum at 100°C. The water washing converts the $-SO_2Cl$ group into $-SO_3H$, generating a sulfonated polymer. I choose this procedure because the chlorosulfonic acid application generates sulfuric acid that can't be distilled and the products were not easy the handle.

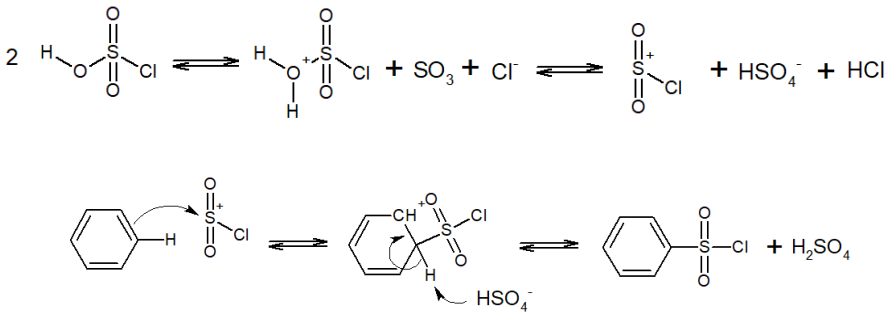

*Figure 4-3 - Scheme of sulfonation by fuming sulfuric acid*

The step_1b was performed by using fuming sulfuric acid as solvent. The initial tests showed that the polymers in pellet form were functionalized only in the outer layer. Consequently, it is important to obtain these raw materials with as high surface as possible. The polymers were dispersed in acetone, dropped in water, recovered, and dried at 80°C in vacuum for one hours. In this way, I obtained the starting materials with higher surface area than the pellet form. After that, the expanded polymers were put in a balloon with ice bath and then fuming acid was added slowly under stirring. When the flash warms to room temperate, the dehydrating valve was connected and the solution was heated up to 60°C for 3 hours. The products were recovered with water washing and dried at 100°C in vacuum.

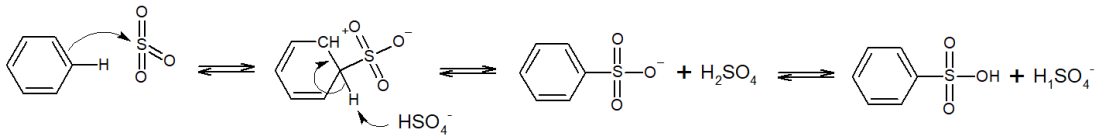

*Figure 4-4 - Scheme of sulfonation by fuming sulfuric acid*

## Step_2

The step_2 is the conversion of sulfonic acid into sulfonamide thanks to diamine reaction. Here, I couldn't follow the same procedure of Aquivion® modification (see 2.1.2), because aromatic sulfonic acid has different reactivity than perfluoroalkyl one. A possible alternative synthesis pathway involves the chlorosulfonyl group as an intermediate [9,10,13]. The procedure involves a first conversion of sulfonic acid into chlorosulfonyl group (step_2a) and then the formation of sulfonamide by reaction with the diamine (step_2b).

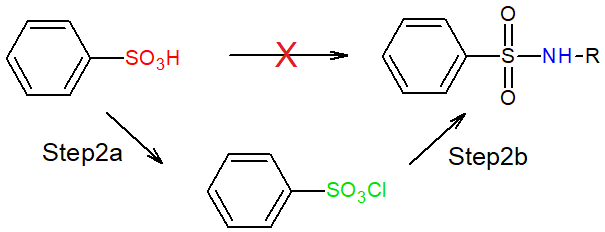


*Figure 4-5 - Graphic scheme of step_2*

In step_2a I used thionyl chloride because It's one of liquid chlorinating agent that could be removed by distillation. $SOCl_2$ reacts energetically with water producing HCl and $SO_2$, for this reason the reaction was carried out in anhydrous conditions.

I used double neck balloon equipped with Vigreux column followed by Liebig refrigerant and storage flask.

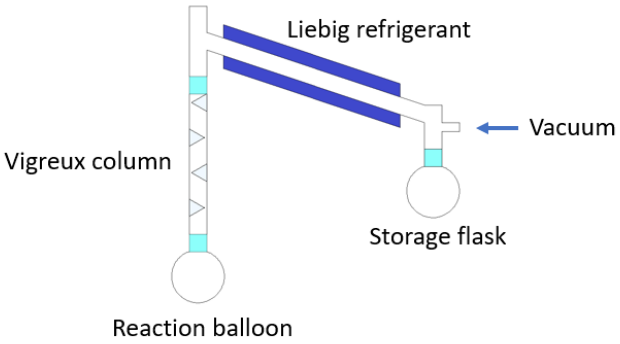


*Figure 4-6 - Sketch of the glassware of Step_2a*

The dried polymers were put in the balloon and then 3 nitrogen-vacuum washing cycles were performed to remove the traces of moisture in the glassware. Later thionyl chloride was added and heated up to 130°C under stirring. The Vigreux column increases the duration of the process allowing a better contact among the chemicals. After 3 hours, the distillation procedure was completed by working in vacuum conditions to guarantee the completely elimination of $SOCl_2$. The dried products were storage under nitrogen atmosphere to avoid the reaction with moisture.

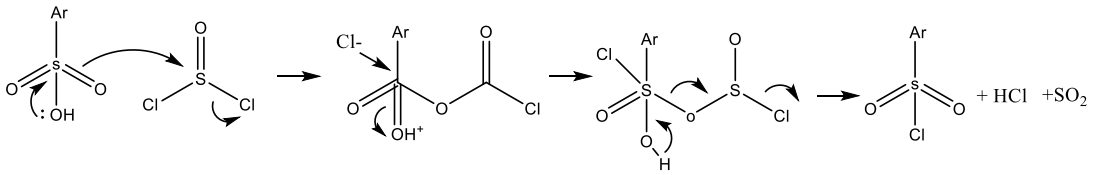


*Figure 4-7 - Mechanism of chlorination through thionyl chloride: Ar is referred to aromatic ring*[10]

In step_2b, the diamine was used as solvent to guarantee a strong excess to react with sulfonyl chloride group and eliminate the HCl produced. The polymers were covered by diamine and let to react for 15 hours in nitrogen atmosphere. After that, the products were washed with water and dried in vacuum at 100°C.

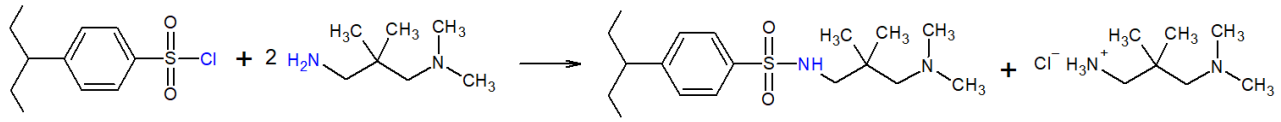


*Figure 4-8 - Scheme of Step_2b*

## Step_3

In the step_3, the ternary nitrogen of N-alkylsulfonamide was methylated forming the quaternary ammonium group. The polymer was soaked in anhydrous acetonitrile for 1 hour and then 500% excess iodomethane was added and let to react for 15h a 40°C. After that, the product was recovered, washed with acetonitrile, then recovered and dried in vacuum at 100°C for 1 hour.

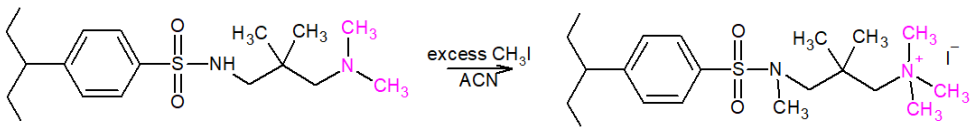


*Figure 4-9 - Scheme of Step_3*

## 4.2 – physical- chemical characterizations

During the synthesis procedure, I monitored the reaction through thermal and elementary analysis, IR spectroscopy and IEC determination. The characterization of raw materials and reaction products are reported below.

### 4.2.1 - Starting materials

#### Poly(4-styrenesulfonic acid) (PSA)

Poly(4-styrenesulfonic acid) is full-sulfonated polystyrene and it's usually sold as 18 - 30 % wt water dispersion. Before using, I casted the solution in Teflon mold, dried at 80°C and then polymer disc was milled to obtain a fine powder.

Figure 10 shows the FTIR spectrum of poly(4-styrensulfonic acid).

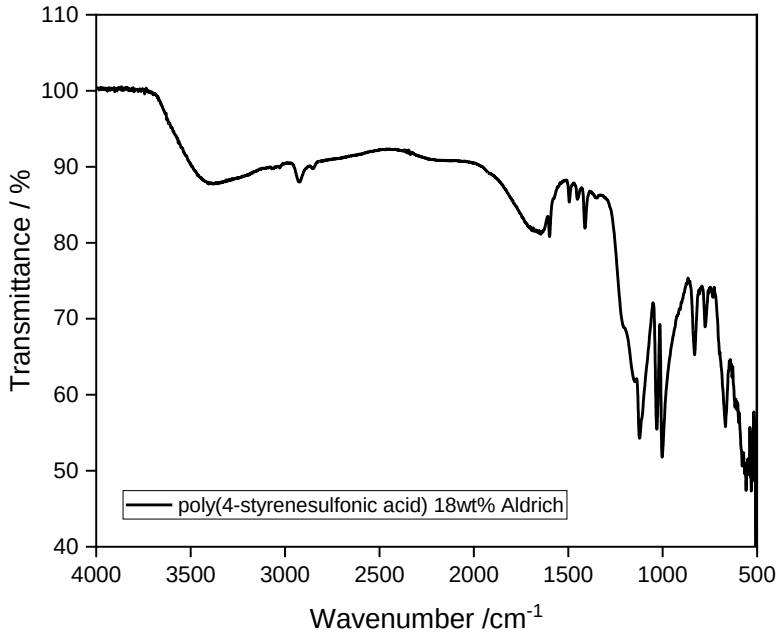


*Figure 4-10 - FTIR of poly(4-styrensulfonic acid)*

The polymer backbone generates the C-H stretching of -$CH_2$- and -CH- at 2930 and 2848 $cm^{-1}$, the -$CH_2$- bending at 1341 $cm^{-1}$ and the C-H stretching out of plane at 733 $cm^{-1}$ [14–16]. The aromatic ring gives the C-H stretching at 3030 $cm^{-1}$, C=C stretching at 1600, 1500, 1448 and 1411 $cm^{-1}$ and C=C

bending at 1031, 1000, 829 $cm^{-1}$ [17,18]. The signals at 1215, 1122 and 1150 $cm^{-1}$ were attributed to sulfuric group [18,19]. Finally, O-H stretching and bending of water were detected at 3400 and 1640 $cm^{-1}$. The presence of water could modify the profile of sulfonyl group signals [20].

The TGA curve in figure 11 could be divided into three zones according to the degradation steps[21]. In region I, 13.6% mass loss was detected and correlated to moisture and coordinating water. The region II is from 250°C to 370°C and the 22.4% mass loss was related to sulfonic group. In region III, the aromatic ring and then the polymer backbone begin to degrade.

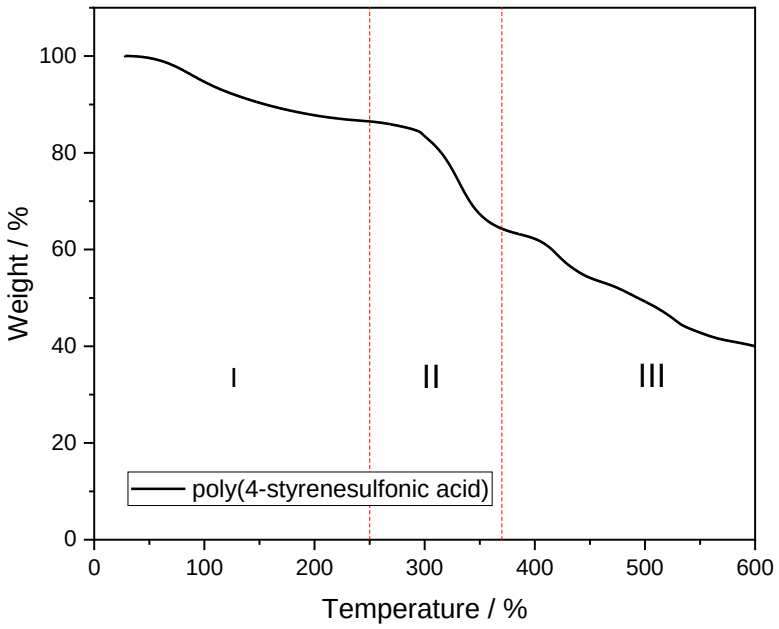


*Figure 4-11 - TGA curve of poly(4-styrensulfonic acid)*

According to TGA analysis, the sample contained about 13% wt of water that could be an obstacle for the further steps. So, I dried the sample at 150°C for 1 hour and at 200°C for 1 hour in vacuum condition. On the dried samples I performed the IR spectra in figure 12.

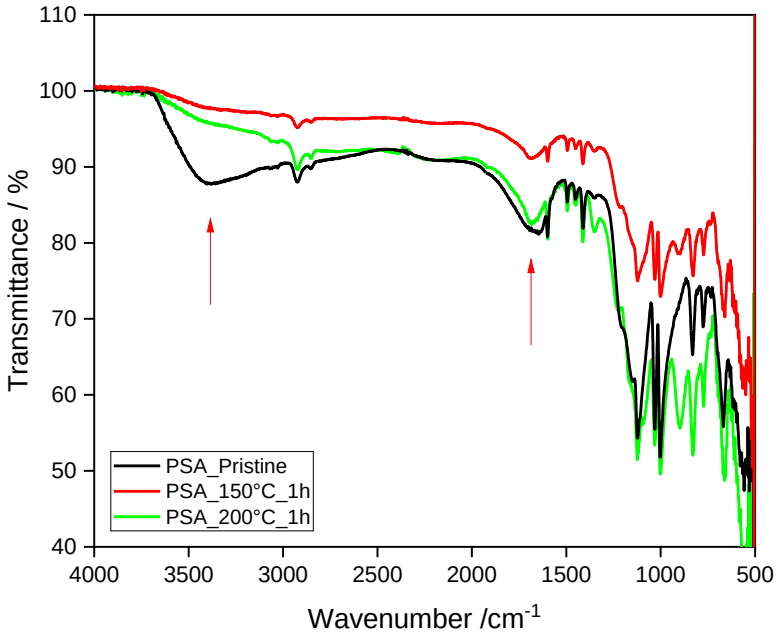


*Figure 4-12 - FTIR of PSA before and after heating process up to 150°C 1h and 200°C: the red arrows indicate the water signals*

Considering the result, in the following I decided to use the treatments at 200°C because it can dry the samples without degrading it.

## Polystyrene (PS)

In figure 13 the IR spectrum of polystyrene is showed.

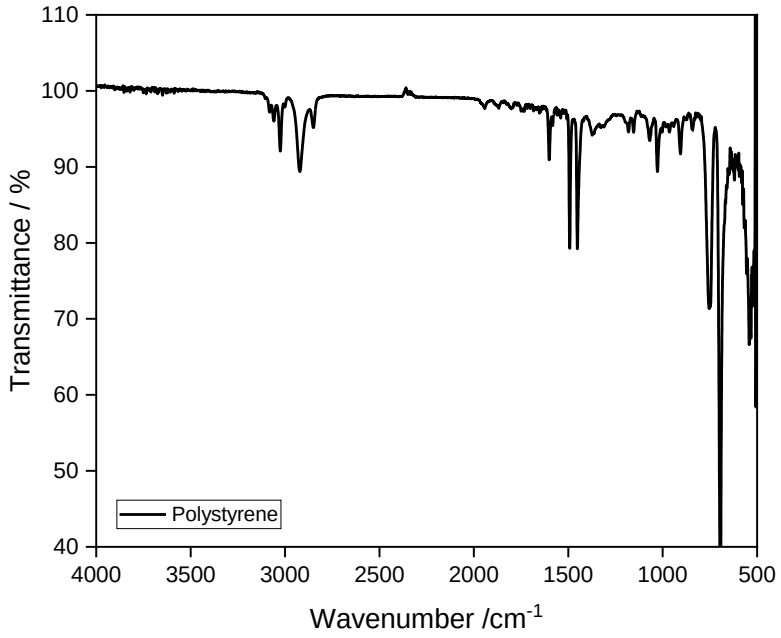


*Figure 4-13 - FTIR spectrum of polystyrene*

The signals of polymer backbone were found at 2930 and 2848 $cm^{-1}$ (the C-H stretching of -$CH_2$- and -CH-), at 1362, 1313 $cm^{-1}$ (the -$CH_2$- bending ) and at 666 $cm^{-1}$(C-H out of plane) [14–16]. The aromatic ring gives the C-H stretching at 3030 $cm^{-1}$, C=C stretching at 1600, 1500 and 1448 $cm^{-1}$ and C=C bending at 1031, 1000, 902 $cm^{-1}$ [17,18]. The signals in 2000 – 1700 zone were the “aromatic finger”.

The TGA curve of polystyrene shows one-step degradation starting from 250°C (fig. 14)

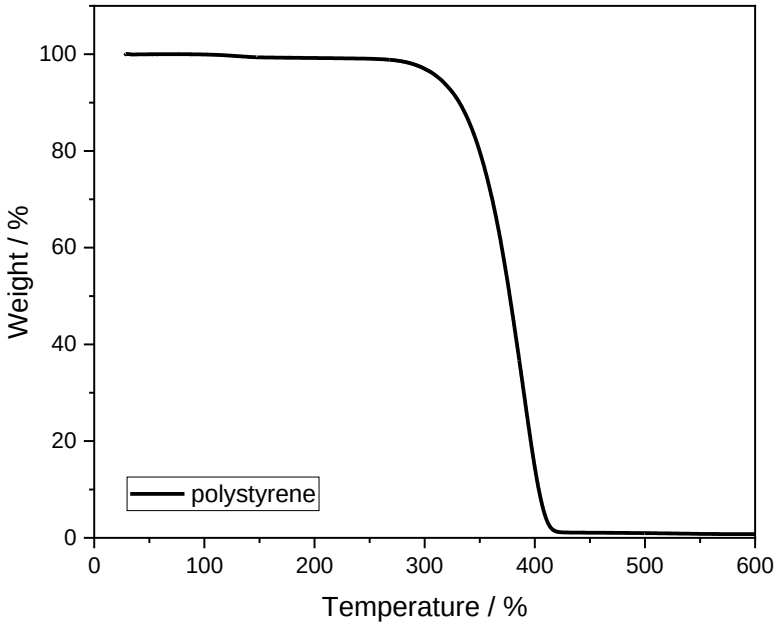


*Figure 4-14 - TGA curve of polystyrene*

## Acrylonitrile-butadiene-styrene (ABS)

This material is a terpolymer of styrene, acrylonitrile, and butadiene, which are present about 47.5, 26.5 and 26 % in weight, respectively. In this polymer matrix, the styrene units are less concentrated than polystyrene, therefore working with 100% of sulfonation degree means to introduce sulfonyl group about 27.7 % wt on the total polymer. This fact is interesting from the point of view of functionalization, because it opens the possibility to regulate the ratio between active sites/polymer and, consequently, the equivalent weight of styrene-based polymer. Moreover, in ABS, also the nitrile group could be used as a potential modifiable group.

The IR spectrum showed the aromatic ring such as the C-H stretching of aromatic system at 3030 $cm^{-1}$, the C=C stretching at 1600, 1500, 1440 $cm^{-1}$ and C-H bending out of plane at 760, 700 $cm^{-1}$ [15,17]. The stretching and bending of -$CH_2$- at 2921, 2843 $cm^{-1}$ [16,18] and the nitrile group at 2230 $cm^{-1}$ were detected[2].

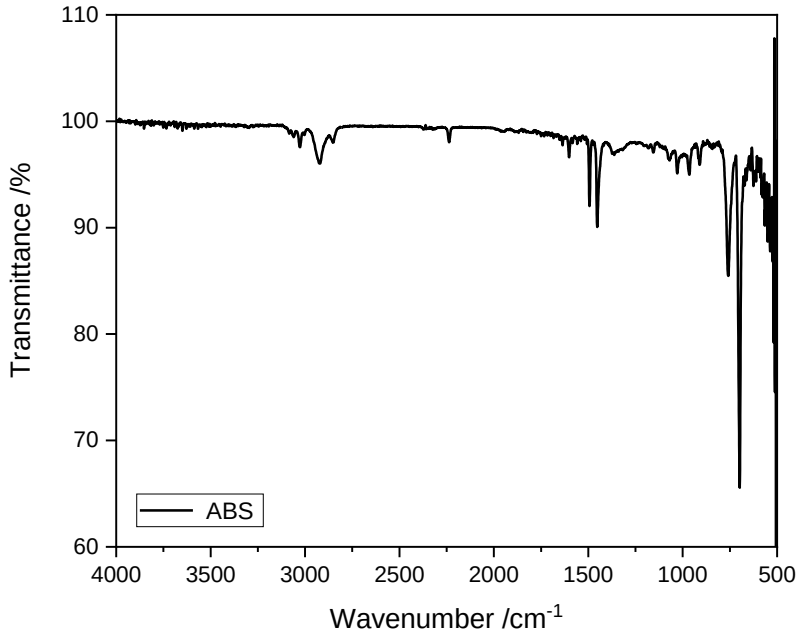


*Figure 4-15 - FTIR spectrum of ABS*

The TGA curve in air of ABS shows a flat zone up to 300°C then a mass loss of 91.8% followed by a smaller one of 6.7% were detected. The first step was correlated to the degradation of polybutadiene followed by styrenic fraction, while the second step was related to acrylic portion[2]

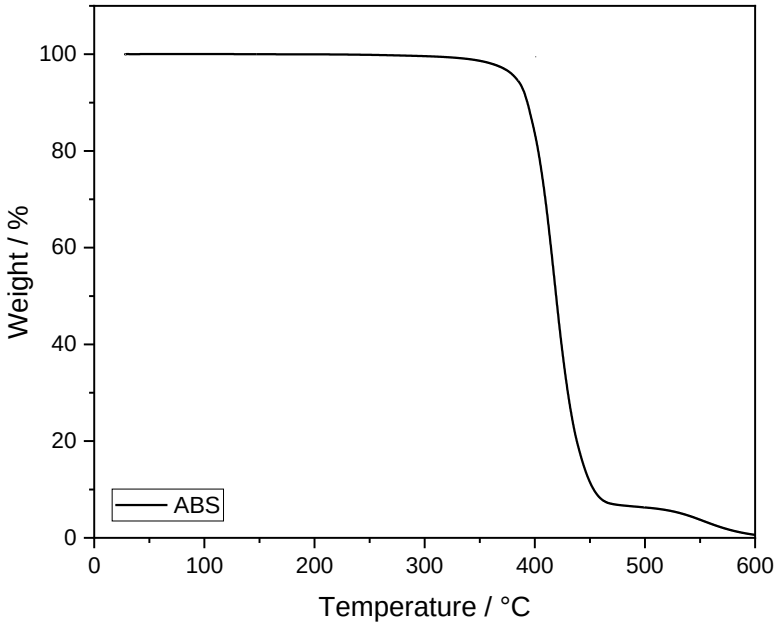


*Figure 4-16 - TGA curve of ABS*

### 4.2.2 -Following the synthesis

#### Poly(4-styrenesulfonic acid) (PSA)

The specific modification pathway is reported below:

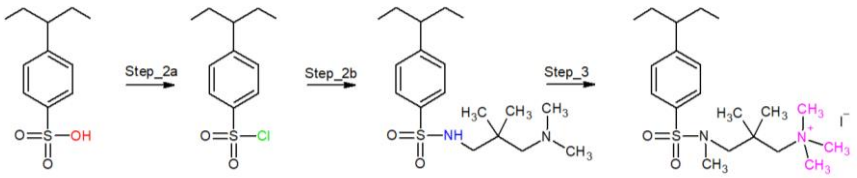


*Figure 4-17 - Scheme for PSA modification*

The first reaction is the chlorination of the sulfonic group. In the figure 18 the comparison between the IR spectra of raw material and step_2a was reported.

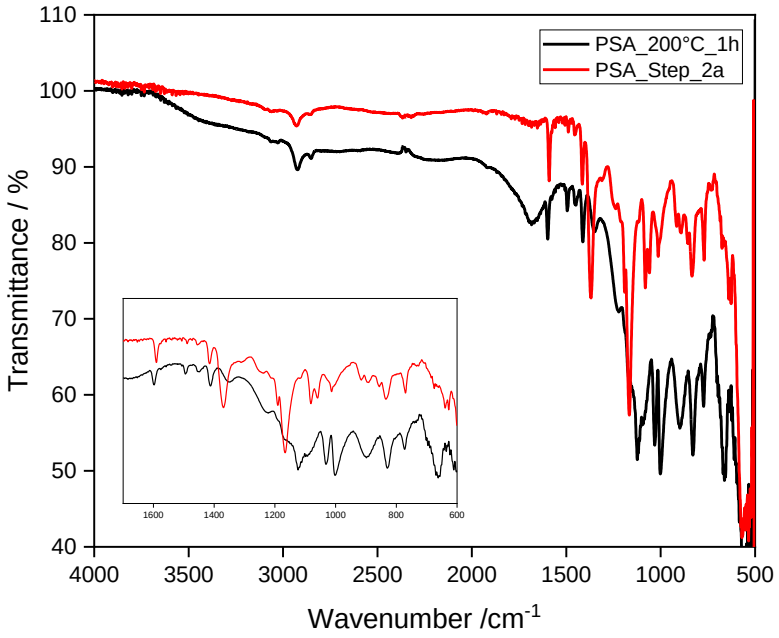


*Figure 4-18 - IR spectra of PSA_200°C_1h and PSA_Step_2a*

It's possible to notice that there are two new peaks at 1380 and 1170 $cm^{-1}$ correlated to stretching of sulfonyl chloride[11]. Moreover, the absence of O-H water signals at 3400, 1750 $cm^{-1}$ is confirming the success of this step. The amplitude of the peaks in 1200-100 $cm^{-1}$ zone could be attributed to different hydration degree[20]. Below, IR spectra of step_2a and 2b are reported.

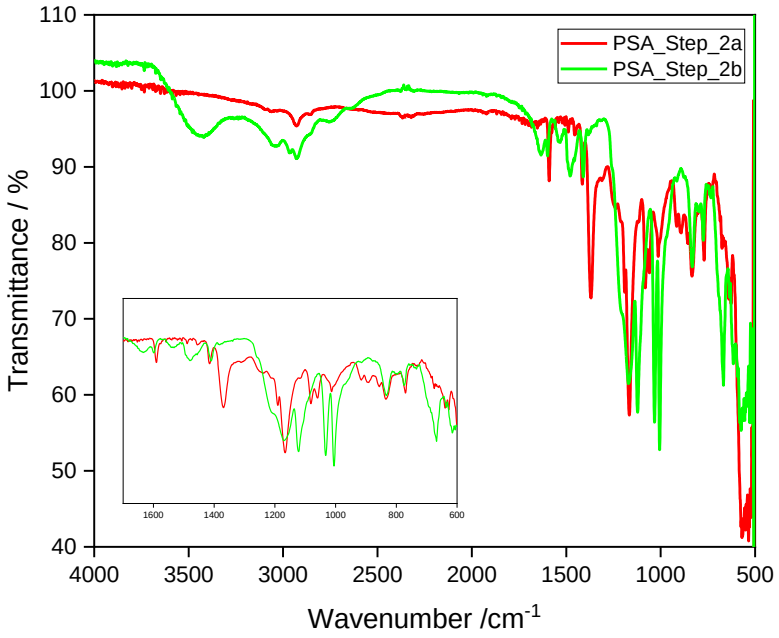


*Figure 4-19 - IR spectra of PSA_Step_2a and Step_2b*

As expected, the diamine C-H signals became visible, while the sulfonyl chloride peaks disappeared. However, the sulfonamide signal at 1325 $cm^{-1}$ was absent [17] and the region 1200-1000 $cm^{-1}$ was similar to PSA one. In order to better understand this result, I performed the reaction between step_2a and triethylamine (TEA).

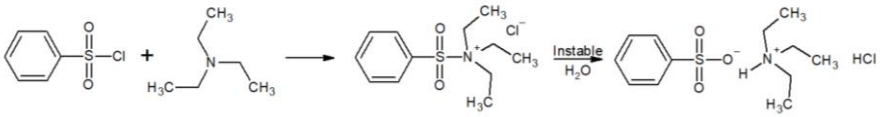


*Figure 4-20 - Scheme of Step_2b using TEA*

This ternary amine has no free hydrogen so it can't generate a sulfonamide bond with step_2a[9,10]. In fact, this reaction generated their corresponding sulfonic salt. In figure 21 the spectra of both step_2b were reported. The main differences are correlated to the use of different amines. As showed, the sulfonyl group signals were similar, denying the sulfonamide formation in favor of salt formation hypothesis.

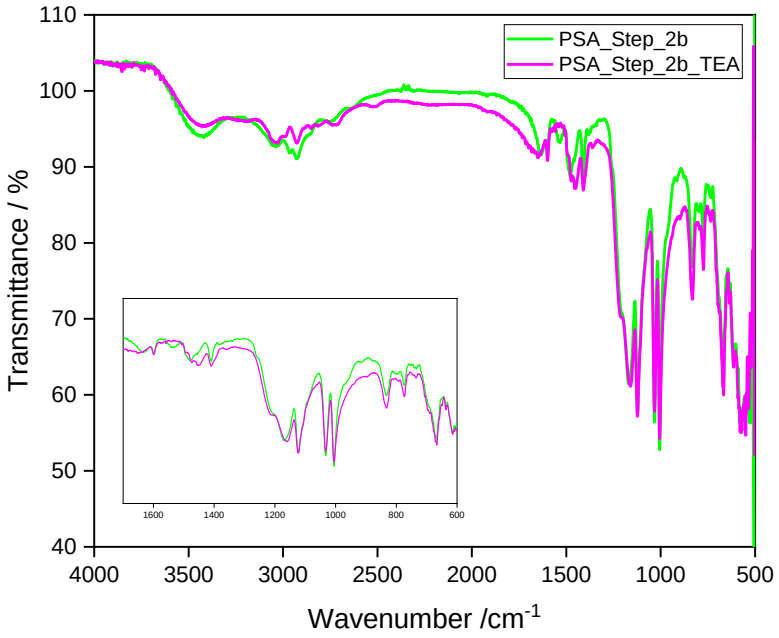


*Figure 4-21 - IR spectra PSA_Step_2b and Step_2b_TEA*

The intensity changes in 3000-2800 zone of Step_3 could be correlated to amine-water exchange during the washing. This is another evidence of salt formation.

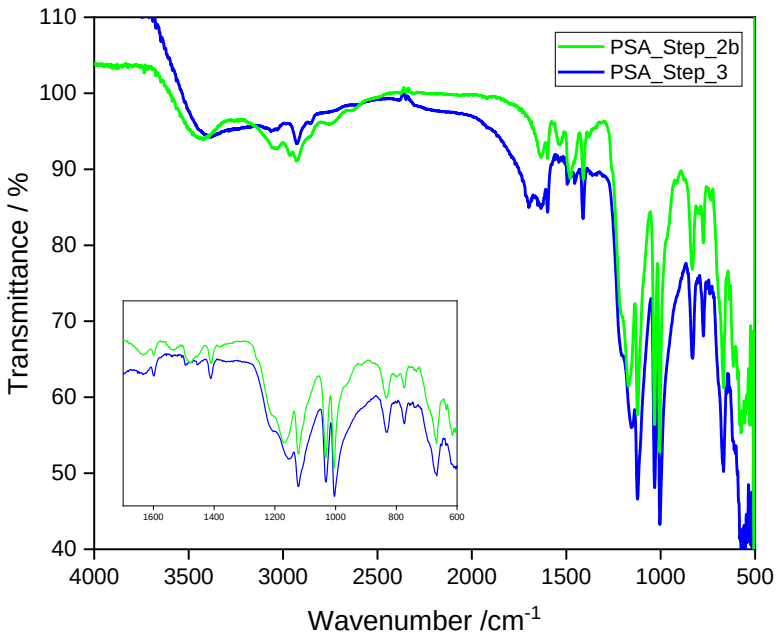


*Figure 4-22 - IR spectra of PSA_Step_2b and Step_3*

The TGA curves in air of PSA products were displayed below.

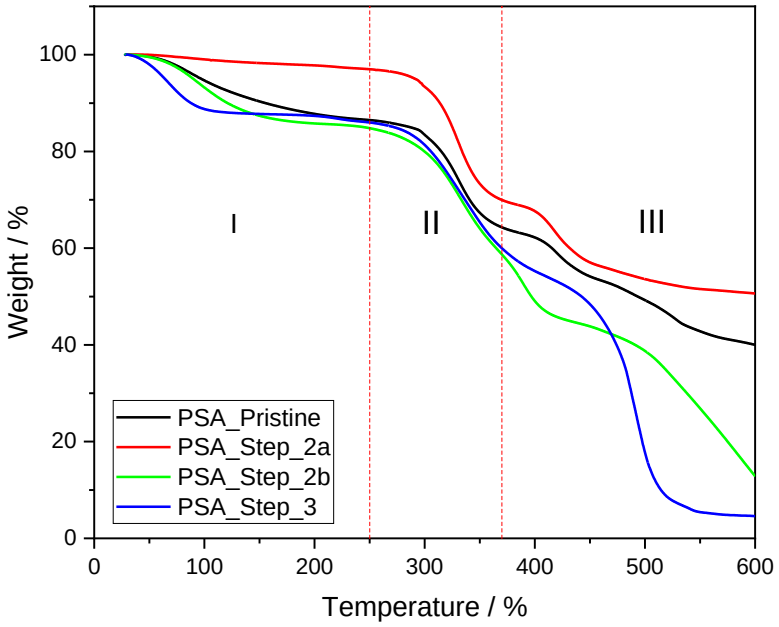


*Figure 4-23 - TGA curves of PSA products: dashed lines are the reference temperature of PSA degradation.*

The step2_a showed a slowly mass loss before 250°C followed by multi-step degradation profile similar to PSA[21]. The mass variations in 250-350 °C zone is higher than to PSA curve by 1.23 factor which is compatible a complete chlorination. The mass losses in region II were 22.4 % for PSA and 27.0 % for Step_2a.

$$\Delta mass\ teorical\ (step\_2a) = \Delta mass\ (PSA) * \frac{PM(SO_2Cl)}{PM(SO_2OH)} = 22.4\ \% * \frac{99.5\ \left(\frac{g}{mol}\right)}{81\ \left(\frac{g}{mol}\right)} = 27.5\ \%$$

The step_2b exhibited a water loss before 100°C, a first degradation at 250°C and a multi-step process at 400°C. This profile is similar to PSA one excepted for a more intense stair at 250°C, that could explain the salt formation. The mass variation is about 38.8 % corresponding to 66.4% of amine as counterion.

$$\Delta mass\ teorical\ (step\_2b) = \Delta mass\ (PSA) * \frac{PM(SO_2NRN)}{PM(SO_2OH)} = 22.4\ \% * \frac{211\ \left(\frac{g}{mol}\right)}{81\ \left(\frac{g}{mol}\right)} = 58.4\ \%$$

$$\%\ amine\ in\ step_{2b} = \frac{\Delta mass\ curve}{\Delta mass\ teorical} * 100 = \frac{38.8\ \%}{58.4\ \%} * 100 = 66.4\ \%$$

The step_3 had thermal profile like PSA validating the water-diamine exchange hypothesis during the procedure as IR result showed.

As confirmed the IR and TGA results, this PSA-synthesis pathway didn't generate the target polymer. Moreover, the products showed water solubility, making them not useful for fuel cell and electrolyzer applications. To address this problem, I studied the sub-stoichiometry SPS with a long polystyrene and ABS functionalization.

### Polystyrene (PS)

The specific modification pathway is reported below:

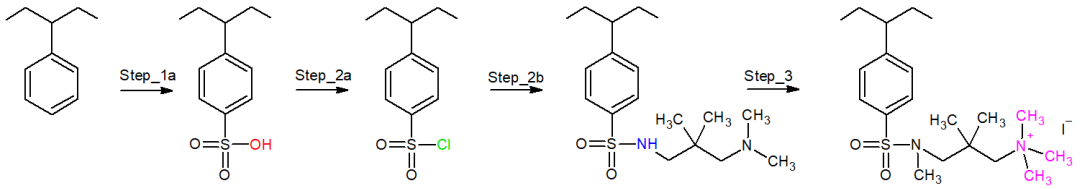


*Figure 4-24 - Scheme of polystyrene modification*

As step_1, I choose the Step_1a procedure obtaining different sulfonated polystyrene (SPS) to explore the sulfonation degree effect on polymer matrix. As example, I reported the IR and TGA results for the products obtained from SPS_0.4 .

In figure 25 the spectra of pristine, sulfonated and chlorosulfonated polystyrene were reported. In step_1 the $SO_3$ stretching in 1250-1000 $cm^{-1}$ zone and O-H water at 3400 and 1750 $cm^{-1}$ were detected. In the chlorination step the expected peaks at 1380 $cm^{-1}$ and 1170 $cm^{-1}$ were detected. It's both case I can confirm the success of the reactions.

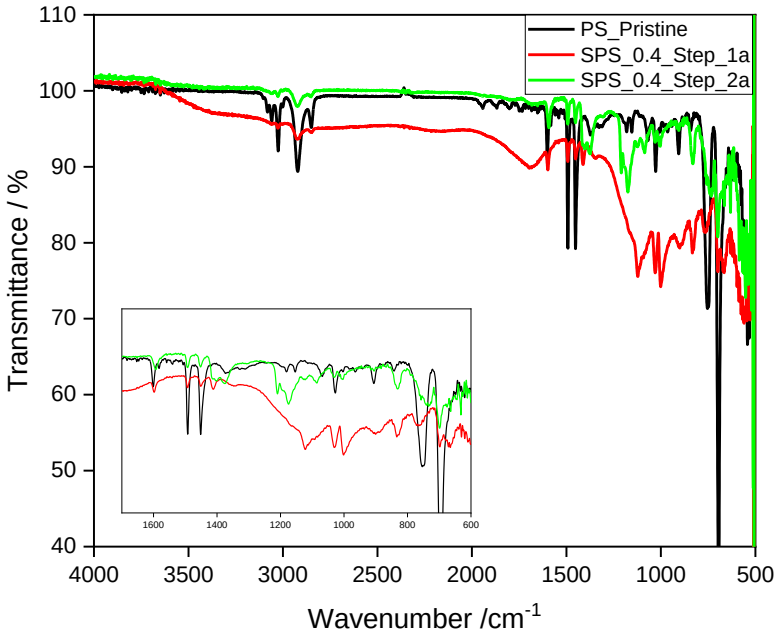


*Figure 4-25 - IR spectra of polystyrene, SPS_0.4_Step_1 and Step_2a*

The figure 26 shows the spectra of Step_2a, 2b, 3. After reaction with diamine, the signal of sulfonyl group shifted from 1380 $cm^{-1}$ to 1325 $cm^{-1}$ correlated to sulfonamide formation[17]. Moreover, the signals of diamine appeared such as the C-H stretching of -$CH_2$-, N-$CH_3$ in 3000-2800 $cm^{-1}$ zone and the N-C and C-H bending in 1500-1400 $cm^{-1}$ zone[22,23]. In the step_3 changes in 3500-2800 zone were detected, due to charged nitrogen at 2730 $cm^{-1}$ [15]. The increase of O-H of water signals at 3500 and 1600 $cm^{-1}$ [24] could be attributed to more hydrophilic system.

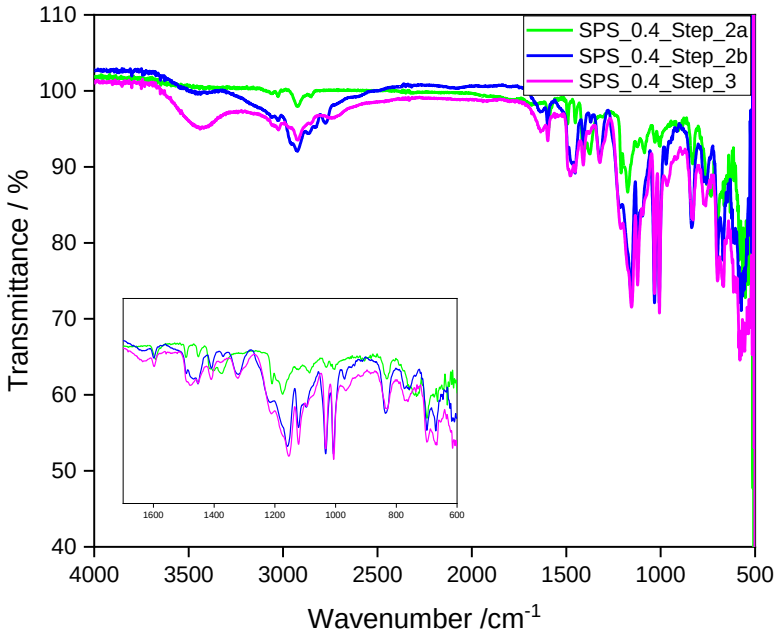


*Figure 4-26 - IR spectra of SPS_0.4_Step_2a, Step_2b and Step_3*

TGA curves in air of SPS_0.4 products were reported below.

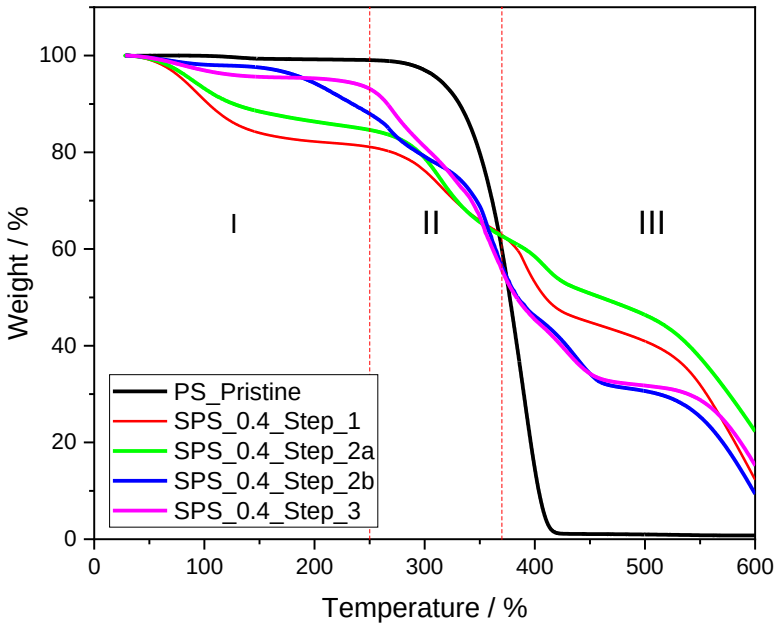


*Figure 4-27 - TGA curves of polystyrene products*

After step_1a functionalization, the thermal resistance of polystyrene decreased in good agreement with poly(4-styrenesulfonic acid) behavior (fig. 23). The step_2a gave thermal profile similar to

step_1b as well as for PSA products. From the calculations the functionalization degree is about 40%.

$$\Delta mass\ teorical\ (SO_3H) = \frac{PM(SO_3H)}{PM(polymer)} * 100 = \frac{81\ \left(\frac{g}{mol}\right)}{185\ \left(\frac{g}{mol}\right)} * 100 = 43.7\ \%$$

$$\%\ sulfonyl\ group\ (step\_1b) = \frac{\Delta mass\ curve}{\Delta mass\ teorical} * 100 = \frac{18.2\ \%}{43.7\ \%} * 100 = 41.6\ \%$$

Step_2b and 3 showed different thermal profiles than the previously samples which may be related to sulfonamide creation. Also in this case, the methylation process increased the polymer thermal stability[6].

However, the functionalized SPS_0.8 and SPS_1.0 showed high water solubility as the pristine PSA, making them not useful for fuel cell and electrolyzer application. In contrast, SPS_0.2, SPS_0.4 and SPS_0.6 showed less solubility, making ion exchange capacity determination interesting. During the procedure (see. ES9) the 0.4 washing solutions became opalescent while 0.2 one remained colorless as showed in the figure below.

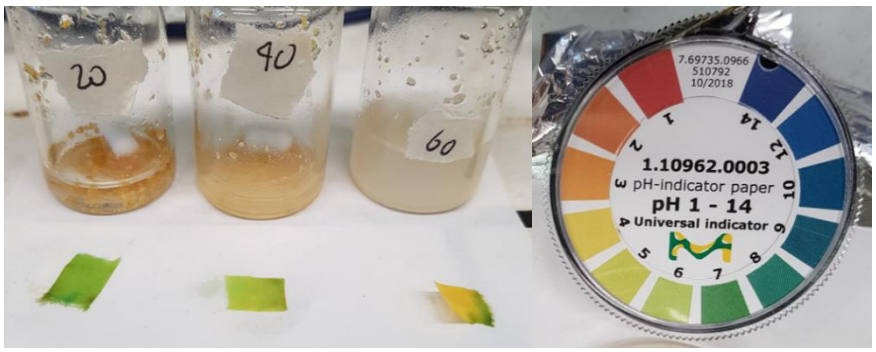


*Figure 4-28 - IEC test of modified polystyrene with 0.2, 0.4 and 0.6 sulfonation degree*

This phenomenon could be attributed to the retro-synthesis of sulfonyl group which causes the release of sulfuric acid in the washing solutions[25]. This hypothesis was validated thanks to the pH values terminated with indicator paper (fig. 27): only the washing of 0.2 sample was neutral. The IEC value determined was 0.33 mmol*$g^{-1}$ and the global modification yield is 15.0 %. This value was comparable with other styrene-based systems i.e. PSEBS, SBS reported in literature[26,27].

$$Maximun\ IEC = \frac{n\ (mmol)}{mass\ (g)} = \frac{\frac{mass\ (g)}{MW\ (g\ mol^{-1})} * 1000}{mass\ (g)} = \frac{1000}{MW\ (g\ mol^{-1})}$$

$$= \frac{1000}{453\ (g\ mol^{-1})} = 2.21\ \frac{mmol}{g}$$

$$\%\ functionalization = \frac{IEC}{Max\ IEC} * 100 = \frac{0.33\ \left(\frac{meq}{g}\right)}{2.21\ \left(\frac{meq}{g}\right)} * 100 = 15.0\ \%$$

The 0.4 and 0.6 solutions were neutralized with sodium bicarbonate in order to allow the Mohr titration method (It can't work in acid environment). However, the values obtained are less than 0.1 meq*$g^{-1}$ confirming that part of the functionalization has been lost in the washes.

To better understand these IEC results, elementary analysis was performed of pristine polystyrene and SPS_0.2, SPS_0.4 and SPS_0.6 (Step_1a). In this way, I could hypnotize a sulfonamide yield and investigate the effect of different sulfonation degree of this functionalization.

| CHNS | % C | % H | % N | % S | % O |
|---|---|---|---|---|---|
| PS_Pristine | 92,17 | 7,692 | 0,03 | 0,021 | 0,09 |
| SPS_0.2 | 79,72 | 6,902 | 0,01 | 5,643 | 7,72 |
| SPS_0.4 | 71,40 | 5,972 | 0,04 | 9,382 | 13,21 |
| SPS_0.6 | 63,20 | 5,394 | 0,00 | 12,474 | 18,93 |

$$C/S\ ratio = \frac{\frac{\%\ C}{WA}}{\frac{\%\ S}{WA}} = \frac{\frac{79.72}{12.01}}{\frac{5.643}{32.01}} = 37.7$$

$$\%\ functionalization = \frac{n°\ C}{C/S} * 100 = \frac{8}{37.7} * 100 = 21.2\ \%$$

From calculations, the SPS_0.2, SPS_0.4 and SPS_0.6 were functionalized for 21.2%, 39.4% and 59.2%, respectively. Unfortunately, only the value of SPS_0.2 is in line with the IEC results.

I conclude that this modification is not suitable for high sulfonation degrees. A possible explanation is related to the concentration of sulfonic groups which increase the hydrophilicity of the polymer. In this situation, the charges increasing along the chains and the high degree of hydration facilitate the retro synthesis process[28]. The global functionalization yield of SPS_0.2 calculated thanks to the IEC measurement is about 15%, which means that not all sulfonic groups were functionalized. From

all sulfonic groups were functionalized. From the data, I can conclude that this modification is not optimal to obtain polystyrene-based anionic conduction polymers with good performance.

## Acrylonitrile-butadiene-styrene (ABS)

The specific modification pathway is reported below:

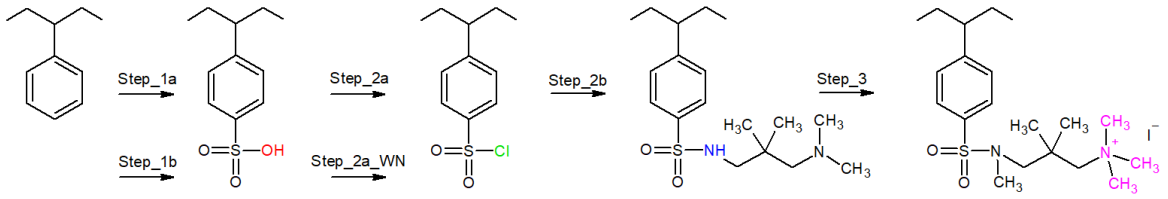


*Figure 4-29 - Scheme of ABS modification*

In this modification I used two sulfonic agents: the first one was chlorosulfonic acid (step_1a) and other was fuming sulfuric acid (step_1b). In figure 30 there is the comparison of pristine ABS, Step_1a and Step_1b IR spectra.

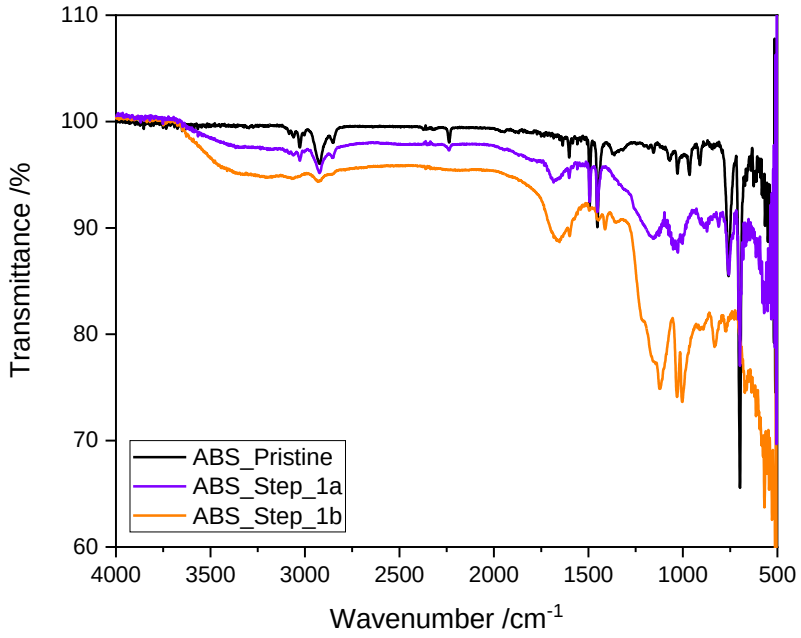


*Figure 4-30 - IR spectra of pristine ABS, step1a and step1b: the red arrow indicates the nitrile signal*

In both the functionalization procedures the expected sulfonic group and water signal were detected but in the Step_1b the nitrile group was converted into carboxyl group (shift from 2234 $cm^{-1}$ to 1690 $cm^{-1}$) [17]. In support I did TGA on Step_1a and 1b obtaining different thermal behaviors.

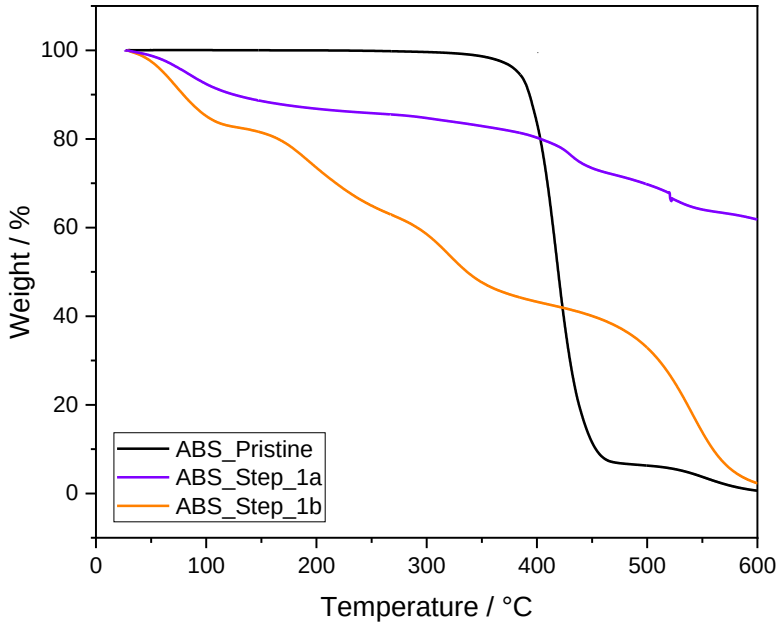


*Figure 4-31 - TGA curves of ABS, Step_1a and Step_1b*

The step_1a displayed a water loss before 100°C and then a multi-steps degradation like SPS. Also in this case, the product could be considered stable up to 250°C. The step_1b showed a more intense water loss before 100°C followed by multi-steps degradation from 130°C compatible with carboxyl and sulfonic groups losses.

$$MW\ ABS\ without\ nitrile = MW(sulfonic\ acid + ethyl\ phenyl + butyl + propionc\ acid) = 311\ \frac{g}{mol}$$

$$MW\ (sulfonic\ and\ corboxy\ acid) = 126\ \frac{g}{mol}$$

$$\Delta\ mass\ theorical = \frac{Mw\ (Acids)}{Mw\ (polymer)} * 100 = \frac{126\ \left(\frac{g}{mol}\right)}{311\ \left(\frac{g}{mol}\right)} * 100 = 40.5\ \%$$

Both the procedures introduced sulfonyl groups in ABS backbone, but step_1b also hydrolyzed the nitrile group to carboxylic acid. So, the step_1b products had two possible chemical functions which could react with diamine generating amide or sulfonamide from carboxyl and sulfonyl groups,

respectively. To better understand the properties of these news polymers, I decided to continue the synthesis procedure with both the products.

In figure 32 the step_1b and step_2a_WN (step_2a_ without nitrile) were reported.

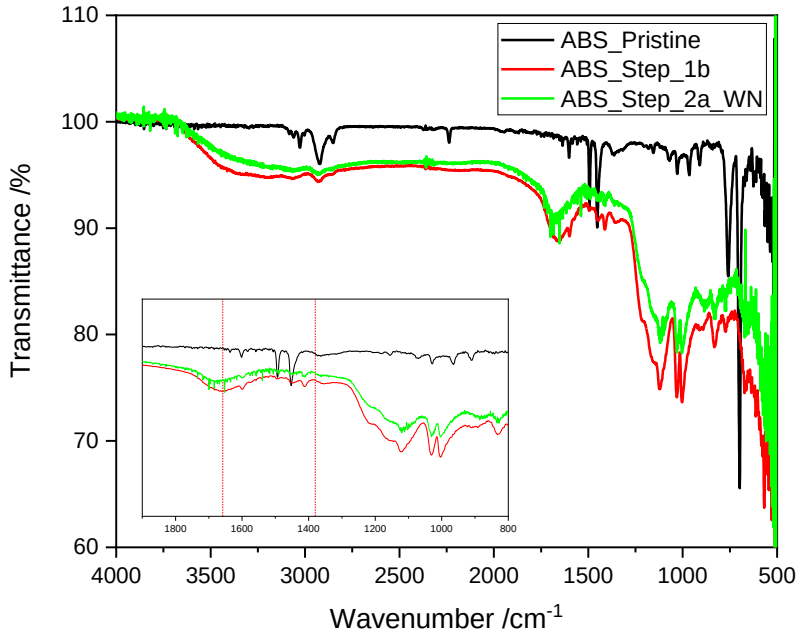


*Figure 4-32 - IR spectra of ABS, step_1b and step_2a_WN*

In step_2a_WN, it's possible to observe the absence of chlorosulfonyl signal at 1380 $cm^{-1}$. Moreover, the large peak at 1658 $cm^{-1}$, composing by O-H stretching water and C=O stretching of carboxyl acid, was reduced. This evidence confirms the dehydration process of Step_2a but, at the same time, the failure of this process. Although this polymer matrix was interesting for selective functionalization, this synthesis pathway will be studied in the future.

The IR spectra of step_1a and its further products are reported below.

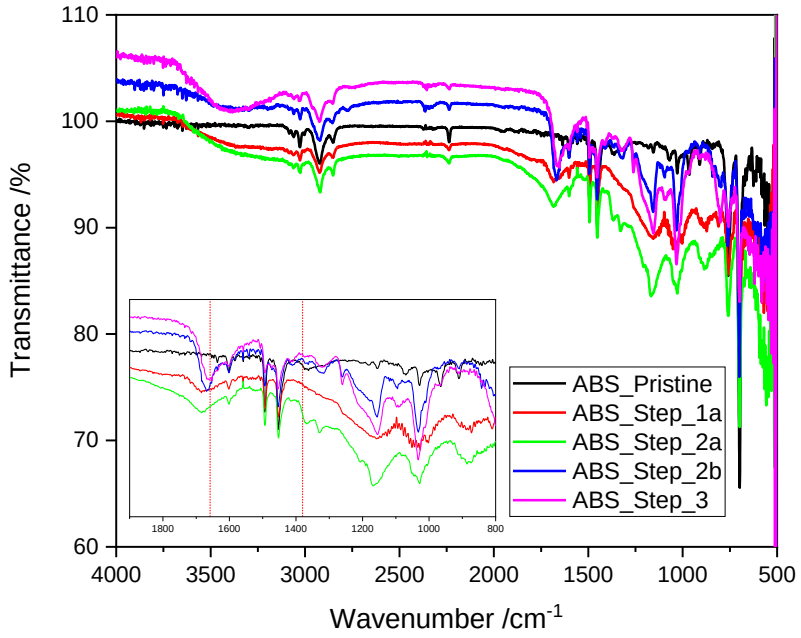


*Figure 4-33- IR spectra of ABS_Step_1a products*

The Step_2a showed the stretching of sulfonyl chloride at 1380 and 1170 $cm^{-1}$, while in Step_2 the sulfonamide signal was detected at 1325 $cm^{-1}$. In Step_3 a small shoulder at 2960 $cm^{-1}$ on the $CH_2$ signal (at 2923 $cm^{-1}$) and some changes in 2800-2600 $cm^{-1}$ zone were noticed. There signals were attributed to the new methyl group and the charged nitrogen [23,29]. In addition, a more intense water peak at 3400 $cm^{-1}$ could be related to more hydrophilic system.

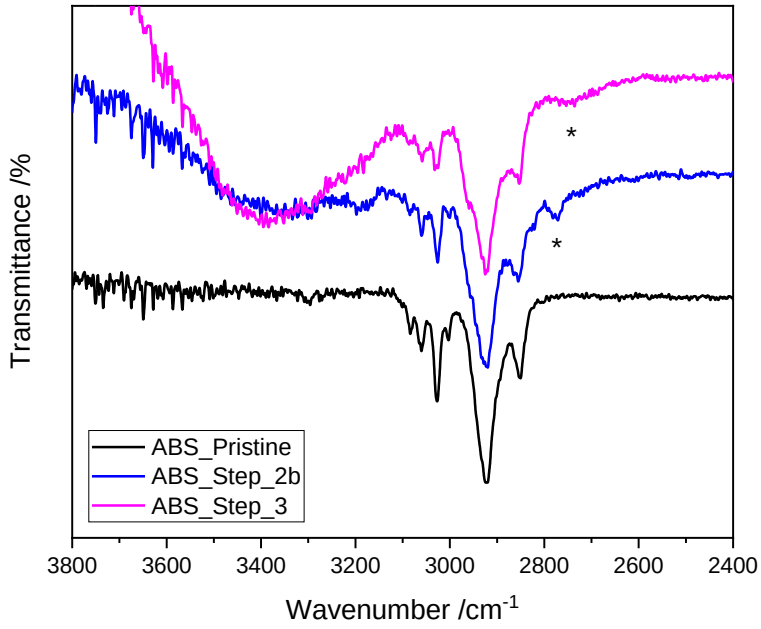


*Figure 4-34 - Zoom of IR spectra of ABS_Step_2b and step_3*

The final product the IEC was 0.69 meq*g$^{-1}$, with a global functionalization yield of 38.7%.

$$Maximun\ IEC = \frac{n\ (mmol)}{mass\ (g)} = \frac{\frac{mass\ (g)}{MW\ (g\ mol^{-1})} * 1000}{mass\ (g)} = \frac{1000}{MW\ (g\ mol^{-1})}$$

$$= \frac{1000}{560\ (g\ mol^{-1})} = 1.78\ \frac{mmol}{g}$$

$$\%\ functionalization = \frac{0.69\ (\frac{mmol}{g})}{1.78\ (\frac{mmol}{g})} * 100 = 38.7\ \%$$

To better understand the IEC result, elementary analysis was performed of ABS and full-sulfonated ABS (Step_1a). As for polystyrene materials, I could hypnotize a sulfonamide yield and also investigate the effect of styrene unit concentration of this functionalization.

| CHNS | % C | % H | % N | % S | % O |
|---|---|---|---|---|---|
| ABS_Pristine | 85,80 | 7,316 | 6,70 | 0,030 | 0,16 |
| ABS_Step_1a | 75,86 | 6,861 | 4,66 | 4,895 | 7,724 |

$$C/S\ ratio = \frac{\frac{\%\ C}{WA}}{\frac{\%\ S}{WA}} = \frac{\frac{75.36}{12.01}}{\frac{4.895}{32.01}} = 41.3$$

$$\%\ functionalization = \frac{n°\ C}{C/S} * 100 = \frac{15}{41.3} * 100 = 36.3\ \%$$

From calculations, the step_1a was functionalized for 36.3%. Within the experimental errors, this value is in line with the IEC value. I could hypothesize that this anionic modification is more efficient for "styrene-diluted" systems than for polystyrene. This phenomenon could be explained by the lower presence of styrene units and, thus, by a greater dispersion of the charged parts in the polymer. This information is in favor of styrene-based copolymer and terpolymer, opening the way for further studies of these materials.

## 4.3 – Chapter conclusion

I reported the preliminary functionalization of styrene-based materials such as polystyrene and acrylonitrile-butadiene-styrene. The functionalization was aimed to generate N-(quaternary ammonium) alkylsulfonamide. The synthesis procedure was based on a first sulfonation process of aromatic rings, to obtain sulfonic groups which were converted into sulfonamide by reaction with diamine. Finally, in the last step, the polymers were methylated, generating a quaternary ammonium group.

Initial studies were carried out on poly(4-styrenesulfonic acid), giving sulfonic salt and consequently soluble polymers. To reduce solubility of the modified polymers, I worked in two directions: the first was the exploration of synthesis of sub-stoichiometry sulfonated polystyrene while, the second one was the functionalization of "diluted" styrene-based matrix such us ABS. For polystyrene, I varied the stoichiometry ratio of sulfonating agent using polystyrene to generate different sulfonated polystyrene (SPS). The higher sulfonation degree polymers were water soluble, so resulting not useful for fuel cell and electrolyzer application. The best result was obtained for the polystyrene with 15% of functionalization, with IEC of 0.33 meq*$g^{-1}$. For ABS, I explored the synthesis of full-sulfonated polymer. The initials test of sulfonation were carried out with two procedures, which can modify or not the nitrile group into carboxy acid (Step_1b and Step_1a, respectively). The polymer

with both acids will be investigate in future works. On the materials with nitrile group, I completed the modification, obtaining an anion conducting polymer with a functionalization of 38.7% and an IEC of 0.69 meq*$g^{-1}$.

These initial functionalization tests demonstrate the possibility of direct functionalization of styrene-based materials to generate anion exchange polymers. This opens the possibility of future recovery and recycling of waste material such as polystyrene, enhancing the economic material value. Although the IEC values are lower than other styrene-based polymers (i.e. prepared by chloromethylation and polymerization[30–32]), this functionalization gives a good information for the development of new direct modifications of styrene-based copolymers and terpolymers. In fact, by choosing the appropriate monomers, it's possible to optimize the equivalent weight of the polymers, increasing the IEC while remaining with a low degree of functionalization[27,33]. In addition, this would also allow a better control on the mechanical and chemical properties of the modified polymer i.e. its hydrophobicity.

## Bibliography


1. Puype F, Samsonek J, Knoop J, Egelkraut-Holtus M, Ortlieb M. Evidence of waste electrical and electronic equipment (WEEE) relevant substances in polymeric food-contact articles sold on the European market. *Food Addit Contam - Part A Chem Anal Control Expo Risk Assess*. 2015;32(3):410-426. doi:10.1080/19440049.2015.1009499

2. Martins JN, Klohn TG, Bianchi O, Fiorio R, Freire E. Dynamic mechanical, thermal, and morphological study of ABS/textile fiber composites. *Polym Bull*. 2010;64(5):497-510. doi:10.1007/s00289-009-0200-6

3. Ma H, Huang J. Tactic polystyrene and styrene copolymers. *Stereoselective Polym with Single-Site Catal*. 2007:363-398. doi:10.1002/14356007.a21

4. Thakur S, Verma A, Sharma B, Chaudhary J, Tamulevicius S, Thakur VK. Recent developments in recycling of polystyrene based plastics. *Curr Opin Green Sustain Chem*. 2018;13:32-38. doi:10.1016/j.cogsc.2018.03.011

5. Couture G, Alaaeddine A, Boschet F, Ameduri B. Polymeric materials as anion-exchange membranes for alkaline fuel cells. *Prog Polym Sci*. 2011;36(11):1521-1557. doi:10.1016/j.progpolymsci.2011.04.004

6. Bonizzoni S, Stilli P, Lohmann-Richters F, et al. Facile Chemical Modification of Aquivion® Membranes for Anionic Fuel Cells. *ChemElectroChem*. 2021;8(12):2231-2237. doi:10.1002/celc.202100382

7. Vijayakumar V, Nam SY. Recent advancements in applications of alkaline anion exchange membranes for polymer electrolyte fuel cells. *J Ind Eng Chem*. 2019;70:70-86. doi:10.1016/j.jiec.2018.10.026

8. Stilli P, Bonizzoni S, Lohmann-Richters F, Beverina L, Papagni A, Mustarelli P. Aquivion®-based anionic membranes for water electrolysis. *Electrochim Acta*. 2022;405:139834. doi:10.1016/j.electacta.2022.139834

9. Loudon M. *Chimica Organica*.; 2010.

10. Clayden J, Greeves N, Warren S. *Organic Chemistry*. Second edi. (Press O university, ed.).

11. Lane JR, Kjaergaard HG. Fluorosulfonic acid and chlorosulfonic acid: Possible candidates for OH-stretching overtone-induced photodissociation. *J Phys Chem A*. 2007;111(39):9707-9713. doi:10.1021/jp074436d

12. Guan R, Zou H, Lu D, Gong C, Liu Y. Polyethersulfone sulfonated by chlorosulfonic acid and its membrane characteristics. *Eur Polym J*. 2005;41(7):1554-1560. doi:10.1016/j.eurpolymj.2005.01.018

13. JIANMING;JI, LI D, WEIGANG D. Method for synthesizing sulfanilamide by using chlorobenzene as raw material.

14. Silverstein RM, Webster FX, J. Kiemle D. *Identificazione Spettrometrica Di Composti Organici*.

15. Millipore Sigma. IR Spectrum Table. *Millipore Sigma*. 2020:1-18.

https://www.sigmaaldrich.com/technical-documents/articles/biology/ir-spectrum-table.html.

16. Fang J, Xuan Y, Li Q. Preparation of polystyrene spheres in different particle sizes and assembly of the PS colloidal crystals. *Sci China Technol Sci*. 2010;53(11):3088-3093. doi:10.1007/s11431-010-4110-5

17. Spectral Database for Organic Compounds SDBS. https://sdbs.db.aist.go.jp/sdbs/cgi-bin/cre_index.cgi.

18. Wei W, Lin S, Reddy DHK, Bediako JK, Yun YS. Poly(styrenesulfonic acid)-impregnated alginate capsule for the selective sorption of Pd(II) from a Pt(IV)-Pd(II) binary solution. *J Hazard Mater*. 2016;318:79-89. doi:10.1016/j.jhazmat.2016.06.050

19. Danilczuk M, Lin L, Schlick S, Hamrock SJ, Schaberg MS. Understanding the fingerprint region in the infra-red spectra of perfluorinated ionomer membranes and corresponding model compounds: Experiments and theoretical calculations. *J Power Sources*. 2011;196(20):8216-8224. doi:10.1016/j.jpowsour.2011.05.067

20. Lowry SR, Mauritz KA. An Investigation of Ionic Hydration Effects in Perfluorosulfonate Ionomers by Fourier Transform Infrared Spectroscopy. *J Am Chem Soc*. 1980;102(14):4665-4667. doi:10.1021/ja00534a017

21. Jiang DD, Yao Q, McKinney MA, Wilkie CA. TGA/FTIR studies on the thermal degradation of some polymeric sulfonic and phosphonic acids and their sodium salts. *Polym Degrad Stab*. 1999;63(3):423-434. doi:10.1016/S0141-3910(98)00123-2

22. Krueger PJ. Intramolecular hydrogen bonds in ethylenediamines and other aliphatic diamines. *Can J Chem*. 1967;45. doi:https://doi.org/10.1139/v67-348

23. Hine J, Li W-S. Synthesis of Some cis- and trans-2-Dimethylaminomethy1.CycliAc mines and Related Diamines. *J Org Chem,*. 1975;Vol. 40:1-4. doi:https://doi.org/10.1021/jo00891a005

24. Wang Z, Tang H, Li J, Zeng Y, Chen L, Pan M. Insight into the structural construction of a perfluorosulfonic acid membrane derived from a polymeric dispersion. *J Power Sources*. 2014;256:383-393. doi:10.1016/j.jpowsour.2014.01.096

25. Kucera. F., Jancar. J. Homogeneous and Heterogeneous Sulfonation of Polymers: A Review. *Polym Eng Sci*. 1998;3(5):783-792.

26. Vinodh R, Ilakkiya A, Elamathi S, Sangeetha D. A novel anion exchange membrane from polystyrene (ethylene butylene) polystyrene: Synthesis and characterization. *Mater Sci Eng B Solid-State Mater Adv Technol*. 2010;167(1):43-50. doi:10.1016/j.mseb.2010.01.025

27. Lin B, Xu F, Su Y, et al. Facile Preparation of Anion-Exchange Membrane Based on Polystyrene-b-polybutadiene-b-polystyrene for the Application of Alkaline Fuel Cells. *Ind Eng Chem Res*. 2019;58(49):22299-22305. doi:10.1021/acs.iecr.9b05314

28. Khomein P, Ketelaars W, Lap T, Liu G. Sulfonated aromatic polymer as a future proton exchange membrane: A review of sulfonation and crosslinking methods. *Renew Sustain Energy Rev*. 2021;137(September 2019):110471. doi:10.1016/j.rser.2020.110471

29. Hine J, Shyong L. Internal Hydrogen Bonding and Positions of Protonation in the Monoprotonated Forms of Some 1,3- and 1,4-Diamines. *J Org Chem*. 1975;40(12):1795-1800.

doi:10.1021/jo00900a026

30. Gupta G, Scott K, Mamlouk M. Soluble Polystyrene-b-poly (ethylene/butylene)-b-polystyrene Based Ionomer for Anion Exchange Membrane Fuel Cells Operating at 70 °C. *Fuel Cells*. 2018;18(2):137-147. doi:10.1002/fuce.201700176

31. Tsai TH, Maes AM, Vandiver MA, et al. Synthesis and structure-conductivity relationship of polystyrene-block- poly(vinyl benzyl trimethylammonium) for alkaline anion exchange membrane fuel cells. *J Polym Sci Part B Polym Phys*. 2013;51(24):1751-1760. doi:10.1002/polb.23170

32. Chae JE, Lee SY, Yoo SJ, et al. Polystyrene-based hydroxide-ion-conducting ionomer: Binder characteristics and performance in anion-exchange membrane fuel cells. *Polymers (Basel)*. 2021;13(5):1-13. doi:10.3390/polym13050690

33. Golubenko D V., Van der Bruggen B, Yaroslavtsev AB. Novel anion exchange membrane with low ionic resistance based on chloromethylated/quaternized-grafted polystyrene for energy efficient electromembrane processes. *J Appl Polym Sci*. 2020;137(19):1-10. doi:10.1002/app.48656

# Chapter 5: Conclusion

Green hydrogen, as energy vector, is expected to replace fossil hydrocarbon fuels. In a circular hydrogen-based economy, electrolyzers and fuel cells technologies play a crucial role in vector generation and conversion, respectively. In particular, Anion Exchange Membrane Fuel Cells (AEMFCs) and ELectrolyzers (AEMELs) are expected to represent a breakthrough with respect to the state of the art, allowing the use of low-cost catalysts, in principle avoiding Platinum Group Metals (PGM) and other critical raw materials. The main drawbacks of using an alkaline working environment are mainly related to the polymeric membrane: a lower conductivity of $OH^-$, combined with the low stability and durability of the polymer electrolytes, do not allow a large-scale diffusion of this technology.

During my PhD, I studied and investigated chemical modification procedures to produce anionic conduction polymers for fuel cell and electrolyzer applications, starting from commercial polymers. In particular, I worked on the modification different classes of polymers, including perfluorinated systems (Aquivion®), aliphatic polyketones, and polystyrene.

For the perfluorinated systems, I modified a commercial proton-exchange membrane to obtain an anionic conducting membrane. The Aquivion® membranes were functionalized by reaction with aqueous diamine solution to obtain sulfonamide AEM. This allows to maintain the same mechanical and chemical resistance of the pristine material but at the same time, it increases the thermal stability thanks to the formation of sulfonamide bonds. In addition, this functionalization was carried out in an aqueous media, which is clearly advantageous from the environmental point of view. The synthesis was confirmed by using several techniques i.e. IR and NMR spectroscopies and TGA and DSC measurements. The modified membranes showed an ionic conductivity of 26 $mS*cm^{-1}$ at 80°C and 100% relative humidity, with IEC of 0.77 $meq*g^{-1}$. I investigated the chemical and electrochemical stability using ex-situ and in-situ methods. As ex-situ treatments, I checked the durability of membranes by soaking them in KOH solution by varying the concentration, temperature and duration of the tests. The results demonstrated that the membranes were stable in alkaline environment and the changes of physical-chemical properties (i.e., conductivity) were negligible. For in-situ test, the membranes were used in electrolyzer using nickel foam as electrode, 1M and 3M KOH solutions as supply feed at 80°C. The best results, in terms of current, were

obtained with the 50 µm modified Aquivion® at 2V after 144 hours obtaining 100 mA*cm$^{-2}$ and 130 mA*cm$^{-2}$ for 1M and 3M KOH solution, respectively.

For the aliphatic polyketones, I modified a commercial polyketones thanks to the Pall Knorr reaction. This reaction allows to introduce a heteroatom aromatic ring inside the polymer chain, modifying for example its mechanical and thermal properties. I investigate the formation of pyrrole-based and furan-based polymer systems. For pyrrole-based polymer, the synthesis procedure involved the reaction of polyketones with a primary-ternary diamine. In the first step, the primary nitrogen was used for the formation of the pyrrole ring thanks to the Pall Knorr reaction, and then, in the secondary step, the ternary nitrogen was methylated in order to obtain a quaternary ammonium conductive polymer. In the first phase, I investigated the effect of time on the reaction yield to identify an optimal process duration and then I studied the effect of the different diamine stoichiometry and the properties of the pyrrole-derivates. The best result was for the 57,4 % functionalized pyrrole-based polymers with an IEC of 1.67 meq*g$^{-1}$. The advantages of this reaction are related to the possibility of obtaining a conductive polymer in only two steps, working in mild conditions and with a relative low-cost material. For furan-based polymers, the synthesis procedure involved two steps. In the first, furan-based derivatives were obtained by reaction of Pall-Knorr, then, in secondary step, I functionalized them through the Dials-Alder reaction, introducing the active site with an appropriate dienophilic. In the first phase I studied and developed a new method for obtaining funanic derivatives, using sulfuric acid. This procedure doesn't employ organic solvents making it more sustainable and greener. In the second phase, I investigated the functionalization of the furanic derivate thanks to Diels-Alder reaction, using 1-vinylimidazole. In a first phase the Diels-Alder product was prepared and then, the imidazole ring was methylated making the polymer conductive. The obtained polymer showed an IEC of 0.08 meq*g$^{-1}$ and, although it was low, it demonstrated the feasibility of this synthesis route. The advantages of this process are related to the possibility of using low-cost reagents that can be recycled (e.g. by distillation), making it an economic and potentially scalable process.

For the styrene-based polymer, I studied the modified polystyrene and acrylonitrile-butadiene-styrene. The functionalization was aimed to generate styrene-based N-(quaternary ammonium) alkylsulfonamide. The synthesis procedure was based on a fist sulfonation process of aromatic rings in order to obtain sulfonic groups which were converted into sulfonamide by reaction with diamine. Finally, in the last step, the polymers were methylated, generating a quaternary ammonium group.

The initial studies were carried out on poly(4-styrenesulfonic acid), giving sulfonic salt and consequently soluble polymers. In order to reduce solubility of the modified polymers, I worked in two directions: the first was the exploration of synthesis of sub-stoichiometry sulfonated polystyrene while, the second one was the functionalization of "diluted" styrene-based matrix such us ABS. For polystyrene, I varied the stoichiometry ratio of sulfonating agent using polystyrene in order to generate different sulfonated polystyrene (SPS). The higher sulfonation degree polymers were water soluble resulting not useful for fuel cell and electrolyzer application. The best result was for the polystyrene with 15% of functionalization, with IEC of 0.33 meq*$g^{-1}$. For ABS, I explored the synthesis of full-sulfonated polymer. The initials test of sulfonation were carried out with two procedure which can modify or not the nitrile group into carboxy acid (Step_1b and Step_1a, respectively). The polymer with both acids will be investigate in future works. On the materials with nitrile group, I completed the modification, obtaining an anion conducting polymer with a functionalization of 38.7% and an IEC of 0.69 meq*$g^{-1}$.

In conclusion, the most interesting results were obtained from Aquivion® modification. This new Aquivion®-based anion exchange membranes showed excellent durability in alkaline environment, making them promising materials for AEMFC and AEMWE. The modification procedures of polyketones needed more investigation. However, their benefits, e.g. the production of AEM in few synthesis step and relatively low-cost material, were interesting and potentially useful advantages for the development of low-cost and scalable anion exchange membranes. The functionalization method of polystyrene must be improved and optimized in order to guarantee the possibility of future recovery and recycling of waste material such as polystyrene, obtaining eco-friendly polymers.

# Chapter 6: Information and appendix

# *Additional works*

During my PhD period, I worked on the synthesis and characterization of solid polymer electrolytes for fuel cell and electrolyzer applications.

Here, I report the other types of electrolytes studied for electrochemical applications and the activities which I did for external company.

## AW1 - Lithium conducting system

- "Polymer-in-Ceramic Nanocomposite Solid Electrolyte for Lithium Metal Batteries Encompassing PEO-Grafted $TiO_2$ Nanocrystals"

*Abstract:*

Lithium Metal Batteries (LMB) require solid or quasi-solid electrolytes able to block dendrites formation during cell cycling. Polymer-in-ceramic nanocomposites with the ceramic fraction exceeding the one normally used as the filler (>10 ÷ 15 wt%) are among the most interesting options on the table. Here, we report on a new hybrid material encompassing brush-like $TiO_2$ nanocrystals functionalized with low molecular weight poly(ethylene oxide) (PEO). The nanocomposite electrolyte membranes are then obtained by blending the brush-like nanocrystals with high molecular weight PEO and LiTFSI. The intrinsic chemical compatibility among the PEO moieties allows a $TiO_2$ content as high as ~39 wt% (90:10 w/w functionalized nanocrystals/PEO- LiTFSI), while maintaining good processability and mechanical resistance. The 50:50 w/w nanocomposite electrolyte (18.8 wt% functionalized TiO2) displays ionic conductivity of $3 \times 10^{-4}$ $Scm^{-1}$ at 70 °C. Stripping/plating experiments show an excellent long-term behavior even at relatively high currents of 200 $\mu Acm^{-2}$. Upon testing in a lab-scale Li/electrolyte/$LiFePO_4$ cell, the material delivers 130 $mAh*g^{-1}$ and 120 $mAh*g^{-1}$ after 40 and 50 cycles at 0.05 and 0.1 mA, respectively, with Coulombic efficiency exceeding 99.5%, which demonstrates the very promising prospects of these newly developed nanocomposite solid electrolyte for future development of LMBs.

Doi: 10.1149/1945-7111/ab7c72

- "Is It Possible to Obtain Solvent-Free, $Li^+$-Conducting Solid Electrolytes Based on Pure PVdF? Comment on "Self-Suppression of Lithium Dendrite in All-Solid-State Lithium Metal Batteries with Poly(vinylidene difluoride)- Based Solid Electrolytes" "

Doi: 10.1002/adma.201907375

## AW2 - Sodium conducting system

- "The properties of highly concentrated aqueous $CH_3COOK$/Na binary electrolyte and its use in sodium-ion batteries"

Abstract:

Highly concentrated aqueous binary solutions of acetate salts are emerging as promising systems for advanced energy storage applications. Together with superior solubility of $CH_3COOK$ helpful in achieving water-in-salt electrolyte concentrations, the presence of $CH_3COOLi$ or $CH_3COONa$ permits intercalation of desired cations in electrode crystalline phases. Although these systems have captured profound scientific attention in recent years, a fundamental understanding of their physicochemical properties is still lacking. In this work, the thermal, rheological, transport, and electrochemical properties for a series of solutions comprising of 20 $mol*kg^{-1}$ of $CH_3COOK$ with different concentrations of $CH_3COONa$ are reported and discussed. The most concentrated solution, i.e., 20 $mol*kg^{-1}$ of CH3COOK with 7 $mol*kg^{-1}$ of $CH_3COONa$ came out to be the best in terms of a compromise between transport properties and electrochemical stability window. Such a solution has a conductivity of 21.2 $mS*cm^{-1}$ at 25°C and shows a stability window up to 3 V in "ideal" conditions, i.e., using small surface area and highly electrocatalytic electrode in a flooded cell. As a proof of concept of using this solution in sodium-ion batteries, carbon-coated $LiTi_2(PO_4)_3$ (NASICON) demonstrated the ability to reversibly insert and de-insert Na+ ions at about -0.7 V vs. SHE with a first cycle anodic capacity of 85 $mAh*g^{-1}$, average charge efficiency of 96% at low current and a 90% capacity retention after 60 cycles. The very good kinetic properties of the interface are also demonstrated by the low value of activation energy for the charge transfer process (0.12 eV).

Doi: 10.26434/chemrxiv-2021-1jxxp

## AW3 - Potassium conducting system

- "A physico-chemical investigation of highly concentrated potassium acetate solutions towards applications in electrochemistry"

*Abstract:*

Water-in-salt solutions, i.e. solutions in which the amount of salt by volume or weight is larger than that of the solvent, are attracting increasing attention in electrochemistry due to their distinct features that often include decomposition potentials much higher than those of lower concentration solutions. Despite the high solubility of potassium acetate (KAC) in water at room temperature (up to 25 moles of salt per kg of solvent), the low cost, and the large availability, the use of highly concentrated KAC solutions is still limited to a few examples in energy storage applications and a systematic study of their physical–chemical properties is lacking. To fill this gap, we have investigated the thermal, rheological, electrical, electrochemical, and spectroscopic

features of KAC/water solutions in the compositional range between 1 and 25 mol*kg$^{-1}$. We show the presence of a transition between the ‘‘salt-in-solvent’’ and ‘‘solvent-in-salt’’ regimes in the range of 10–15 mol*kg$^{-1}$. Among the explored compositions, the highest concentrations (20 and 25 mol*kg$^{-1}$) exhibit good room temperature conductivity values (55.6 and 31 mS*cm$^{-1}$, respectively) and a large electrochemical potential window (above 2.5 V)

Doi: 10.1039/d0cp04151c

## AW4 - Electrocatalyst for fuel cells

- “Waste Face Surgical Mask Transformation into Crude Oil and Nanostructured Electrocatalysts for Fuel Cells and Electrolyzers”

*Abstract:*

A novel route for the valorization of waste into valuable products was developed. Surgical masks commonly used for COVID 19 protection by stopping aerosol and droplets have been widely used, and their disposal is critical and often not properly pursued. This work intended to transform surgical masks into platinum group metal-free electrocatalysts for oxy- gen reduction reaction (ORR) and hydrogen evolution reaction (HER) as well as into crude oil. Surgical masks were subjected to controlled-temperature and -atmosphere pyrolysis, and the produced char was then converted into electrocatalysts by functionalizing it with metal phthalocyanine of interest. The electrocatalytic performance characterization towards ORR and HER was carried out highlighting promising activity. At different temperatures, condensable oil fractions were acquired and thoroughly analyzed. Transformation of waste surgical masks into electrocatalysts and crude oil can open new routes for the conversion of waste into valuable products within the core of the circular economy.

Doi: 10.1002/cssc.202102351

## AW5 - Works for external company

- AMSA (Anonima Materie Sintetiche Affini), Como, Italy.

Aim: Determination of the surface resistance of polymeric film by EIS measurements

- De Nora, Milano, Italy.

Aim: Determination of the resistance of membranes in alkaline environment

- ALUSERVICE, Milano, Italy.

Aim: Determination of ions concentration of by electrochemical methods

# *Overview of activities*

Below find in attached the list of my PhD period activities.

## List of publications

- S. Khalid, N. Pianta, S. Bonizzoni, P. Mustarelli, and R. Ruffo, “The properties of highly concentrated aqueous CH 3 COOK / Na binary electrolyte and its use in sodium-ion batteries,” pp. 1–29.

- P. Stilli, S. Bonizzoni, F. Lohmann-Richters, L. Beverina, A. Papagni, and P. Mustarelli, “Aquivion®-based anionic membranes for water electrolysis,” Electrochim. Acta, p. 139834, 2022.

- M. Muhyuddin, J. F.ilippi, L. Zoia, S. Bonizzoni et al., “Waste Face Surgical Mask Transformation into Crude Oil and Nanostructured Electrocatalysts for Fuel Cells and Electrolyzers,” ChemSusChem, vol. 14, pp. 1–15, 2021.

- Bonizzoni S, Stilli P, Lohmann-Richters F, et al. Facile Chemical Modification of Aquivion® Membranes for Anionic Fuel Cells. ChemElectroChem. 2021;8(12):2231-2237. doi:10.1002/celc.202100382

- Stigliano PL, Pianta N, Bonizzoni S, et al. A physico-chemical investigation of highly concentrated potassium acetate solutions towards applications in electrochemistry. Phys Chem Chem Phys. 2021;23(2). doi:10.1039/d0cp04151c

- Colombo F, Bonizzoni S, Ferrara C, et al. Polymer-in-Ceramic Nanocomposite Solid Electrolyte for Lithium Metal Batteries Encompassing PEO-Grafted TiO 2 Nanocrystals . J Electrochem Soc. 2020;167(7):070535. doi:10.1149/1945-7111/ab7c72

- Callegari D, Bonizzoni S, Berbenni V, Quartarone E, Mustarelli P. Is It Possible to Obtain Solvent-Free, Li+-Conducting Solid Electrolytes Based on Pure PVdF? Comment on “Self-Suppression of Lithium Dendrite in All-Solid-State Lithium Metal Batteries with Poly(vinylidene difluoride)-Based Solid Electrolytes.” Adv Mater. 2020;1907375:1-3. doi:10.1002/adma.201907375

- Bonizzoni S, Ferrara C, Berbenni V, Anselmi-Tamburini U, Mustarelli P, Tealdi C. NASICON-type polymer-in-ceramic composite electrolytes for lithium batteries. Phys Chem Chem Phys. 2019;21(11). doi:10.1039/c9cp00405j

## Poster and oral presentation

- Oral presentation - Aquivion®-Based Alkaline Exchange Membrane for Fuel Cell and Electrolyzer Applications at “European Fuel Cell and Hydrogen, Piero Lunghi conference 2021” online.
- Oral presentation - Aquivion®-Based Alkaline Exchange Membrane for Fuel Cell and Electrolyzer Applications at “XXVII Congresso Nazionale della Società Chimica Italiana” at, Milan Italy.
- Oral presentation - Aquivion®-Based Anion Exchange Membrane for Fuel Cell and Electrolyzer Applications at “29th Topical Meeting of the International Society of Electrochemistry” at Mikulov, Czech Republic.
- Poster - “Synthesis of Stable Polyfluorinated Anion Exchange Membrane by Chemical Modification of Aquivion®” at “71st Annual Meeting of the International Society of Electrochemistry” at Belgrade.
- Poster - "PEO-grafted TiO2 filler as Solid Polymer Electrolyte for rechargeable lithium batteries" at GEI 2019 Padova.

**Congress and workshop**

- “European Fuel Cell and Hydrogen, Piero Lunghi conference 2021” virtual conference (15th-17th December 2021). With oral presentation.
- “XXVII Congresso Nazionale della Società Chimica Italiana” at Milan, Italy, Online (14th - 23th September 2021). With oral presentation.
- “29th Topical Meeting of the International Society of Electrochemistry” at Mikulov, Czech Republic, Online (18th - 21th April 2021). With oral presentation.
- Workshop “GISEL: First Italian Workshop on Energy Storage”, Online (24th - 26th February 2021).
- “71st Annual Meeting of the International Society of Electrochemistry” at Belgrade, online (31st August - 4th September 2020). With poster.
- Online conference “European perspectives on batteries of the future” held by the BATTERY 2030+ (25th - 26th May 2020).
- Workshop “HorizonChem 2019” at University of Milano Bicocca (5th April 2019).
- Conference "Giornate elettrochimiche italiane (GEI) 2019” at Padova, Italy (8th - 12th September 2019). With poster.

## Courses

- Surfing the academic job market: how to publish in high impact international journals (1 CFU)
- Giovani & impresa (1 CFU)
- Principles of electrochemical energy conversion (2 CFU)
- Frequency response analysis in electrochemical systems (1 CFU)

## Seminar

- Maximising the impact of your research
- Tailored Nanoparticles Prepared in Superfluid Helium Droplets
- Van der Waals epitaxy and characterization of quasi-two-dimensional Ge-Sb-Te alloys and superlattices
- Dynamic Molecular Crystals: The Bigger Picture
- Porous materials without a framework

## Schools

- 12th International Symposium of Electrochemical Impedance Analysis at Stuttgart, Germany, Online (from 29th to 30th November 2021).
- Spring school "International Spring School of Electrochemistry" ISSE 2019 at Castellammare del Golfo, Italy (from 19th to 23th May 2019).

## Stages

- Stage at University of Padova, Italy, under the supervision of Prof Vito Di Noto. (from 27th November 2018 to 23th December 2018). Activity: to learn basic knowledge and Know-how for the realization of a synthesis implant of polyketones.
- Stage at University of Padova, Italy, under the supervision of Prof Vito Di Noto. (from 27th to 29th January 2020). Activity: to learn knowledge and Know-how for the realization of protonic and anionic MEA for fuel cells.

## Thesis tutoring

- Laboratory tutor for curricular internship of two bachelor students.
- Co-supervisor of six bachelor degree thesis
- Co-supervisor of two master degree thesis

## Didactic activities

- Tutor for didactic activities of “Progetto Lauree Scientifiche (PLS)” 2020, at University of Milano Bicocca, Italy (February 2020).
- Workshop for orientation day at Highschool “ITIS E.Molinari”, Milan, Italy (4th November 2019)
- Tutor for didactic activities of “Alternanza scuola-lavoro” 2019, at University of Milano Bicocca, Italy (June 2019)
- Workshop for orientation day at Highschool “ITIS G.Cardano”, Pavia, Italy (6th February 2019).
- Tutor for didactic activities of “Progetto Lauree Scientifiche (PLS)” 2019, at University of Milano Bicocca, Italy (February 2019).

# *Experimental section*

In this section, the experimental details of the measurement and the method applied were reported.

### ES1 – Infrared spectroscopy (FTIR)

The infrared spectroscopy (IR) is a useful technique based on the vibrations transition, that allows to investigate and detect the main chemical functions of a material. The vibrational modules of a chemical bond, i.e. stretching and bending, are characterized by a specific energy that is related to the strength of the bond and to the type of atoms involved in it [1]. For this reason, it's possible correlate an IR signal with the opportune vibration transition and, consequently, to a specific chemical function. In this way, the IR spectroscopy can give qualitative information about the structure of a sample. The advantages of IR spectroscopy are the low-cost instrumentation, easy optical design and operation, simple surface selection rule, and wide applicability to various materials[2]. In particular, I used Attenuated Total Reflectance Fourier transform Infra-Red spectroscopy (ATR-FT-IR). With this set-up, the beam of infrared light is passed through the ATR crystal in such a way that it reflects at least once off the internal surface in contact with the sample. This reflection forms an evanescent wave which extends into the sample, being the penetration depth of this wave a characteristic peculiar of the sample itself. In fact, mainly the intensity of ATR-IR spectra is minor than transmittance one [3] but, at same time, ATR set-up allows a more easier analysis of liquid and solid samples.

The Infrared (IR) spectra were obtained on Jasco FT/IR-4100 spectrometer equipped with ATR accessory and the data were analyzed with Spectra Manager™ Suite software. The measurements were recorder from 4000–500 $cm^{-1}$ with resolution of 2.0 $cm^{-1}$. The IR spectra were showed as % transmittance in function of wavenumber expressed in $cm^{-1}$.

## ES2 – Nuclear magnetic resonance spectroscopy (NMR)

The nuclear magnetic resonance spectroscopy (NMR) is one of the powerful techniques to investigate and analyze the structure of a material, that is rely on measuring the difference amongst the energy nuclear spin states caused by the presence of a strong eternal magnetic field[4,5]. This spectroscopy can only operate with the nuclei which have a nuclear magnetic spin moment because when they are in the magnetic field, they can assume specific orientation with precise energy levels. The energies distribution follows the formula:

$$\mu=\gamma P=m\gamma\hbar$$

Where μ is the magnetic moment, $\gamma$ is the gyromagnetic ratio, $P$ is the spin moment, $m$ is the quantic spin number of the nucleus, and $\hbar=h/2\pi$, in which $h$ is Planck's constant.

From a mechanical point of view, in the presence of a magnetic field, the magnetic moment of each spin starts to rotate doing a processional motion around the applied magnetic field axis, occupying different nuclear levels whose energy differences are proportional to the frequency. The nuclear levels are 2S+1, with spin vector (S), the energy gaps are $\Delta E= \gamma B0\hbar$, with $B0$ as applied magnetic field, and correlated frequencies are calculated as $v=\Delta E/h$. In order to obtain structural information, the nuclei must be excited causing a spin transition from one nucleal energy level to another. To do this, the sample must be irradiated with a radiofrequency with an energy equal to the energy jump of the levels. In the presence of different nuclei (with different spin systems and magnetic moments), it is possible to observe different absorptions phenomena at different frequencies due to the interactions of their electron cloud with the applied magnetic field causing the shielding or the de-shielding of the nuclei ($B_i$). These particular phenomena comport that each nucleus has a precise energy gap due to the total magnetic field ($B_o+B_i$), and consequently, a precise frequency. The effect of the different in frequency between the sample's and the reference's resonance frequency is called "chemical shift". In this way, it's possible associate the chemical shift of NMR signal with to the presence of specific vicinal group, obtaining information of the sample structure.

From a quantum mechanical point of view, each individual nucleus and the properties of the whole system are derived as an average ensemble. Each Hamiltonian operator $\hat{H}$, which describes the energy state of a system, is applied to each wave functions $\psi$, which instead describes the state of a systems, so that, in the end, a single global Hamiltonian can be identified:

$$H_{tot,interactions} = H_z + H_{RF} + H_{CS} + H_D + H_j + H_q + H_p + H_{exp}$$

Which includes the Zeeman interaction ($H_z$) between the nucleus and the external field, the interaction between the nucleus and the applied RF pulse ($H_{RF}$), the chemical shielding defining the interaction between the nucleus and the local change in the magnetic field due to changes in electron density ($H_{CS}$), the dipolar coupling trough space between two nuclei ($H_D$), the indirect spin coupling that defines the interaction trough bonds of the nuclei ($H_J$), the electric quadrupole interaction that affects the Zeeman energy level although it is an electric effect ($H_Q$), the interaction with unpaired electrons ($H_P$). In terms of sheer analysis, even more interactions are used to calculate the state of a molecule, like the anisotropic chemical shift, the dipolar coupling and the quadrupolar interactions, all involving the magnetic dipole moment and the orientation, described via the calculation of "interaction tensors" of each nucleus referred to the other ones.

Differently from standard liquid-state NMR, in solid-state NMR, since the analyzed matrix has no or little mobility, nuclei can be considered to find themselves in a static, uniform magnetic field [6], so anisotropic local fields and interactions, that are basically averaged by Brownian motion in liquids, assume bigger relevance. Every solid-state NMR experiment needs special techniques, like cross-polarization (CP), magic angle spinning (MAS), 2D experiments, and enhanced probe electronics [7], in order to have more high-definition spectra. The anisotropic part of a specific interaction can provide information about the local structure, being strongly related to the local environment of the nuclei. On the contrary, it also gives origin to broadening which can be so significant to lead to strong overlapping between the signals from different sites, lowering the global resolution of the spectrum. Among the first two techniques, cross-polarization consists in a transfer of polarization from abundant nuclei (such as $^{1}H$ and $^{19}F$) to rare nuclei ($^{13}C$), while the magical-angle-spinning is used to mimic the averaging of the orientations as it happens in solutions, by physically spinning the sample via an air turbine mechanism at a fixed angle (54.74°) with respect to the magnetic field. It is also possible to couple the MAS technique to other averaging method (especially quantum pulse sequences) to address specific problems.

Solid state NMR data were collected for each step reported in the schemes of the reaction on an Avance III Bruker 400 MHz spectrometer (9.4 T magnet) using a 4 mm MAS probe. $^{1}H$ spectra were collected with a single-pulse sequence adopting a $\pi/2$ pulse of 2.5 ms, the delay time was checked for each sample and averaged over 128 scans under MAS conditions (10 KHz).

$^{13}C$ spectra were acquired with $^{13}C$-$^{1}H$ CP-MAS sequence under the same MAS conditions. The $^{1}H$ π/2 pulse was 2.5 ms, the delay time 5–200 s depending on the sample, as previously determined with 1H experiments, the contact time 2.5 ms, and the signals were averaged over 1k–8k acquisitions.

The quantitative $^{13}C$ spectra were acquired under high-power decoupling conditions (HPDEC pulse program) with a π/2 pulse of 4.7 μs, recycle delay of 40 s and SPINAL-64 heteronuclear decoupling scheme. $^{1}H$ and $^{13}C$ spectra were referenced to the signal of adamantane (as a secondary standard with respect to TMS). Chemical shifts for both $^{1}H$ and $^{13}C$ have been referred to adamantane signals as a secondary standard with respect to tetramethylsilane (TMS, 0 ppm). The spectra were acquired, processed, and analyzed with the software package Topspin 3.1 (Bruker).

### ES3 – Thermogravimetric analysis (TGA)

Thermogravimetric Analysis (TGA) is a technique in which changes in weight are measured as a function of increasing temperature giving information about many physical and chemical phenomena of a sample[8]. The basic instrumental requirements are a precision balance and a furnace that allows accurate temperature controller working in dynamic or static modes. The TGA experiments could be performed in inert condition using nitrogen, argon or in reacting atmosphere with air, oxygen[9]. This technique gives information about the thermal stability, fusion, vaporization, absorption and adsorption, decomposition, solid-state and solid-gas-state reactions [8]. In general, the data curves could be elaborated to determinate the concentration of some species of known processes. However, in some case, this information is not enough the understand the thermal processes involved, so, TGA can be coupled with a spectroscopy such as FTIR or mass spectroscopy. With this improvement, it's possible understand the nature of the fragments during the mass losses of TGA curve.

The TGA measurements were carried out by heating the samples up to 600°C, with a heating rate of 10°C/min in air flux by using Mettler Toledo TGA/DSC1 and elaborating the data with STARe System software.

### ES4 – Thermogravimetric analysis coupled with infrared spectroscopy (TGA-IR)

To better understand the degradation processes of Aquivion®-based and polyketones-base materials, I performed the TGA coupled with FTIR. The TGA/DSC 1 star® system (Mettler Toledo) was connected to Nicolet™ iS20 FTIR Spectrometer. The exhaustive gas-line of the TGA furnace was connected to TGA-IR Module (Nicolet™ FTIR Spectrometers) that is placed in the spectrometer compartment.

I used the following protocol: 15 min at 30°C, heat up to 600°C, with a heating rate of 10°C/min using air atmosphere with 100 ml/min as flux. The first step is for the purging of the connector and IR measurement chamber. The data was elaborate by OMNIC™ Series Software (Thermofischer™). The data were plotted as transmittance in function of wavenumber or IR signal intensity in function of time.

### ES5 – Differential scanning calorimetry (DSC)

The differential scanning calorimetry is useful technique to study and investigate the polymer properties[9]. DSC is based on the measurement of heat flow of a sample which could be correlated to melting, crystallization, and mesomorphic transition temperatures, and the corresponding enthalpy and entropy changes, and characterization of the glass transition and other effects which show either changes in heat capacity or a latent heat[10].

The DSC protocol for Aquivion® samples:
From 25°C to 280°C at 10 °C/min, 3 min at 280°C, from 280°C to 25°C, 3 min at 25°C and from 25°C to 280°C.

The DSC protocol for polyketones samples:
From 0°C to 150°C at 10 °C/min, 3 min at 150°C, from 150°C to 0°C, 3 min at 0°C and from 0°C to 150°C.

All measurements were performed in nitrogen atmosphere with 80 ml/min flux, using a Mettler Toledo DSC 1 instrument, elaborating the data with STARe System software.

### ES6 – Elementary analysis (CHNS)

The elementary analysis (CHNS) is a rapid technique that allow the determination of carbon, hydrogen, nitrogen and sulfur in organic matrices and other types of materials[11]. the CHNS consists in high temperature combustion in an oxygen-rich environment that converts carbon into carbon dioxide, hydrogen into water, nitrogen into $NO_x$ and sulfur into sulfur dioxide. Then, these gases are conveyed in Gas-Chromatography-Mass spectroscopy (GC-MS) system separated and then quantified. The CHNS analysis were performed by using the varioMICRO V1.9.3 instrument in CHNS Mode, with ElementarAnalysensysteme GmbH software.

### ES7 - Scanning electron microscope (SEM)

A Scanning Electron Microscope (SEM) is used to analyze the surface of a materials in order to obtain information on its morphology, topography and composition, thanks to the interactions between an electron beam and the sample. The microscope works under high vacuum conditions to avoid interactions and contamination with gaseous external atmosphere. The electron beam excites the atoms of the surface and induces an emission scattered primary electrons, secondary electrons, and X-rays[12]. Primary electrons are the electrons of the incident beam, which are scattered through 90°-180° and emerge back out of the specimen surface, are called backscattered electrons (BSEs). Transmitted primary electrons and BSEs may have experienced elastic or inelastic scattering and have energy higher than 50 eV. They can give information on the average atomic number of the area. Secondary electrons are generated by several inelastic scattering mechanisms. They come from the external orbitals of superficial atoms and have energy lower than 50 eV. They can give information on sample topography. X-Rays are produced when primary electrons knock an electron out of an atom, and the subsequent transition of a second electron between energy states causes an emission of specific energy. They can be used to be directly attributed to a specific element in the sample, and thus used for chemical analysis (Energy Dispersive X-Ray Analysis, EDS).

The SEM images of Aquivion® membrane were performed in surface and cross-section. The cross-section samples were frozen in liquid nitrogen for sufficient time and then ripped with tweezers. All sample were carbon-coated with DC sputter. The images were acquired with a Gemini 500 Microscope (Zeiss), using a 5kV beam. Samples were coated in graphite with an automatic coater.

### ES8 - Contact angle measurement

The contact angle measurements provide information on the hydrophobicity of a surface. The experiment consists in depositing a drop of water on the surface and evaluating its sphericity. The evaluation parameter is the value of the angle between the tangent line of tears and the horizon. If the value is more the 90°C the surface has a hydrophobic behavior while if the value is less, the material shows hydrophilic behavior[13].

To make these measurements, a video of the falling drop is made and then the appropriate frames are separated (30 frames/second). The equipment necessary used are a photonic 5100 lamp, the hydrostatic pump “11 pico plus elite”, the “fast cam” camera. The videos were analyzed by Phototron fastcam viewer 4 and the measurement were performed by using ImaJ program.

### ES9 - Ion exchange capacity (IEC)

The ion exchange capacity (IEC) is a key parameter for ion conducting polymers. It’s defined as the millimole of active sites for a specific dried mass of a sample. Generally speaking, a high IEC is desired to insure adequate ionic conductivity of the membrane, but an excessively high IEC will be detrimental to membrane stability. In fact, higher value of IEC means higher concentration of charge portion in the polymer increasing the swelling of the membrane. At the same time, the cations will be more exposed to alkali attack and the gas permeability of membrane could be reduced[14]. The common method is a titration specific for cation and anion. Although this seems to be the simplest analysis, it is useful to repeat the measurements at least three times in order to have a more mitigated error and a more trustful value[15].

From proton conducting materials, the ion-exchange capacity (IEC) of the membrane was determined by the acid basic retro-titration[16]. A strip 2×4 cm2 of PEM was activated and washed at least 3 times in distilled water. After that, it was immersed in accurate-volume excess of 0.1 M KOH solution for 24 h. Subsequently, the excess of the KOH solution is titrated with a 0.1 M HCl standard solution. The membrane was recovered, washed and dried at 120 °C under vacuum for 2 h and then weighed.

$$IEC\ \left(\frac{meq}{g}\right) = \frac{(V_{(excess)} - V_{(stoichiometric)})(mL) * Conc.HCl\ \left(\frac{meq}{mL}\right)}{dry\ mass\ (g)}$$

From anion conducting, materials The ion-exchange capacity (IEC) of the membrane was determined by the Mohr titration method[17]. A strip 2×4 cm2 of AEM was immersed in a 0.5 M NaCl solution for 24 h, washed in water for 5 h and then immersed in a 0.2 M NaNO3 solution for 24 h. Finally, the NaNO3 solution was titrated with a 0.01 M AgNO3 standard solution using K2CrO4 as the indicator. The membrane was dried at 120 °C under vacuum for 2 h and weighed. The IEC was calculated as the ratio of the milliequivalents of membrane and its dry mass as following formula:

$$IEC\ \left(\frac{meq}{g}\right) = \frac{Stechiometric\ volume\ (mL) * Conc.AgNO_3\ \left(\frac{meq}{mL}\right)}{dry\ mass\ (g)}$$

### ES10 - Electrochemical impedance spectroscopy (EIS) - Conductivity measurements

The electrochemical impedance spectroscopy (EIS) is powerful technique that allows the investigation and the studies of electrochemical systems [18,19]. Impedance spectroscopy takes advantage of the large spectrum of timescales over which different processes within the electrochemical system occur to separate their individual effects. The commonly evaluated phenomena include ohmic (bulk) resistance, electrode properties such as charge transfer resistance and double-layer capacitance, and transport (diffusion) effects[20]. Electrochemical impedance spectroscopy is an experimental technique that involves imposing a small sinusoidal AC voltage or current signal of known amplitude and frequency to an electrochemical cell and monitoring the AC amplitude and phase response of the cell. The AC perturbation is typically applied over a wide range of frequencies, from 100 kHz to less than 1 Hz. The ratio and phase-relation of the AC voltage and current signal response is the impedance ($Z$).

A sinusoidal current signal of amplitude $I_{AC}$ and frequency $\omega$ can be defined as:

$$I(\omega) = I_{AC} * \sin(\omega t)$$

Where $t$ is time. The output AC voltage signal from e electrochemical cell can be defined as:

$$V(\omega) = V_{AC} * \sin(\omega t - \theta)$$

Where $V_{AC}$ is the amplitude of the output voltage signal, and $\theta$ is the phase angle. Appling the Ohm's law for the AC case, the Impedance is expressed as:

$$Z(i\omega) = \frac{V(i\omega)}{I(i\omega)} = \frac{V_{AC} * \sin(\omega t - \theta)}{I_{AC} * \sin(\omega t)}$$

This equation clearly explains that impedance is a complex number and can be written in complex notation as $Z$=$Z'$+$Z''$, where the real part is represented by $Z'$, and the imaginary part is $Z''$ and, consequently, the magnitude can be calculated as $|Z|$=√($Z'$)$^2$+($Z''$)$^2$. The impedance experiment can be described with the following four parameters: real and imaginary impedance ($Z'$, $Z''$), the impedance magnitude ($|Z|$), and the phase angle ($\theta$). The typically graph representation are the Nyquist plot, that is the imaginary part ($Z''$) versus real part ($Z'$), and Bode plots which can be displayed as the log $|Z|$ versus log ($\omega$) or phase angle ($\theta$) versus log ($\omega$). In order to better understand the impedance data could be fitted by an equivalent circuit. The idea is simulate the sample behavior due to electrochemical processes through the combinations of circuit components i.e. resistor, capacitor [20]. For a polymer electrolyte, the impedance response can be approximated by an equivalent circuit composed of resistances R and capacitor C in parallel [21] giving a semi-circle in the Nyquist plot. The value of Z' where the semi-circles end is the resistance of the sample. From this value, it's possible calculate the specimen conductivity take in account the its geometry:

$$K = \frac{l\ (cm)}{S\ (cm^2)}$$

$$Conductivity\ = \frac{K\ (\frac{1}{cm})}{R\ (ohm)} = \frac{1}{ohm * cm} = \frac{S}{cm}$$

Where $l$ is the thickness (cm), $S$ is the surface area (cm$^2$) of the membrane.

The in-plane conductivity of AEMs was determined by means of Electrochemical Impedance Spectroscopy using a VSP-300 multichannel (Biologic), with a 4-electrodes conductivity cell mounted in Fuel Cell Test System 850e (Scribner). The home-made, four electrodes cell is made with Teflon®. The electrodes are made of Pt wire 0.6 mm in diameter. The distance between the inner contacts is 0.5, the distance between the outer contacts is 1.8 cm. The measurements were carried out under nitrogen flux at 80°C in the frequency range 100 Hz–1 MHz, and in the relative humidity range 60%–

100%. Before the measurements, the membrane was activated and then washed at least three times to eliminate the excess of acid/basic. The protonic conducting membrane were activated using 1M $H_2SO_4$ solution while for alkaline ones 1 M KOH solution was used.

## ES11 – Stability test protocols

The durability of the membrane was investigated by using ex-situ and in-situ accelerated ageing tests[15,22,23]. The tests protocols were defined considering different ageing conditions in order to investigate the effects of KOH concentration and temperature on the polymer degradation.

*Ex-situ test*

For these tests the membranes were soaked in KOH solution varying the solution concentration, the duration and the temperature of the treatments. Strips of 0.8 cm x 5 cm of modified membranes were activated by immersion in 1M KOH solution at room temperature for 48 hours under inert atmosphere. After that, samples were washed with water to remove the basic excess. The strips were immersed in a 20 ml vial in the respective degassed ageing KOH solutions at a precise temperature according the protocols.

For the test performed in 6M KOH at room temperature, the membrane was recovered from the ageing solution, washed and placed in the conductivity cell. After measurement, the membrane was soaked again in 6M KOH solution to continue the testing. The measurements cell was assembled and disassembled in the wet box to avoid carbon dioxide contamination and the EIS was performed using a VSP-300 multichannel (Biologic), with a 4-electrodes conductivity cell mounted in Fuel Cell Test System 850e (Scribner). The SEM images of aged membrane were done as described in ES7.

For the test performed in temperature, I used three different ageing conditions: “Light ageing” 1M KOH solution at 60°C, “Medium ageing” 1M KOH at 80°C, “Heavy ageing” 3M KOH at 80°C. The samples were extracted after 48 and 144 hours, to evaluate the effects over time. All the samples were subjected to Ion exchange capacity (IEC) and weight loss measurements, Electrochemical Impedance Spectroscopy (EIS) and Scanning Electron Microscopy (SEM) analyses. The IEC and SEM were performed as described in ES9 and ES7 while the IES measurement were recorded using an EG&G Princeton Applied Research potentiostat galvanostat, and a Schlumberger SI 1250 Frequency

Response Analyzer. The FTIR and CHNS analysis of aged membrane were done as described in ES1 and ES9.

*In-situ test*

For the in-situ tests, modified membranes were used in an electrolyzer at fixed potential of 2V, using nickel foam as electrodes and different KOH solution as supply feed. According to ex-situ protocol, the “Medium ageing” 1M KOH at 80°C and “Heavy ageing” 3M KOH at 80°C were applied.

From outside to inside, the test cell was made by two external steel plaques and the two stainless steel bipolar plates, which were separated by a PTFE-glass fiber composite gasket and Nickel-foam electrodes which were placed on the flow fields, directly in contact with the modified membrane. The used Ni-foam electrodes had a catalytic charge of 500 $g*m^{-2}$, thickness of 300 µm and area of about 5 $cm^2$. To guarantee a perfect seal, additional PTFE gasket were placed between the bipolar plates and the membrane, with a hole to perfectly fit the electrode. The whole system was closed by tightening screws passing through the plates, with a torque force of 10 N*m.

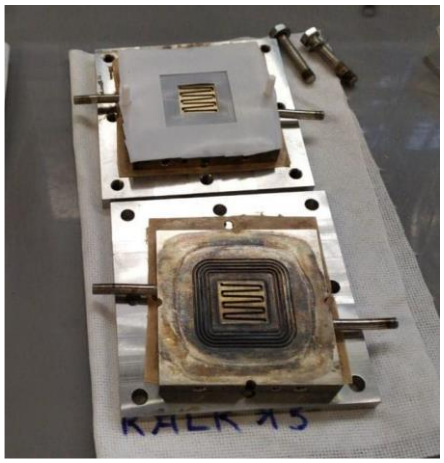

*ES 1 - Photo of in-situ measurements cell*

To investigate the ageing effects, the resistance of the system and the current overtime were recorded at 2V while the polarization curves were performed sweeping the potential from 2 to 1.2 V. Below is reported the protocol of measurement for one cycle (two hours).

Every experiment was made of many cycles of potentiostatic experiments, used to “age” the membrane inside of the cell. A constant potential of 2 V was applied for 1hour and 32min during

which the current was constantly recorded, followed, in the end, by a PEIS experiment. Then the voltage was dropped each 0.1 V to 1.2V, waiting 3 minutes in order to let the system equilibrate and record the current. The PEIS measurements were made every two 0.1 V voltage drop Every cycle lasted about 2 hours, so, for 2 and 6 days the number of cycles were 24 and 72, respectively. The EIS spectroscopy measurements were performed sweeping the frequency from 10 kHz to 2 Hz at fixed potential, while the electrolyzing system was running, using a BCS-815 Biologic Potentiostat/Galvanostat connected with BTLab software control.

## Bibliography


1. Skoog DA, Holler JF. *Chimica Analitica Strumentale*. (Edises, ed.).

2. Wang H, Zhou YW, Cai W Bin. Recent applications of in situ ATR-IR spectroscopy in interfacial electrochemistry. *Curr Opin Electrochem*. 2017;1(1):73-79. doi:10.1016/j.coelec.2017.01.008

3. Koenig JL. *Spectroscopy of Polymers*. Elsevier Science doi:https://doi.org/10.1016/B978-0-444-10031-3.X5000-2

4. Fitzgerald JJ, DePaul SM. Solid-state NMR spectroscopy of inorganic materials: An overview. *ACS Symp Ser*. 1999;717:2-133. doi:10.1021/bk-1999-0717.ch001

5. Holzgrabe U, Deubner R, Schollmayer C, Waibel B. Quantitative NMR spectroscopy - Applications in drug analysis. *J Pharm Biomed Anal*. 2005;38(5 SPEC. ISS.):806-812. doi:10.1016/j.jpba.2005.01.050

6. Kornyshev AA, Kuznetsov AM, Spohr E, Ulstrup J. Kinetics of Proton Transport in Water. 2003:3351-3366. doi:10.1021/jp020857d

7. Editors G, Hodgkinson P, Wimperis S, et al. This paper is published as part of a PCCP Themed Issue on : Solid-State NMR Spectroscopy. 2009. doi:10.1039/b914008p

8. Bottom R. Thermogravimetric Analysis. *Princ Appl Therm Anal*. 2008;1(906):87-118. doi:10.1002/9780470697702.ch3

9. Menczel JD, Prime RB. *Thermal Analysis of Polymers: Fundamentals and Applications*.

10. Schick C. Differential scanning calorimetry (DSC) of semicrystalline polymers. *Anal Bioanal Chem*. 2009;395(6):1589-1611. doi:10.1007/s00216-009-3169-y

11. Paper G. Evaluation of analytical instrumentation. Part XIX: CHNS elemental analysers. *Accredit Qual Assur*. 2006;11(11):569-576. doi:10.1007/s00769-006-0185-x

12. Hübschen G, Altpeter I. *Materials Characterization Using Nondestructive Evaluation (NDE) Methods*.

13. Goswami S, Klaus S, Benziger J. Wetting and Absorption of Water Drops on Nafion Films. 2008;51(Nafion 112):8627-8633. doi:doi.org/10.1021/la800799a

14. Cheng J, He G, Zhang F. A mini-review on anion exchange membranes for fuel cell applications: Stability issue and addressing strategies. *Int J Hydrogen Energy*. 2015;40(23):7348-7360. doi:10.1016/j.ijhydene.2015.04.040

15. Mao J, Iocozzia J, Huang J, Meng K, Lai Y, Lin Z. Graphene aerogels for efficient energy storage and conversion. *Energy Environ Sci*. 2018;11(4):772-799. doi:10.1039/c7ee03031b

16. Smitha B, Sridhar S, Khan AA. Synthesis and characterization of proton conducting polymer membranes for fuel cells. *J Memb Sci*. 2003;225(1-2):63-76. doi:10.1016/S0376-7388(03)00343-0

17. Kim E, Lee S, Woo S, et al. Synthesis and characterization of anion exchange multi-block copolymer membranes with a fluorine moiety as alkaline membrane fuel cells. *J Power Sources*. 2017;359:568-576. doi:10.1016/j.jpowsour.2017.05.086

18. Springer TE, Zawodzinski TA, Wilson MS, Gottesfeld S. Characterization of Polymer Electrolyte Fuel Cells Using AC Impedance Spectroscopy. *J Electrochem Soc*. 1996;143(2):587-599. doi:10.1149/1.1836485

19. Lasia A. *Electrochemical Impedance Spectroscopy and Its Applications*.; 2005. doi:10.1007/0-306-46916-2_2

20. Ciucci F. Modeling electrochemical impedance spectroscopy. *Curr Opin Electrochem*. 2019;13:132-139. doi:10.1016/j.coelec.2018.12.003

21. Snyder KA, Ferraris C, Martys NS, Garboczi EJ. Using Impedance Spectroscopy to Assess the Viability of the Rapid Chloride Test for Determining Concrete Conductivity. *J Res Natl Inst Stand Technol*. 2000;105(4):497-509. doi:10.6028/jres.105.040

22. Lin C, Gao Y, Li N, et al. Quaternized Tröger's base polymer with crown ether unit for alkaline stable anion exchange membranes. *Electrochim Acta*. 2020;354. doi:10.1016/j.electacta.2020.136693

23. Mustain WE, Chatenet M, Page M, Kim YS. Durability challenges of anion exchange membrane fuel cells. *Energy Environ Sci*. 2020;13(9):2805-2838. doi:10.1039/d0ee01133a

# *Appendix*

In this section are reported some extra information about the PhD work.

## A1 - Polyketones implant

The aliphatic polyketones are produced by co-polymerization between carbon monoxide and olefin such as ethylene or propylene. In general, the main working condition for this process are 50 - 60 bar at 90 - 100 ° C and, consequently, the use of an autoclave is necessary. For the specific synthesis of poly(ethyl-ketone), the two gaseous precursors must be mixed, so, the implant needs a premixing zone before the autoclave. For this reason, I design the functional structure of this implant. Unfortunately, for technical problems, not depending by me, the implant is not already finished. In figure below, the general sketch of implant and the details of premixing system are reported.

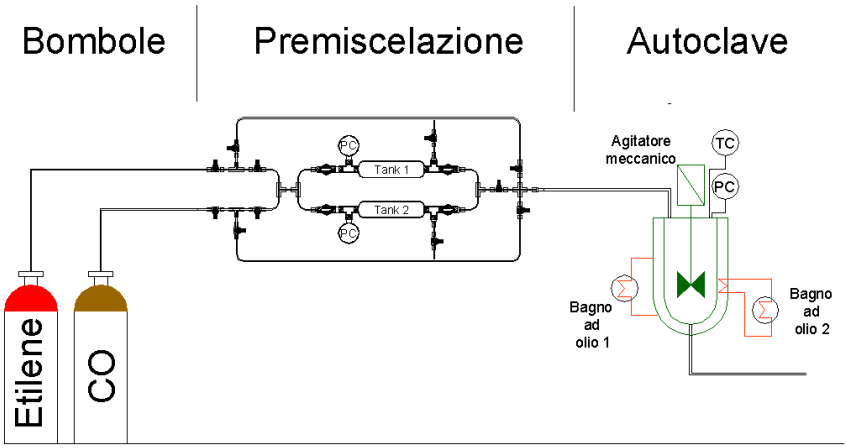

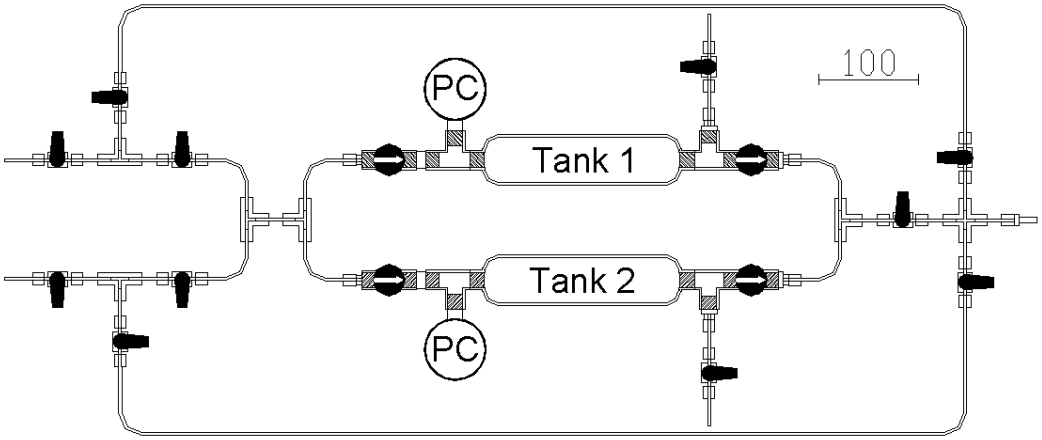


*Appendix 1 – General scheme of polyketones implant (top) and the sketch of pre-mixing zone (down)*

## A2 - Homemade Wet box

The alkaline exchange materials react with carbon dioxide generating carbonates. To prevent this reaction, my materials were conserved and activated in wet box. This lab equipment guarantees a $CO_2$-controlled working zone filled by nitrogen. During my PhD I realized and fixed a homemade wet box for lab activities as reported in photo.

*Technical data:*

Body material: PMMA

Cylinder: Nitrogen, 99.99995, with pressure gauge to work at 0.1 bar

Carbon dioxide detector: AMI 2.0 VWR®

Water solution: water milli-q, 1M KOH, 6M KOH, saturated KOH and waste

*Appendix 2- Photo of wet box in materials science department*


*Appendix 3 - Details of wet box: a) double check valves on the in-gas line of wet box, b) workbench, c) pre-chamber, d) needle valve on the out-gas line of the wet box, e) gases trap, f) AMI 100 carbon dioxide detector*

## A3 - In-plane conductivity cell

Impedance spectroscopy is a powerful technique to study and understand the properties of an electrochemical system. In order to explore in-plane conductivity and surface resistance of polymeric materials, in-plane conductivity cell is necessary. During my PhD I designed and realized the measurement cell reported in photo.

*Technical data:*

Body material: PTFE

Wire: platinum, 0.6 mm diameter, length about 50 cm

Distance between outer wires: 1.8 cm

Distance between inner wires: 0.5 cm

Optimal sample: polymer film, 1 cm * 4 cm

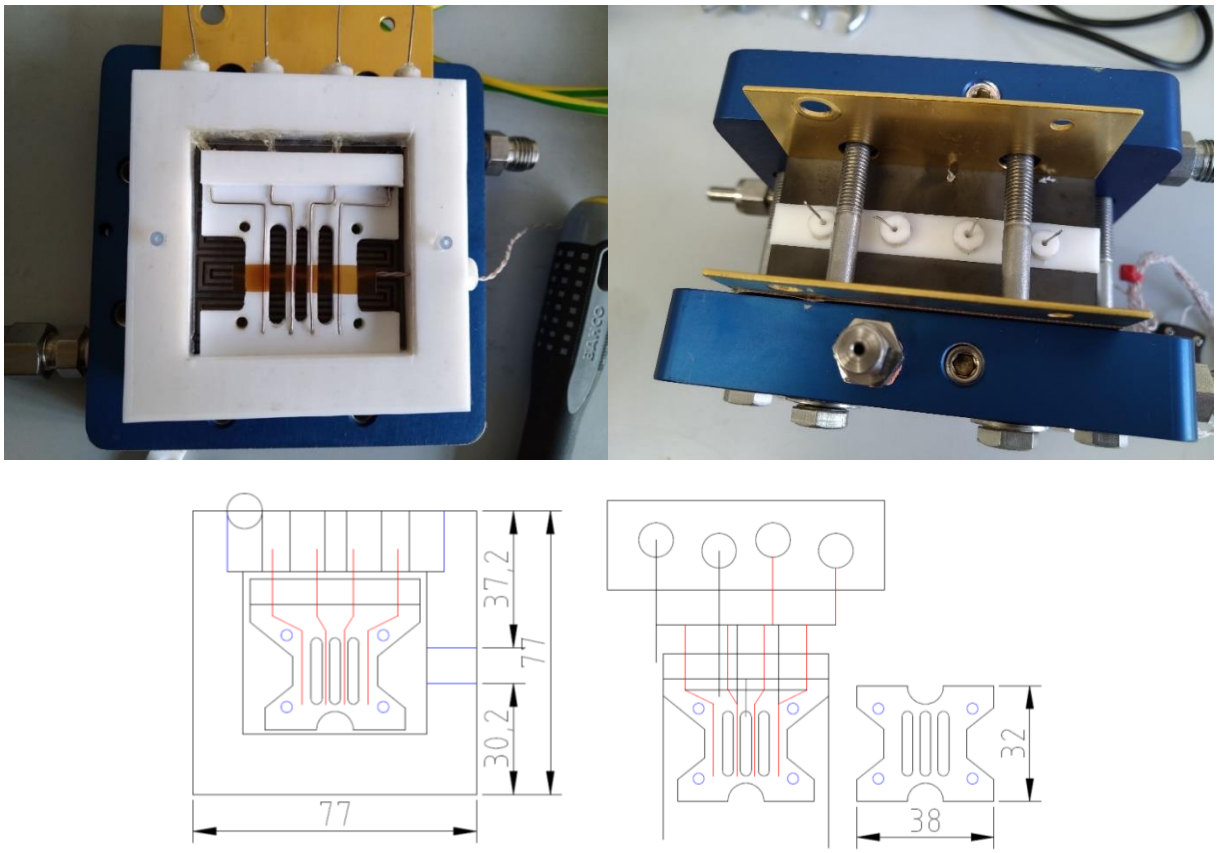


*Appendix 4 - Photos of in-plane conductivity cell (top) and Some sketch of my CAD_2D file (down)*

## A4 – Fuel cell testing stand station

During my PhD I realized and fixed the fuel cell testing stand station reported in photo. In order to optimize the maximum working condition of this testing station, I design and realized the multi-gas selector and the backpressure system.

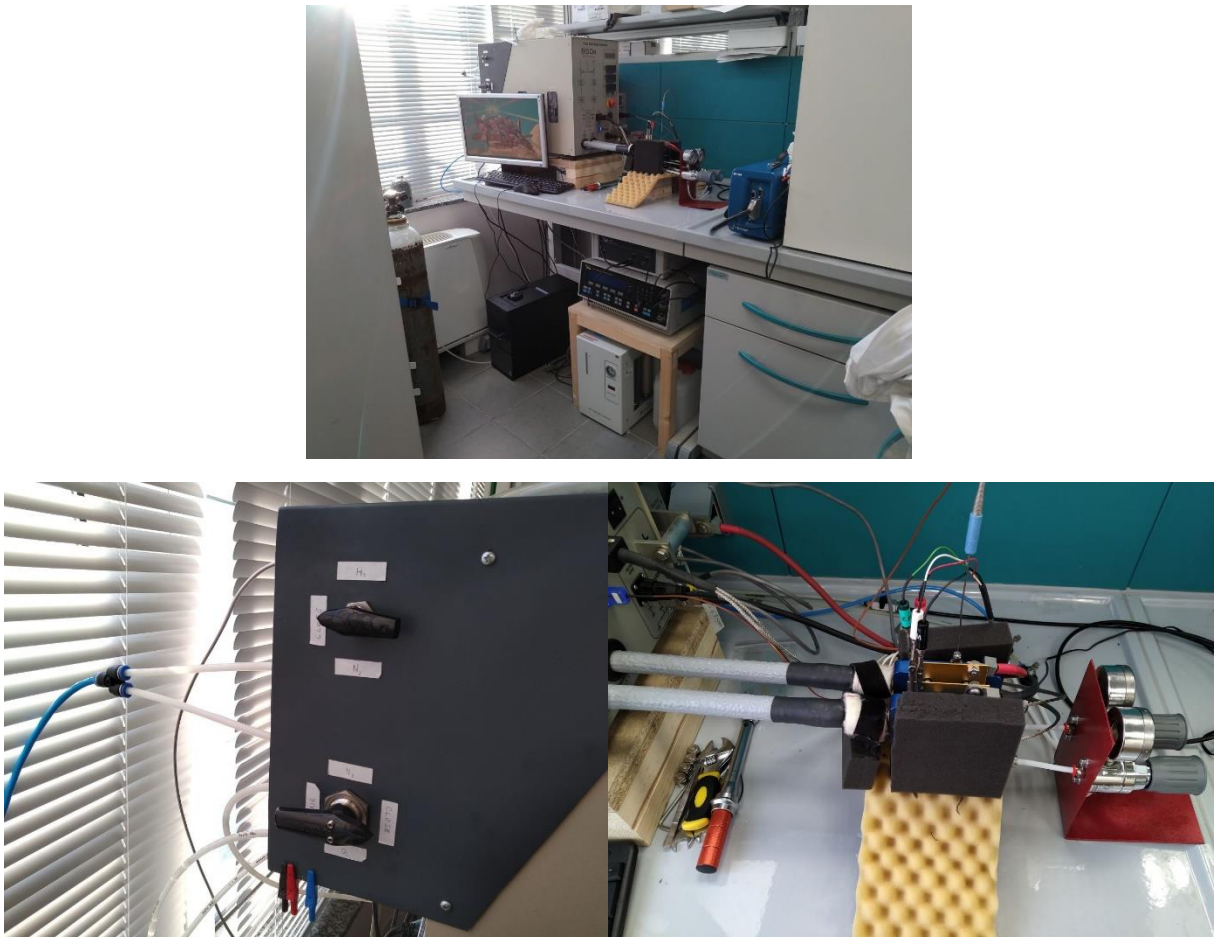

*Appendix 5 - Photos of Fuel Cell testing stand station (top), multi-gas selector (down left) and backpressure system (down right)*

## A5 – Project "Dipartimento dei eccellenza" (2018-2022) - FLEXILAB project

The project Electrical Power and Energy Vectors from Renewable Sources - FLEXILAB of the Department of Materials Science of the University of Milano – Bicocca is funded by the "Fondo per il finanziamento dei dipartimenti universitari di eccellenza – D.L. n.232 del 11/12/2016, Vol I, Commi 314-338". Such competitive funding from the Italian Government was granted to the best 180 Italian Departments (807 in total) by means of a selection based on the Department productivity and the quality of a development project. The Department of Materials Science resulted among the best 11

in the area of Chemical Sciences. The total cost of FLEXILAB is 10.700.000 € with a direct funding from MIUR of 6.500.000 €. FLEXILAB has the ambition to constitute a Departmental Laboratory, open to collaboration with external stakeholders, on materials for a sustainable energy cycle. (reference: website of Department of Materials Science).

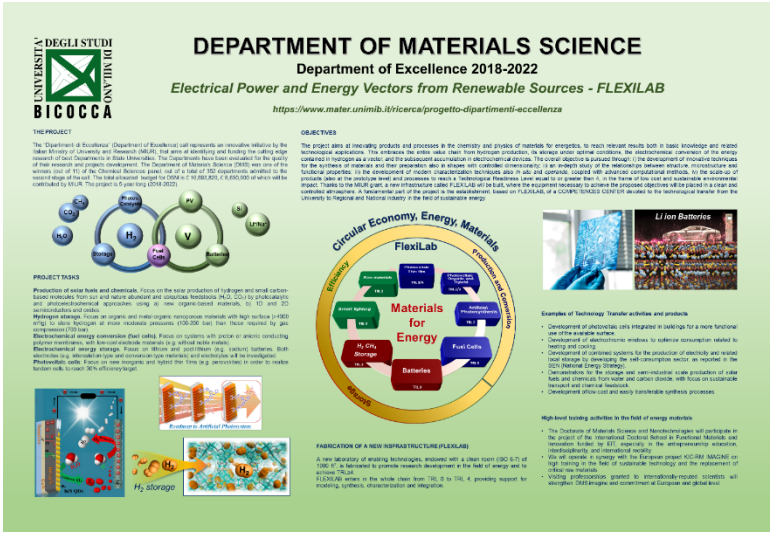


*Appendix 6 - overview of FLEXILAB project*

Fuel cell activities represent a new research for the Department (Work Packages 3, WP3). I am the first PhD student who has worked since the beginning of this project. During this period, I contributed to the realization of the working methods and laboratory equipment necessary for this purpose.